Sustainable Carbon Materials

Review

Open Access

https://doi.org/10.48130/scm-0025-0011

Microwave-assisted pyrolysis for advanced sustainable carbon materials

Tianhao Qiu[1], Kaihan Xie[1], Chaoyue Liu[1], Faizan Ahmad[1], Wenke Zhao[1], Müslüm Arıcı[2] and Yaning Zhang[1*]

Received: 28 August 2025

Revised: 19 November 2025

Accepted: 26 November 2025

Published online: 30 December 2025

Abstract

Driven by global carbon neutrality goals and resource cycling demands, sustainable carbon materials have emerged as strategic solutions for addressing environmental and energy crises, owing to their broad raw material sources (including biomass, municipal solid waste, and industrial exhaust gases), and multifunctional properties (such as energy storage, environmental remediation, and microwave absorption). This review systematically compares the performance differences between conventional pyrolysis (CP), and microwave-assisted pyrolysis (MAP) technologies in producing carbon materials of varying dimensions, revealing that MAP significantly enhances material performance and process efficiency through its volumetric heating mechanism (eliminating temperature gradients), low thermal mass characteristics (response time of less than 3 min), and energy-selective transfer (activation energy reduction of 40–150 kJ/mol). Research demonstrates that: in the 1D material domain, MAP-synthesized carbon nanofibers reduce reaction time from hours to minutes, compared to traditional chemical vapor deposition, while significantly lowering energy consumption; for 2D graphene, microwave reduction of graphene oxide elevates electrical conductivity from 0.07 to 10^4 S/m within 2 s, whereas conventional thermal reduction requires temperatures exceeding 800 °C under inert atmospheres and yields products with resistivity as high as 796 $\mu\Omega/cm^2$. In the 3D porous carbon field, MAP exhibits exceptional structural control capabilities: biochar prepared via 15-min MAP achieves a specific surface area of 455.9 m^2/g, far exceeding the 288.60 m^2/g of biochar from CP after 120 min; for electromagnetic wave absorption applications, MAP-derived tremella-carbon (a fungus) achieves breakthrough performance with a minimum reflection loss RL_{min} = −77.9 dB and an effective absorption bandwidth EAB = 8.5 GHz. Despite MAP's significant advantages in energy consumption (energy recovery efficiency reaching 97.96%), processing efficiency (heating rate exceeding 100 °C/min), and product performance, its industrialization still faces challenges in equipment costs and scaled reactor design. Future efforts must integrate hydrothermal pretreatment with AI-driven parameter optimization to develop mesopore-oriented processes, thereby advancing this technology in energy storage (target specific capacitance > 500 F/g) and electromagnetic protection (target EAB > 8 GHz) applications.

Keywords: Sustainable carbon material, Production, Microwave pyrolysis technology, Conventional pyrolysis technology

Highlights

- Microwave pyrolysis offers a more environmentally friendly production than conventional methods.
- Microwave pyrolysis reduces production time for carbon nanofibers and graphene.
- Microwave pyrolysis produces biochars with better properties.
- The challenges lie in large-scale production, especially in reactor design and equipment cost.

* Correspondence: Yaning Zhang (ynzhang@hit.edu.cn)

Full list of author information is available at the end of the article.

Graphical abstract

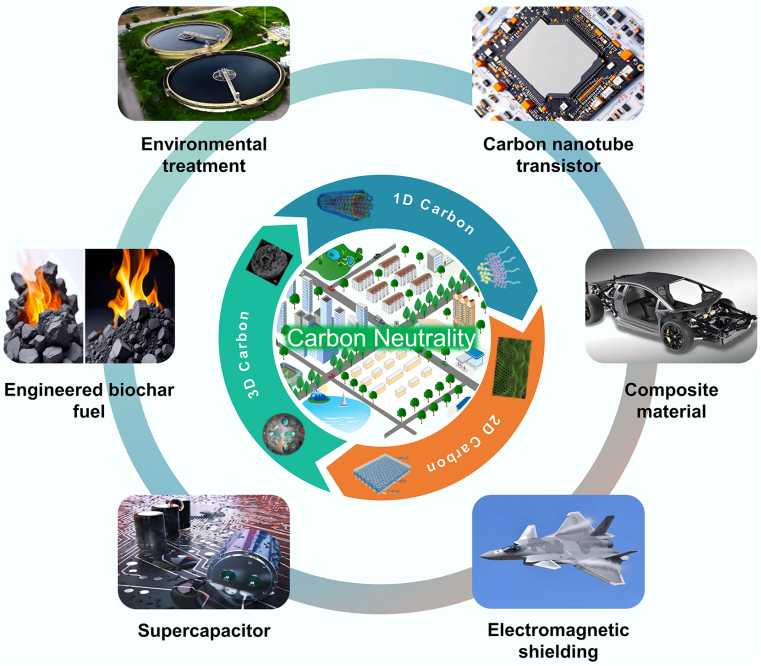

Introduction

Against the backdrop of the current global scene, facing severe environmental and energy crises, the urgency of carbon neutrality goals, and the necessity of resource recycling have become an international consensus. Issues such as intensifying climate change, depletion of fossil fuel resources, and environmental pollution continue to drive the search for sustainable solutions. In this context, developing environmentally friendly and sustainable materials emerges as a key solution to these challenges, with carbon materials becoming a research focus due to their unique strategic value[1]. The core advantage of carbon materials lies first in their source sustainability. They can utilize biomass (such as agricultural residues, forestry byproducts), municipal solid waste (such as plastics, rubber), or industrial exhaust gases (such as CO_2) as feedstocks. Through processes like pyrolysis and activation, these feedstocks are transformed into high-value-added carbon materials, achieving a circular economy through waste-to-resource conversion. Secondly, carbon materials exhibit exceptional structural designability. From 1D carbon nanotubes and 2D graphene, to 3D porous carbon frameworks, different dimensional structures exhibit distinct physicochemical properties, such as ultra-high specific surface area (SSA), excellent electrical conductivity, and mechanical strength. This structural versatility provides a solid foundation for diverse functional applications. More significantly, carbon materials play pivotal enabling roles in several critical fields. In energy storage, they serve as electrode materials for lithium/sodium-ion batteries that enhance energy storage density[2]. In environmental remediation, their adsorption capabilities efficiently remove heavy metals and organic pollutants from water bodies[3]. In microwave absorbing applications, lightweight, highly conductive carbon foams provide effective adsorption of electromagnetic radiation pollution in the 5G era[4]. The wide-ranging applications of various carbon materials are illustrated in Graphic abstract. Owing to this multi-functionality, carbon materials serve as a bridge connecting environmental governance and green energy, holding profound significance for achieving the dual carbon goals.

Traditional carbonization methods face multiple technical bottlenecks for preparing carbon materials. Firstly, high-temperature thermal treatment (typically requiring 500–1,200 °C) results in persistently high energy consumption. Secondly, the pyrolysis process of raw materials often releases pollutants such as residues, acidic gases (e.g., H_2S), and polycyclic aromatic hydrocarbons, entailing secondary environmental risks. Thirdly, conventional methods lack the capability to regulate microstructure. This limitation impedes the precise construction of hierarchical pore structures or targeted surface functional groups. These defects severely constrain the application efficacy of carbon materials in high-end fields, such as the rate capability of supercapacitor electrode materials and the selectivity of adsorbent materials. Therefore, developing green processes such as low-temperature catalytic carbonization and microwave-assisted pyrolysis (MAP), or employing novel technologies like molten salt electrolysis and plasma activation, is critical to overcoming the tripartite challenge of energy consumption, pollution, and performance limitations. A comparative summary of these pyrolysis technologies, highlighting their fundamental characteristics and limitations, is provided in Table 1. As electromagnetic waves with wavelengths ranging from 0.001 to 1 m (frequency 300 MHz–300 GHz)[5], microwaves have been widely applied in fields such as radar, microwave ovens, and wireless communication due to their characteristics of easy beam focusing, strong directionality, and linear propagation[6,7]. The industrial application of their heating technology is built upon an in-depth understanding of the electromagnetic wave-matter interaction mechanism. Particularly, studies on the dynamic response of polar molecules in alternating electromagnetic fields have revealed the core of electromagnetic-to-thermal energy conversion, which is the energy loss process in dielectric materials. When a substance is exposed to a microwave field, internal charged particles exhibit three typical response mechanisms. The first mechanism is dipole polarization[8], where the

Table 1 Comparison of different pyrolysis technologies for sustainable carbon material production

Technology	Heating mechanism	Key advantage	Inherent limitation
Conventional pyrolysis	External conduction/ convection	Mature technology, simple setup	High energy consumption, slow heating
Microwave-assisted pyrolysis	Volumetric heating via dielectric loss	Rapid and selective heating, high energy efficiency, superior product performance, excellent microstructure control	Potential hotspots, specialized equipment needed, scalability challenges
Low-temperature catalytic carbonization	Catalytic lowering of activation energy	Lower operating temperature, potential for targeted reactions	Catalyst cost and deactivation, limited feedstock adaptability
Molten salt electrolysis	Electrochemical reduction in molten salt	Utilize CO_2 or wastes as feedstock, direct conversion	High energy input, corrosive environment, complex operation
Plasma activation	Ultra-high temperature from ionized gas	Extremely fast reactions, can handle refractory materials	Very high energy consumption, expensive equipment

inherent dipole moments of polar molecules repeatedly reorient in a high-speed alternating electric field (billions of times per second), generating frictional heat due to intermolecular retardation forces. Zhao et al.[9] discovered during their study of hierarchical porous flower-like biphasic sulfides that interfacial lattice distortion and defects significantly enhanced dipole polarization, enabling microwave absorption performance with a minimum reflection loss (RL_{min}) of −45.8 dB and an effective bandwidth of 3.8 GHz. The second is the ionic conduction mechanism[10], where free ions in dielectric media exhibit phase lag under the rapid polarity reversal of the microwave field (~4.9 GHz), leading to collisions with surrounding media and converting into thermal energy. The third is the interfacial polarization mechanism[11], where, in heterogeneous systems, heterointerfaces form accumulated space charges due to differences in dielectric constant (Maxwell-Wagner effect). For example, Sun et al.[12] grafted a SiO_2 coating onto the surface of chopped carbon fibers. Through enhanced interfacial polarization, the material achieved a reflection loss value of −29.3 dB at a 2 vol% filling rate. Notably, besides the aforementioned thermal effects, non-thermal effects induced by quantum interactions between the electromagnetic field and molecules also exist during microwave heating[13]. Thermal effects arise from bulk temperature increase due to dielectric loss, while non-thermal effects involve direct microwave-induced quantum state modulation. This non-thermal effect primarily enhances molecular collision probability and reduces activation energy. Specifically, microwaves accelerate molecular vibration frequency, promote chemical reactions, and induce energy-level transitions to excited states, thereby altering reaction kinetics[14]. Research indicates that non-thermal effects precede thermal effects, influencing intermolecular forces to generate initial thermal energy. Thermal effects gradually dominate as energy accumulates. The differences in heating mechanisms between conventional pyrolysis (CP) and MAP are shown in Fig. 1. This unique energy transfer mechanism overcomes the limitations of traditional heat conduction and provides a new paradigm for green chemical engineering.

Compared with conventional electrical pyrolysis, MAP has attracted significant attention due to its unique advantages. One key advantage is heating uniformity[18], which results from the direct interaction of microwaves with polar molecules inside the material. This interaction forms volumetric heating that eliminates temperature gradients caused by surface heat conduction, making it particularly suitable for porous or bulky materials. Another advantage is low thermal mass[19], which allows instantaneous system response that synchronizes with microwave activation/deactivation. This eliminates the need for preheating or cooling while achieving instant and precise temperature control. The process also exhibits high energy efficiency and low consumption[20], benefiting from the selective heating of polar components by microwaves, which reduces energy loss pathways. This is evidenced by the activation energy for biomass MAP being reduced by 40–150 kJ/mol, and the pyrolysis temperature range decreasing from the conventional 300–500 to 250–300 °C[21]. Additionally, high pyrolysis efficiency[22], originating from rapid heating rates (> 100 °C/min) and the microwave field promoting chemical bond cleavage, significantly shortens reaction time. Extensive experimental evidence supports these advantages. For example, Ellison et al.[23] reported that selective heating during MAP of low-rank coal generated local hotspots, accelerating pore development. Zhang et al.[24] compared microwave and CP of pepper straw, confirming that biochar prepared by MAP exhibited 47.6% higher SSA and 55.7% higher specific capacitance. Jankovská et al.[25] efficiently converted waste tires into microporous carbon black using microwaves for xylene adsorption. Precisely due to the significant advantages of MAP in time, energy consumption, and product performance, converting waste biomass into porous biochar via this technology has been widely recognized as an environmentally friendly and efficient resource utilization approach[26].

This review critically analyzes recent advances in different-dimensional (1D/2D/3D) carbon materials produced by both conventional and microwave methods. It compares the differences between various technical pathways and comprehensively evaluates the advantages and disadvantages of the two methods in terms of energy efficiency, product characteristics, etc. It focuses on analyzing the regulatory mechanisms of microwave process parameters on carbon material performance. By reviewing the role of microwave technology in the preparation of sustainable carbon materials, it provides a theoretical basis and practical guidance for selecting green carbon material preparation technologies targeting carbon neutrality goals.

1D carbon materials

1D carbon materials refer to carbon-based substances with nanostructures featuring macroscopic lengths and nanoscale diameters. Among them, carbon nanotubes (CNTs) and carbon nanofibers (CNFs) are two of the most prominent examples[27,28]. CNTs are formed by rolling single or multiple layers of graphene into hollow tubular structures with diameters of 2–20 nm and lengths of 0.1–10 μm. Depending on the number of layers, they are classified as single-walled (SWCNT) or multi-walled (MWCNT), possessing excellent tensile strength[29], electrical conductivity[30], optical properties[31], and room-temperature thermal conductivity[32]. SWCNTs can exhibit metallic or semiconducting behavior due to their unique electronic structure, which depends on their chiral indices, making them highly promising for nano-electronic devices. In contrast, MWCNTs exhibit higher mechanical strength and thermal stability due to their multi-layered structure, making them outstanding for composite reinforcement.

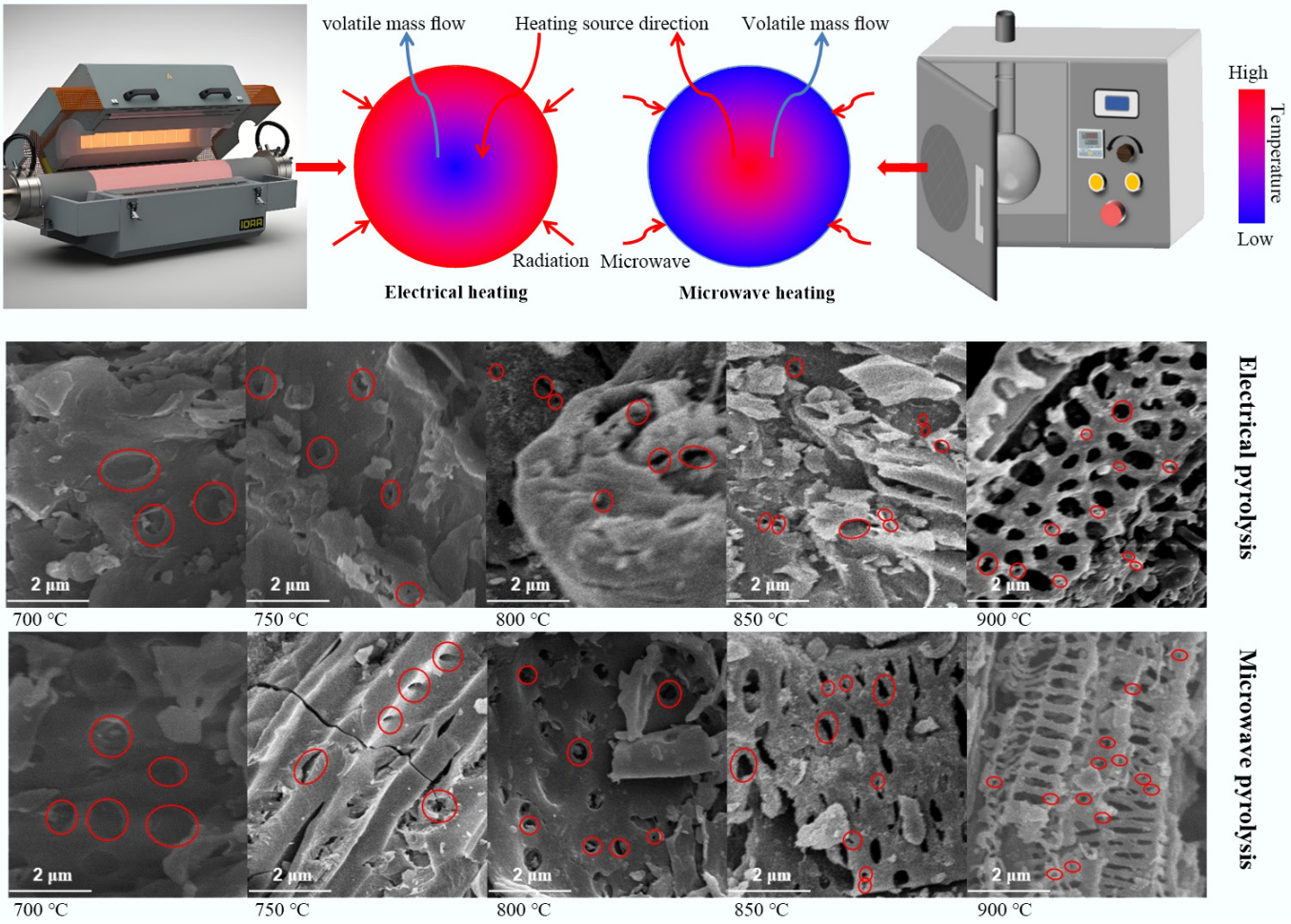

Fig. 1 Schematic diagram of temperature distribution, heat transfer, and mass transfer for conventional electrical heating and microwave-assisted heating[15–17].

Comparatively, CNFs (diameter 10–500 nm), as solid quasi-1D nanostructures, possess abundant edge defects and functional groups on their surfaces, resulting in significantly higher active site density than CNTs. This structural characteristic enables CNFs to demonstrate superior performance in electrochemical applications, such as achieving higher specific capacitance in supercapacitors. Their unique characteristics, such as lightweight nature, high electrical conductivity, and chemical stability[33,34], make applications possible in energy storage[35], catalysis[36], biomedicine[37], and environmental remediation[38]. Particularly in biomedicine, the large SSA and surface functional groups of CNFs enable effective drug molecule loading for targeted drug delivery. Similarly, in environmental remediation, the adsorption capacity of CNFs for heavy metal ions is significantly superior to traditional activated carbon materials.

Traditional CNT synthesis techniques primarily include arc discharge, laser ablation, and chemical vapor deposition (CVD) (Fig. 2a)[39,40]. These methods employ high-energy sources (high-voltage arcs/laser beams/plasma) to disassociate carbon sources, forming nanoclusters that drive growth on catalyst surfaces. Arc discharge is the earliest technique enabling mass CNT production, but its products suffer from low purity and require complex purification processes. Laser ablation can produce high-quality SWCNTs, but entails high equipment costs and limited yield. CVD has become the primary method for industrial production due to its strong controllability and relatively low cost. Controlling reaction temperature, gas flow rate, and catalyst type enables directional CNT growth. Despite their advantages, these methods share significant limitations, including the requirement for extremely high temperatures (> 600 °C) to ensure crystallinity[41], reliance on inert gases to prevent oxidation, safety risks from using flammable/explosive gases (acetylene/hydrogen) in CVD, and bulk heating mechanisms leading to high energy consumption and difficulty in localized growth control. Particularly, the high-temperature requirement restricts direct growth on flexible polymer substrates, and the reliance on inert gas protection substantially increases production costs. Collectively, these limitations hinder the *in-situ* construction of nanodevices on low-melting-point substrates[42,43].

Microwave methods overcome these limitations (Fig. 2b)[44], utilizing differential microwave absorption between substrates and catalysts to achieve selective localized heating[45]. This heating mode offers significant energy-saving advantages, reducing reaction times to below 1/10 of those of traditional methods. Catalyst particles are rapidly heated to reaction temperatures within seconds to 3 min[46,47], while transparent substrates remain at low temperatures, creating reaction conditions without requiring hazardous gases. The microwave method is particularly suitable for growing CNTs on temperature-sensitive substrates, enabling the direct construction of flexible electronic devices on paper or polymer films. Regarding products, traditional CVD can produce long SWCNTs (length of 0.1–100 mm, diameter of 0.6–4.0 nm)[48,49], suitable for

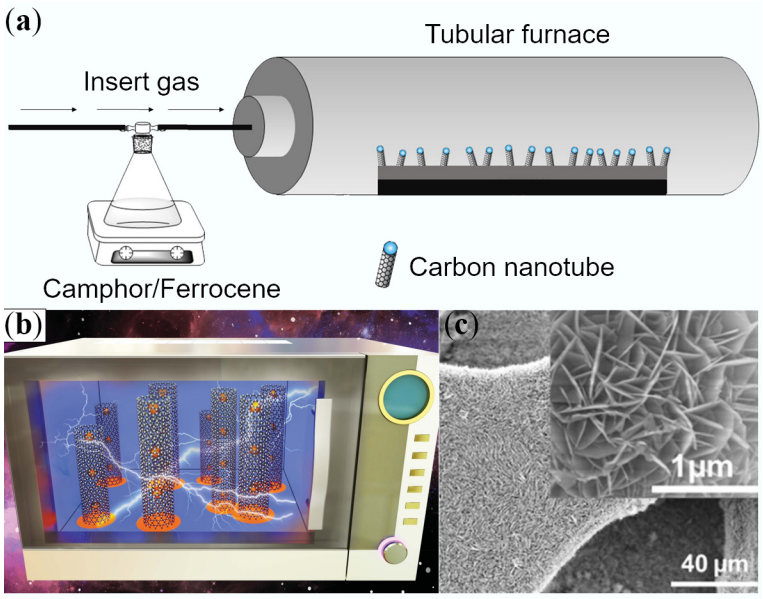

Fig. 2 Production of CNTs by (**a**) chemical vapor deposition[39], and (**b**) microwave irradiation[44]. (**c**) SEM images of CNTs[50] prepared by microwave irradiation.

polymer composites. These ultra-long CNTs uniquely benefit the preparation of high-strength fibers with tensile strengths exceeding 50 GPa. Conversely, microwave synthesis primarily yields short MWCNTs (length of 1–20 μm, diameter of 10–200 nm) (Fig. 2c)[50]. Its localized heating characteristic is particularly conducive to the *in-situ* growth of brush-like structures on conductive/porous substrates. CNT arrays with this unique morphology exhibit excellent performance in applications like field emission displays and supercapacitor electrodes. Notably, microwave-grown CNTs often possess more structural defects, which, rather than being a detriment, become advantageous in certain catalytic applications as defect sites can serve as active centers enhancing catalytic efficiency. Beyond this, the rapid temperature ramping inherent to microwave synthesis facilitates the formation of unique branched structures or heterojunctions, which may possess novel functional properties in optoelectronic devices.

Traditional CNF production primarily focuses on electrospinning (Fig. 3a)[51] and CVD. Electrospinning utilizes electrostatic fields to stretch polymer solutions, combined with pre-oxidation and carbonization post-treatment, to obtain continuous structures with diameters ranging from 10 nm to 10 μm, achieving random, core-shell, and aligned morphologies. Aboagye et al.[52] obtained smooth CNFs with an average diameter of 250 nm by electrospinning polyacrylonitrile nanofibers followed by carbonization. After loading platinum nanoparticles via redox reactions, these CNFs exhibited conversion efficiencies of 7%–8% as counter electrodes in dye-sensitized solar cells. Notably, this performance approaches that of traditional platinum counter electrodes while significantly reducing costs, offering new possibilities for the large-scale commercialization of solar cells. Li et al.[53] fabricated 3D porous interconnected CNFs with diameters of 100–200 nm using electrospinning combined with an Ar/air mixed-atmosphere carbonization process. Their unique micro/mesoporous structure endowed them with a high specific capacity of 1,780 mA·h/g, demonstrating potential to replace graphite in flexible lithium battery anodes. This 3D porous structure not only provides more lithium-ion storage sites but also significantly improves ion transport kinetics, enabling excellent cycle stability even at high current densities. Furthermore, this flexible electrode material can be directly integrated into wearable electronics, opening new avenues for the development of next-generation flexible energy storage devices.

The CVD method uses hydrocarbons as carbon sources (500–1,500 °C) to produce CNFs with high aspect ratios and high conductivity, albeit at higher costs. For example, Simon et al.[54] employed CVD using methane as the carbon source and palladium as the catalyst to grow CNTs and CNFs on single-channel porous ceramic Al_2O_3 substrates at different temperatures. At a synthesis temperature of 800 °C, a mixture of two types of bamboo-like CNFs was obtained. This unique bamboo-joint structure imparts distinctive mechanical properties and electron transport characteristics, holding significant application value in composite reinforcement and conductive fillers. Additionally, Xing et al.[55] utilized a dual-template strategy employing porous anodic aluminum oxide (AAO) membranes and colloidal silica to prepare mesoporous carbon nanofibers (MCNFs). The resulting MCNFs possessed not only high SSA and mesopore volume but also a hierarchical nanostructure comprising hollow macro-channels derived from the AAO template, large mesopores (~22 nm) formed by removing silica particles, and micropores formed by phenolic resin carbonization. This multi-level pore structure maximizes mass transfer efficiency, exhibiting outstanding performance in energy storage systems like supercapacitors and lithium-sulfur batteries. Ren et al.[56] demonstrated that efficient solar and conventional energy can electrolytically convert atmospheric CO_2 dissolved in molten carbonate into CNFs on inexpensive steel or nickel electrodes. This breakthrough technology not only realizes the resource utilization of greenhouse gases but also significantly reduces CNF production costs. A cheaper source of CNFs will promote their adoption as a societal resource, and using CO_2 as a reactant to produce value-added products like CNFs provides an incentive to consume this greenhouse gas to mitigate climate change. Scaling up this process promises to achieve carbon-negative production, making significant contributions to global carbon neutrality goals.

Combining microwave technology with traditional methods can significantly improve efficiency. Microwave-assisted CVD (Fig. 3b)[57] and microwave hydrothermal methods have emerged as novel

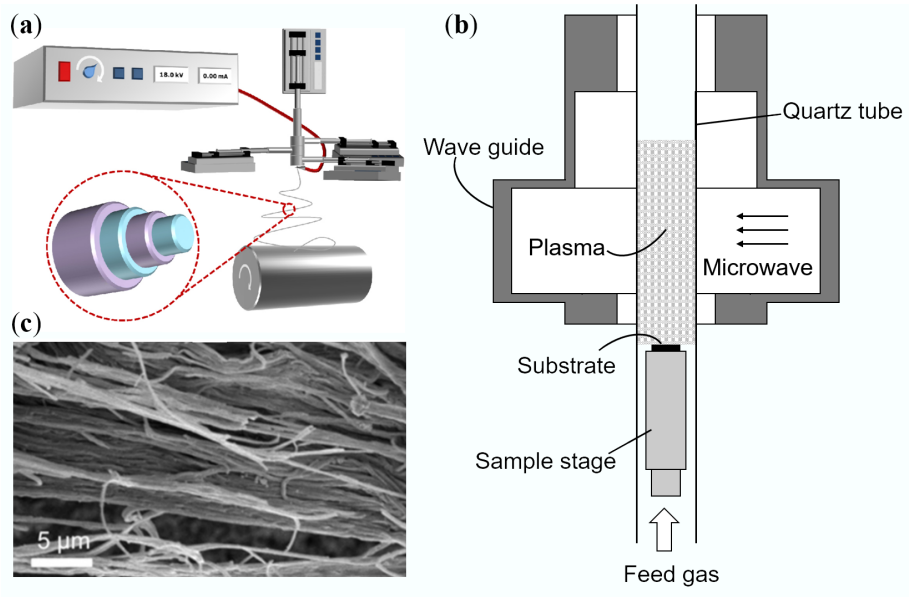

Fig. 3 Production of CNFs by (**a**) chemical vapor deposition[51], and (**b**) microwave irradiation[57]. (**c**) SEM images of CNFs[60] prepared by microwave irradiation.

approaches. For instance, Bigdeli & Fatemi[58] utilized a 900 W microwave-assisted CVD to prepare morphologically uniform carbon nanofibers on ordinary activated carbon surfaces. Compared to conventional CVD, this method reduced reaction time from hours to minutes, while significantly lowering energy consumption, demonstrating substantial energy-saving advantages. Gupta et al.[59] employed a simple and feasible microwave-assisted hydrothermal method, synthesizing CNFs at 400 W after a 2-h hydrothermal reaction at 400 °C for use as rapid adsorbents for methamphetamine. This approach enables CNFs grown on substrates like activated carbon and fibers to exhibit unique morphologies (Fig. 3c)[60]. A notable feature of microwave-assisted synthesis is its ability to achieve uniform heating at the molecular level, facilitating the formation of more uniform nanostructures while avoiding temperature gradient issues inherent in conventional heating. Although electrospinning and CVD (including microwave variants) remain mainstream, developing economical, green, and scalable techniques capable of precise structural control (porosity/orientation) remains a crucial goal. In recent years, emerging technologies such as plasma-enhanced CVD, supercritical fluid technology, and biotemplating methods have also begun to show promise in CNF preparation. These methods exhibit unique advantages in controlling fiber diameter, orientation, and surface chemistry, providing new tools for tailoring CNF properties. Particularly noteworthy is the introduction of artificial intelligence into the CNF preparation process. Optimizing process parameters through machine learning algorithms holds promise for the precise design and performance prediction of CNF structures, which will significantly accelerate the development of novel CNF materials. Furthermore, developing green synthesis routes based on sustainable feedstocks (e.g., biomass, plastic waste) and exploring low-cost, large-scale production technologies for CNFs remain key future research directions. With continuous breakthroughs in these technologies, CNFs are poised to play important roles in more fields such as energy, environment, and healthcare, driving the rapid development of the nanotechnology industry.

In summary, the synthesis of 1D carbon nanomaterials via MAP demonstrates revolutionary advantages in reaction efficiency and process mildness, compared to conventional CVD. Traditional CVD requires high temperatures (> 600 °C), inert gas protection, and reaction times on the order of hours, suffering from high energy consumption and difficulty in localized growth control due to bulk heating mechanisms. In contrast, MAP leverages differential microwave absorption between substrates and catalysts to achieve selective localized heating. This reduces reaction times from hours to minutes or even seconds (response time < 3 min), with catalyst particles being heated to reaction temperatures within seconds while microwave-transparent substrates remain cool. This unique heating mode not only offers significant energy-saving benefits but also enables the direct construction of flexible electronic devices on temperature-sensitive substrates like paper or polymer films.

2D carbon materials

Graphene is a 2D atomic crystalline material composed of a single layer of carbon atoms tightly packed via sp^2 hybridization into a perfect hexagonal honeycomb lattice[61,62], with a thickness of only one-millionth of the diameter of a human hair. As the first experimentally confirmed 2D material, it is not only a pivotal member of the carbon allotrope family but its single-atomic-layer structure imparts extraordinary properties, such as exceptional strength (far exceeding steel)[63,64], excellent flexibility, superior electrical/thermal conductivity, and outstanding optical transparency (~97.7%)[65–68], along with gas impermeability and chemical functionality. This unique structural characteristic originates from the strong covalent bonding between carbon atoms. Simultaneously, graphene exhibits electron mobility at room temperature far surpassing that of traditional semiconductor materials, granting it unparalleled advantages for high-speed electronic devices. Endowed with these unmatched characteristics, graphene has rapidly become a focal point of research and is hailed as one of the most revolutionary materials of the 21st century. With the maturation of production techniques and cost reduction (e.g., micromechanical exfoliation, CVD, chemical oxidation-reduction methods[69]), graphene is progressively moving towards widespread application. Particularly, the development of CVD has enabled the preparation of large-area,

high-quality graphene films, laying the foundation for industrial applications. The oxidation-reduction method, due to its simplicity and low cost, has become the primary laboratory method for graphene preparation. Although the product quality is slightly inferior to CVD, it holds significant advantages for large-scale production.

In electronics and optoelectronics, its superior electrical properties make it an ideal material for developing ultra-high-frequency transistors, flexible displays, and efficient photodetectors. The cut-off frequency of graphene transistors far exceeds that of traditional silicon-based devices, promising to advance terahertz communication technology. In flexible electronics, graphene's excellent mechanical properties and conductivity make it an ideal choice for the backplanes of foldable displays. In composites and coatings, the incorporation of graphene can significantly enhance the mechanical strength, corrosion resistance, self-healing efficiency, and flame retardancy of matrix materials like epoxy resins, finding applications in aerospace, construction, and protective coatings[70]. In energy storage and conversion, graphene serves as an ideal electrode material for supercapacitors and batteries which possess a high theoretical specific capacitance, greatly improving energy storage efficiency[71]. The energy density of graphene-based supercapacitors has exceeded 50 W·h/kg, with charge-discharge cycle lifetimes exceeding 100,000 cycles, showing immense potential in electric vehicles and smart grids. Furthermore, it can enhance the performance of dye-sensitized solar cells or function as a high-thermal-conductivity filler, significantly improving the thermal management of heat storage systems (thermal conductivity enhanced by up to 220%)[72]. In environmental protection, graphene filters show great promise and have been successfully applied for highly efficient CO_2 capture (high permeability and selectivity)[73], and purifying severely polluted water sources (e.g., Graph-Air technology)[74]. The CO_2/N_2 selectivity of graphene membranes far surpasses that of traditional polymeric membrane materials. In biomedicine, graphene and its derivatives (e.g., graphene oxide (GO), graphene quantum dots) exhibit broad applicability, including antibacterial effects (against Gram-positive and Gram-negative bacteria), targeted drug delivery (pH-responsive carriers), orthopedic implants (promoting angiogenesis and bone regeneration), and biosensors[75]. GO, owing to its abundant oxygen-containing functional groups and good biocompatibility, has become a research hotspot for drug carriers, enabling pH-responsive controlled release and improving targeting for tumor therapy. Additionally, its applications extend to catalysis, self-healing smart coatings, high-performance sensors (e.g., strain sensing), desalination, cryptography, lightweight electric vehicles, and even space technology. In catalysis, nitrogen-doped graphene has demonstrated oxygen reduction reaction activity comparable to precious metals, substantially reducing fuel cell costs. Importantly, graphene serves as the fundamental building block of the carbon material family (CNTs can be viewed as rolled-up graphene, and fullerenes as wrapped graphene)[76,77], and its continuously demonstrated versatility and research breakthroughs indicate it will profoundly transform numerous industries and deliver revolutionary solutions[78]. In recent years, significant progress has also been made in research on heterostructures of graphene with other 2D materials. Bandgap engineering enables the design of material systems with entirely new functionalities, providing novel approaches for next-generation optoelectronic devices and quantum computing technologies. With continuous breakthroughs in preparation techniques and in-depth application research, graphene will undoubtedly demonstrate its unique value and broad application prospects in even more fields.

Synthesis of graphene-based materials primarily relies on bottom-up methods (e.g., CVD[79]) and top-down methods (e.g., reduced graphene oxide [rGO]). Among them, reduction of GO presents the most scalable pathway due to its low raw material cost and solution hydrophilicity[80]. Although CVD can produce high-quality graphene films, its significant equipment investment and complex process limit large-scale application. In contrast, the GO reduction method is simple to operate and utilizes readily available raw materials, making it more suitable for industrial production. Traditional reduction primarily relies on chemical reduction methods[81–84], which use reductants such as hydrazine, sodium borohydride as shown in Fig. 4a or thermal reduction methods[85–87], as shown in Fig. 4b, but both possess significant limitations. Chemical reduction requires highly toxic reagents, and the products are prone to aggregation with relatively low electrical conductivity. Hydrazine-based reductants are not only harmful to humans but also cause environmental pollution, while sodium borohydride ($NaBH_4$), although less toxic, exhibits poor reduction efficiency. Simultaneously, thermal reduction requires an inert atmosphere and high-temperature environment (> 800 °C), which introduces lattice defects and consumes excessive energy[88].

High-temperature treatment not only has high energy consumption but can also damage the layered structure of graphene, affecting its conductive properties. These drawbacks have prompted researchers to explore greener alternatives. Under potential control, electrochemical reduction (as shown in Fig. 5a) produces rGO (C/O ≈ 6) within 3 min[89–91], but suffers from non-uniform electrode contact[92,93]. This issue arises because the limited contact area between the electrode and the GO solution makes uniform reduction difficult, leading to inconsistent product performance. Reduction using solar irradiation (as shown in Fig. 5b) is environmentally friendly but requires 16–30 h of irradiation, with the C/O ratio generally below 4[94–96]. Although photoreduction avoids chemical reagents, its long reaction time and limited reduction degree make it difficult to meet practical application demands. In contrast, microwave reduction technology stands out due to its efficiency, energy-saving nature, and environmental friendliness, becoming a core breakthrough development in recent years. Microwave reduction utilizes molecular polarization and dielectric loss effects, enabling completion of the reduction process within minutes without requiring toxic reagents or high-temperature conditions. This method is not only simple to operate but also preserves the intact structure of graphene, yielding reduced products with excellent electrical conductivity. Furthermore, microwave reduction enables selective heating, facilitating control over the reduction degree and product morphology, thereby offering new possibilities for the functional applications of graphene.

The unique advantages of microwave reduction stem from its energy transfer mechanism. Microwaves excite dipole rotation and ion migration within GO, generating volumetric heating that induces localized ultrahigh temperatures (> 400 °C) within seconds, thereby enabling effective cleavage of oxygen groups and restoration of the carbon skeleton[97]. This distinct heating mechanism fundamentally differs from conventional thermal conduction heating; that is, it achieves selective heating at the molecular level, avoiding thermal gradient issues inherent in conventional heating methods. The rapid movement of polar molecules and ions in the microwave field not only provides efficient heating but also promotes the directed cleavage and reorganization of functional groups on the GO surface. This technology has achieved breakthroughs in three key areas. Regarding revolutionizing reaction speed, Li et al.[98] first achieved microwave thermal reduction of GO. Under 500 W irradiation for 2 s, the electrical conductivity of GO increased from 0.07 to 10^4 S/m, and the ID/IG ratio decreased from 1

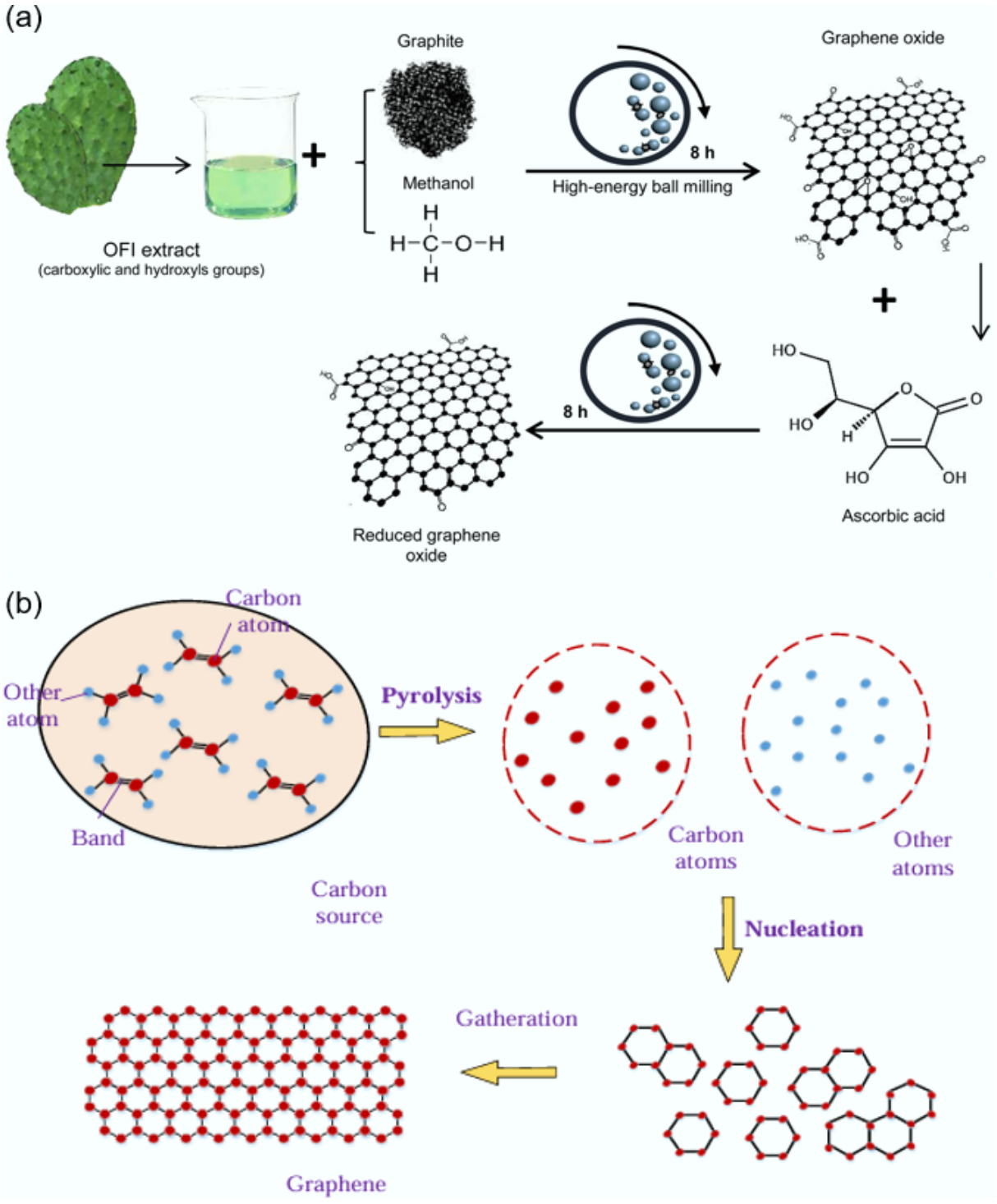

Fig. 4 Synthesis of rGO by (**a**) chemical reduction[84], and (**b**) thermal reduction[87].

to 0.3. This ultrafast reaction speed enables continuous industrial production, significantly enhancing efficiency. Voiry et al.[99] developed a gradient reduction strategy involving pre-reduction via annealing at 300 °C followed by 1,000 W microwave irradiation for 1–2 s, obtaining graphene structures similar to CVD with only 4% oxygen content, and a prominent Raman 2D band.

This step-wise approach ingeniously combines the advantages of conventional thermal reduction and microwave reduction, ensuring high product quality while improving reaction efficiency. Conventional thermal reduction requires continuous inert gas protection, whereas the microwave method can operate in air, greatly simplifying the process conditions. This feature significantly reduces equipment requirements and operational difficulty, removing barriers to industrial production. For example, Jiang et al.[100] employed a triggering-reduction method, placing pre-reduced rGO fragments on the GO surface. Irradiation at 800 W for 2–5 s achieved deep deoxygenation via arc discharge, with XPS analysis confirming the complete disappearance of C–O bonds. The instantaneous high temperature generated by this localized arc discharge enables precise control over the reduction degree, avoiding increased defects

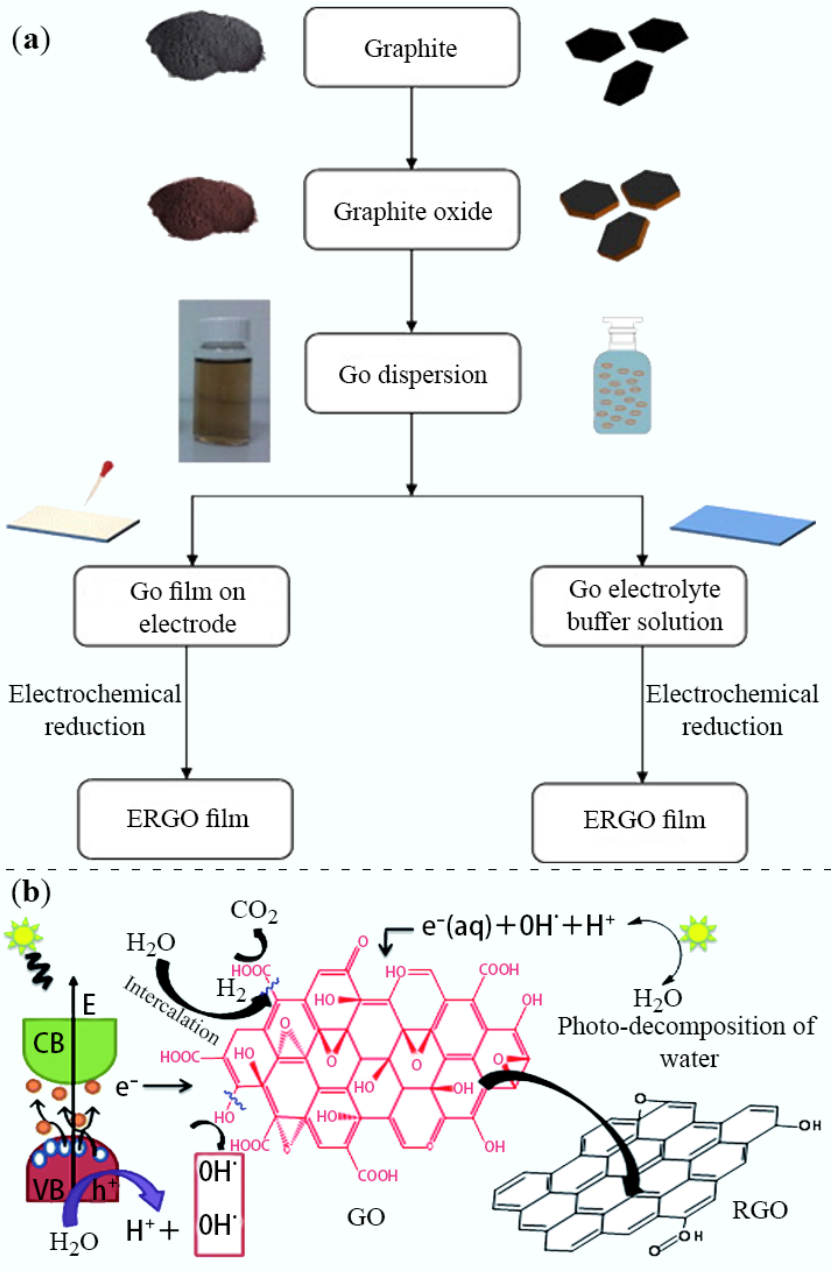

Fig. 5 Synthesis of rGO by (**a**) electrochemical reduction[89], and (**b**) sunlight reduction[94].

due to over-reduction. Wan et al.[101] used a copper wire to trigger microwave arcing, obtaining highly crystalline rGO within 2 s. This metal-assisted microwave reduction method further enhances energy utilization efficiency, making the reaction more controllable. Figure 6 illustrates the microwave-assisted thermal reduction process of GO[102]. Concerning breakthrough optimization of product quality, microwave-induced instantaneous high temperatures promote carbon atom rearrangement, significantly repairing structural defects. Han et al.[103] treated GO films with low-temperature microwave at 42 W for 5 min, reducing the ID/IG ratio from 2.89 to 1.56, and increasing the C/O ratio from 7.8 to 17.5. These gentle microwave conditions are particularly suitable for preparing thermally sensitive graphene derivatives. Jiang et al.[100] found that arc-discharge-reduced GO exhibited a sheet resistance as low as 40 μΩ/cm^2, representing a 20-fold improvement over samples thermally reduced at 800 °C (796 μΩ/cm^2). This excellent electrical conductivity gives microwave-reduced graphene a unique competitive edge in electronic devices.

Microwave synergistic strategies further enhance the reduction effect. In chemical-microwave combinations, Zedan et al.[104] achieved a higher degree of reduction using 2 min of microwave irradiation in DMSO solvent compared to 7 h of conventional thermal treatment. This approach, leveraging chemical-physical synergy, fully utilizes the dual advantages of solvent effects and microwave heating for a more thorough reduction process. Kumar et al.[105] demonstrated that HI/CH_3COOH reductants achieved deoxygenation equivalent to 48 h of conventional reaction after just 4 h of microwave treatment. This significant efficiency boost highlights the immense potential of microwave-assisted chemical reduction. Figure 7 shows the microwave-assisted chemical reduction process of GO[106]. Regarding pretreatment optimization, Voiry et al.[99] constructed a conductive network through $CaCl_2$ crosslinking and

gentle annealing significantly enhancing the microwave absorption capacity of GO at 2.45 GHz. This pretreatment method cleverly addresses the low microwave absorption efficiency caused by the low dielectric loss of GO. Concurrently, the intense degassing and high pressure generated during microwave reduction simultaneously promote the exfoliation of GO, yielding thinner rGO flakes. This self-exfoliation effect facilitates the preparation of monolayer or few-layer graphene, providing a novel approach for high-quality graphene production. The industrialization potential of this technology is already evident in multiple fields. For instance, in energy storage, microwave-reduced GO electrodes, leveraging high electrical conductivity (1,490 S/m)[107], enable supercapacitors to achieve a specific capacitance of 265.9 F/g[108]. This superior electrochemical performance is primarily attributed to the porous structure formed during microwave reduction and the retained oxygen-containing functional groups, which collectively provide more active sites and fast ion transport channels. In flexible electronics, microwave-reduced graphene films exhibit excellent mechanical flexibility and conductive stability, making them ideal materials for wearable devices. In composites, stronger interfacial interactions form between microwave-reduced GO and polymer matrices, significantly enhancing the mechanical properties and functional characteristics of the composites.

The parameters of microwave reduction starkly contrast with those of conventional methods, highlighting its superior process efficiency. Traditional thermal reduction necessitates an inert atmosphere and prolonged treatment at extreme temperatures (> 800 °C), yielding products with a high sheet resistance of 796 μΩ/cm^2. Chemical reduction employs highly toxic reagents and results in relatively low conductivity. Conversely, microwave reduction is typically performed in air without an inert gas blanket, completing the deoxygenation process within seconds (2–5 s) at moderate power levels (500–1,000 W). This ultrafast process yields reduced graphene oxide with a spectacular increase in electrical conductivity from 0.07 to 10^4 S/m and a remarkably low sheet resistance of 40 μΩ/cm^2, representing a 20-fold performance enhancement over conventional thermal reduction and underscoring the dual breakthrough of MAP in speed and product quality. Although challenges remain regarding process standardization (e.g., matching power intensity to sample volume), microwave reduction, with its core advantages of secondary reaction times, elimination of inert atmosphere requirements, and high product quality, has

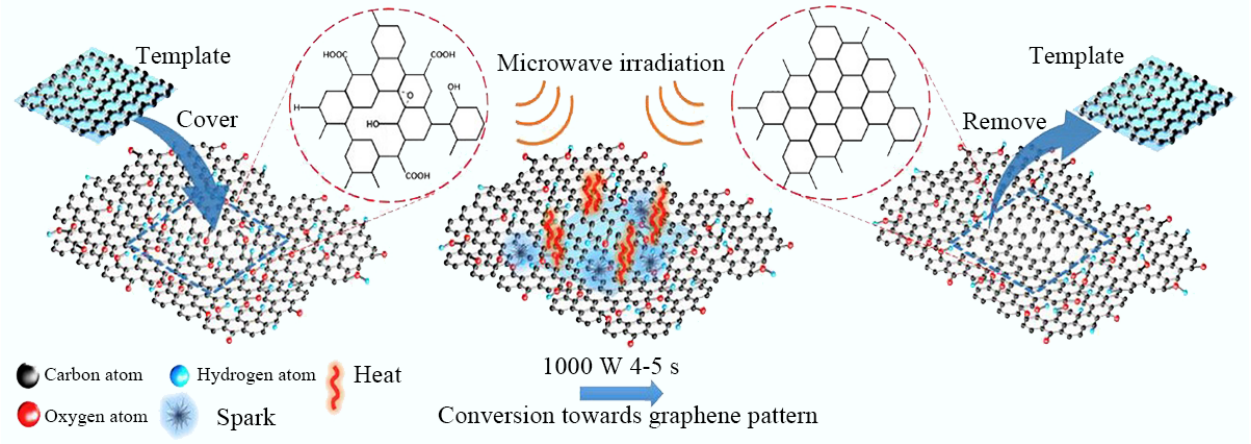

Fig. 6 Synthesis of rGO by microwave-assisted thermal reduction[102].

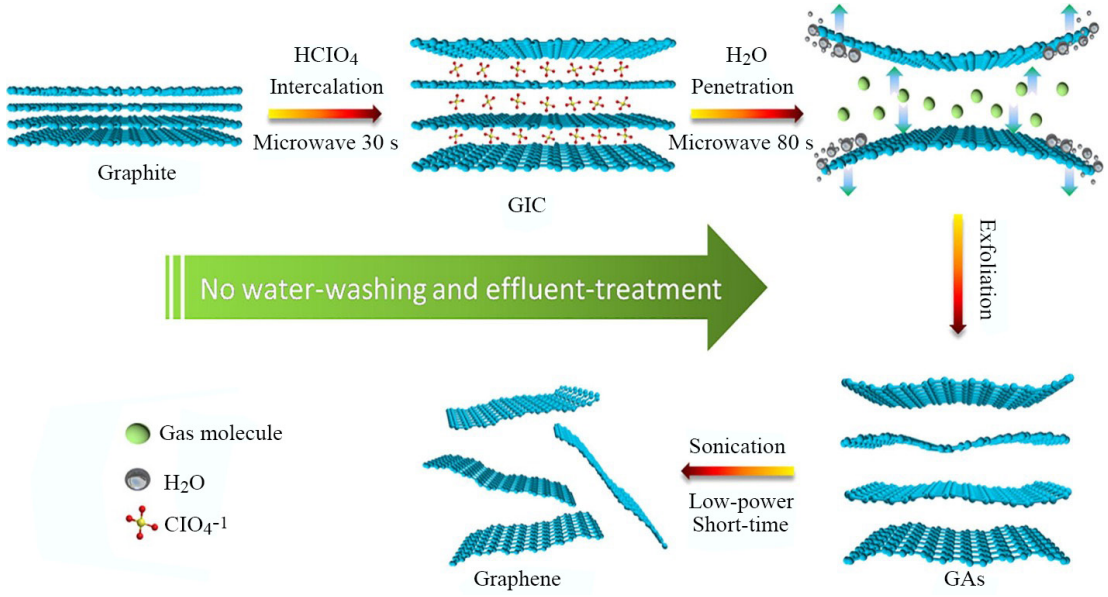

Fig. 7 Synthesis of rGO by microwave-assisted chemical reduction[106].

become a key technology driving the large-scale production of graphene. With continuous advancements in microwave engineering and optimization of process parameters, microwave reduction technology is poised for breakthrough applications in even more fields, providing strong technical support for the industrialization of graphene. Future research should focus on key issues such as the scale-up design of microwave reactors, intelligent control of process parameters, and online monitoring of product quality to propel this technology from the laboratory to industrial production.

3D carbon materials

As detailed in the preceding sections, MAP is a versatile technique for producing carbon materials across various dimensions. This section concentrates specifically on 3D carbon architectures, and is organized around their primary application domains. It aims to present a coherent narrative from material design and controlled MAP synthesis to final functional performance. While the application landscape for MAP-derived 3D carbons is broad, as previewed in Graphic abstract—encompassing promising uses in composites, construction, and catalysis—this section will maintain a focused and in-depth discussion by examining four of the most representative and high-impact areas: their use as solid fuels, for environmental remediation, as microwave absorbers, and in energy storage.

Carbon materials with high heating value (HHV)

With the advancement of the dual carbon goals, biomass energy, as the largest component of clean energy (with a capacity equivalent to twice that of hydropower and 3.5 times that of wind power), holds strategic significance for adjusting the energy structure through efficient conversion. Agricultural and forestry residues, as the primary biomass resource (annual production of 740 million tons in China with a calorific value equivalent to 460 million tons of standard coal), can be converted into high-calorific-value biochar through thermochemical conversion, serving as a low-carbon solid fuel alternative to fossil fuels[109,110]. This material is characterized by a low H/C ratio (0.2–1.6) and O/C ratio (0.2–0.8). Their coal-like properties originate from the significant reduction of oxygen-containing functional groups (such as O–H and C–O–C bonds) caused by deoxygenation and dehydration reactions during pyrolysis, thereby enhancing hydrophobicity and energy density[111]. The preparation process of biochar directly affects its physicochemical properties and application performance, among which pyrolysis temperature, heating rate, and residence time are key parameters determining the pore structure, surface functional group distribution, and stability of biochar. Studies show that appropriate pyrolysis conditions can promote the formation of a highly developed pore structure in biochar. This not only improves its combustion efficiency as a fuel but also enables it to demonstrate multiple application values in areas such as soil improvement and pollutant adsorption. Furthermore, the carbon sequestration capacity of biochar makes it an important technical pathway for achieving negative carbon emissions. Each ton of biochar can sequester approximately 2–3 tons of CO_2 equivalent, which is of great significance for achieving carbon neutrality goals.

Traditional pyrolysis technologies like torrefaction and hydrothermal carbonization exhibit significant limitations[112]. Torrefaction primarily reduces the content of O–H functional groups through dehydration reactions in an inert atmosphere at 200–300 °C. However, its thermodynamic behavior is complex as it exhibits endothermic characteristics below 230 °C while transitioning to exothermic above 230 °C, which creates challenges for effective energy consumption control[113,114]. Hydrothermal carbonization occurs in subcritical water at 180–260 °C, relying on high-pressure conditions (2–20 MPa) to promote cellulose hydrolysis and lignin repolymerization[115,116]. However, the long residence time (hours to days), and high-pressure requirements substantially increase process costs[117,118]. Additionally, both methods rely on external heat conduction, generating inward temperature gradients that oppose volatile diffusion, leading to low thermal efficiency and poor product uniformity. These traditional methods also face difficulties in precisely regulating product performance, making it challenging to control the pore structure and surface chemistry of biochar according to different application needs. For example, biochar produced by traditional pyrolysis methods often suffers from uneven pore size distribution and insufficient active sites, limiting its performance in advanced applications. Simultaneously, traditional processes have poor adaptability to feedstocks, struggling to handle agricultural and forestry residues with high moisture content or strong heterogeneity, which is also a major factor constraining the large-scale production of biochar. MAP overcomes these bottlenecks through an endogenous heating mechanism. Microwaves (300 MHz to 300 GHz) generate heat through polar molecule collisions, establishing an inward-to-outward temperature gradient aligned with the direction of volatile migration, enabling rapid (heating rates 3–5 times higher than conventional methods[119]), uniform (temperature fluctuation < 5%[120]), and selective heating. Their penetration capability ensures processing ability for various material forms[121]. Feedstocks with weak microwave absorption can be enhanced by adding absorbers like silicon carbide or activated carbon[122]. Once effective coupling is achieved, products are typically optimized by regulating power, temperature, and duration in an inert atmosphere[123,124]. As shown in Fig. 8, compared to conventional methods, microwave biochar exhibits significantly higher yield and calorific value[133], with lignocellulosic-derived biochar being more suitable as a solid fuel[111].

Another advantage of MAP lies in its excellent process controllability. By adjusting parameters such as microwave frequency, power, and time, the pyrolysis depth and product characteristics can be precisely controlled. This controllability allows MAP to be optimized for different feedstock characteristics (e.g., moisture content, particle size, and chemical composition) to obtain biochar products with specific functionalities. For instance, by regulating microwave treatment conditions, activated carbon materials with ultra-high SSA or functionalized biochar rich in specific functional groups can be prepared. Furthermore, microwave systems feature rapid start-stop capability, enabling batch production, which significantly enhances production flexibility and energy utilization efficiency. From an engineering application perspective, MAP equipment has a small footprint, is easy to automate, and facilitates the establishment of distributed biochar production systems. This is of great importance for the *in-situ* conversion and utilization of agricultural and forestry residues. With advancements in microwave generator technology and reduced costs for scaled-up production, MAP technology is poised to become the mainstream process route for the industrial production of biochar.

Critically, pyrolysis temperature is the core parameter controlling biochar properties. As shown in Table 2, biochar yield typically decreases within the 350–550 °C range[151–153], which is attributed to the enhanced secondary cracking of volatiles and cleavage of C–H/C–O bonds at high temperatures. This cracking process follows a free radical reaction mechanism. As temperature increases, the weaker chemical bonds in biomass macromolecular structures preferentially break, generating small-molecule volatiles and active free radicals. These radicals further participate in recombination reactions to form more stable aromatic structures. Conversely, the

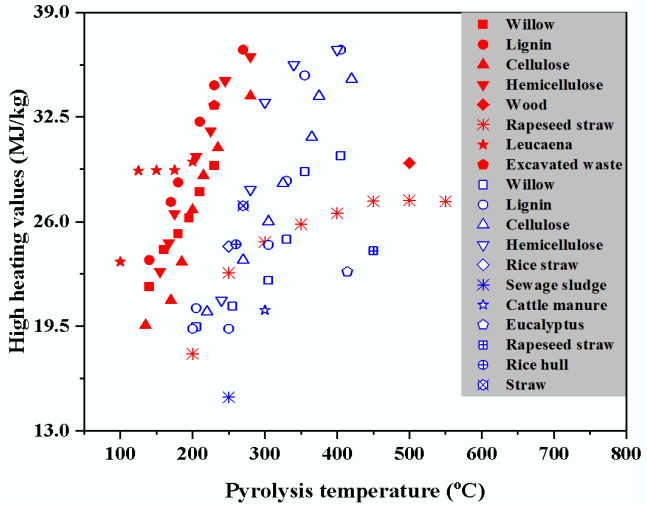

Fig. 8 Comparison of high heating value of biochar produced from feedstocks under different pyrolysis temperatures. The red symbols are data obtained from microwave pyrolysis, and blue symbols are from conventional pyrolysis. Data has been surveyed from previous studies[125–132].

HHV of biochar increases significantly with rising temperature. This phenomenon stems from carbon fixation, where high temperatures drive the release of H and O in the form of H_2O and CO_2, thereby enriching the carbon content[123]. Notably, the temperature gradient also influences the development of biochar pore structure. The medium-temperature zone (400–500 °C) favors micropore formation, while the high-temperature zone (> 600 °C) promotes the development of mesopores and macropores. This evolution of pore structure directly impacts the performance of biochar as an adsorbent or catalyst support. Furthermore, pyrolysis temperature regulates the distribution of surface functional groups on biochar. Low-temperature biochar retains more oxygen-containing functional groups (such as carboxyl and phenolic hydroxyl groups), whereas high-temperature biochar is dominated by aromatic carbon structures. This difference in surface chemistry determines its varied performance in applications like soil remediation and pollutant removal.

Microwave power significantly regulates product distribution. Increasing power generally reduces yield, but exhibits feedstock-dependent fluctuations, as the cellulose-to-lignin ratio affects microwave energy conversion efficiency[154]. Cellulose, due to its higher dielectric loss factor, is more easily heated in the microwave field, while lignin requires a higher field strength for effective energy coupling. This difference leads to significant variations in the response of different feedstocks to microwave power. Pine wood yield shows a trend of first decreasing and then increasing during 600–1,500 W[155], which may be related to localized high-temperature zones (hotspots)[156]. Microwave power exerts a positive influence on HHV[144,157]. The inhomogeneous distribution of hotspots within the microwave field may affect the HHV trend. For instance, localized overheating at high power might compromise the stability of the carbon skeleton[158]. Energy utilization efficiency requires balancing power and yield. For example, peanut shells reach an ERE of 97.96% at 350 W (with maximum yield of 86 wt%)[123], whereas at 900 W, despite the increased HHV, yield drops to 45.37%, leading to a significant decline in ERE. High power may also promote H_2 production (with selectivity up to 50.22 vol%) at the expense of liquid products. Therefore, power optimization is necessary based on feedstock properties and target products. Studies further indicate that microwave density and specific energy input (microwave power and total energy per unit mass) are key parameters regulating pyrolysis efficiency[159], but the interaction mechanism between the two requires in-depth investigation. Spatiotemporal control of microwave power is also crucial. Employing pulsed microwave irradiation or gradient power adjustment can avoid localized overheating while improving energy utilization efficiency. Additionally, the addition of microwave absorbers (such as activated carbon or silicon carbide) can enhance the energy coupling efficiency of feedstocks with low dielectric loss. This auxiliary strategy holds significant application value in industrial scale-up processes.

Notably, residence time control exhibits feedstock specificity. Residence time effects are feedstock-specific[145,160], influencing yield, carbon content, and HHV, as detailed in Table 2. This difference primarily stems from the distinct pyrolysis behaviors of feedstock components. Cellulose-rich materials preferentially undergo carbonization reactions during prolonged pyrolysis, with their degradation following first-order reaction kinetics and extending residence time facilitates more complete reaction progression. Conversely, ash-rich feedstocks (such as sewage sludge) may experience rapid pyrolysis due to catalytic effects from mineral components. Furthermore, excessively long residence time conversely exacerbates degradation of the carbon framework. The common pattern is that extending residence time significantly increases carbon content (69.4–77.4 wt%) and HHV (27.17–31.02 MJ/kg), which results from continuous devolatilization and aromatization. However, energy efficiency exhibits a decreasing trend[161]. When the residence time for peanut shells is extended from 10 to 30 min, HHV increases from 23.48 to 31.02 MJ/kg, but the decline in yield reduces the total energy output, causing ERE to drop from 96.45%

Table 2 Yields and HHVs of biochars obtained under different microwave pyrolysis conditions

Feedstock	Pyrolysis condition	Yield (wt%)	HHV (MJ/kg)	Ref.
Algae	400–600 °C	10.8–13.4	18.6–21.7	[134]
Canola straw	300–500 °C	29.8–41.9	22.3–24.5	[135]
Corn stalk	400–600 °C	24.8–36.4	18.3–22.1	[134]
Corn stover	500–900 °C	28.0–40.0	18.1–29.8	[136]
Manure pellet	300–500 °C	66.7–76.4	4.1–4.7	[135]
Palm kernel shell	500–700 °C	33.0–38.0	23.0–26.0	[137]
Pigeonpea stalk	500 °C	31.0	30.7	[138]
Pinewood	400–600 °C	19.3–33.1	23.2–27.3	[134]
Saccharum bagasse and Waste cooking oil	200–300 °C	59.6–86.7	16.1–24.5	[139]
Sawdust	300–500 °C	24.7–45.3	25.9–32.3	[135]
Sewage sludge	450–600 °C	33.0–62.3	6.5–8.7	[140]
Waste oily sludge	250–650 °C	70.0–70.4	15.4–16.2	[141]
Wheat straw	300–500 °C	31.0–43.3	25.6–26.9	[135]
Cassava stem	550–750 W	70.0–77.0	19.2–20.6	[142]
Corn stalk	900–1,500 W	30.9–41.1	23.0–31.7	[143]
Indian coal	420–560 W	61.9–69.6	15.3–16.8	[144]
Indian coal and rice husk	420–560 W	45.7–61.2	12.0–14.6	[144]
Palm kernel shell	500–700 W	79.0–86.0	23.5–28.4	[145]
Rice husk	420–560 W	34.8–38.3	12.1–12.6	[144]
Wood pellets	2,000–3,000 W	26.2–32.4	30.6–31.8	[146]
Chlorella sp.	15–60 min	50.1–66.7	25.4–27.3	[147]
Chlorella vulgaris	15–25 min	35.4–44.8	23.1–26.2	[148]
Nannochloropsis oceanica	15–60 min	49.6–75.1	23.8–26.4	[147]
Sewage sludge	5–15 min	70.0–87.0	27.2–28.4	[145]
Sewage sludge	30–60 min	30.2–56.5	13.6–16.8	[149]
Sugarcane bagasse	20–30 min	30.1–60.4	19.9–24.7	[150]
Waste oily sludge	60–120 min	68.6–70.8	15.3–16.0	[141]

to 79.49%[123]. The rise in the C/H ratio (palm kernel shells increase from 1.25 to 1.43[160]) further corroborates the positive correlation between the degree of aromatization and energy density. Residence time also affects the electrical conductivity of biochar. Appropriately extending the treatment duration facilitates the growth and oriented arrangement of graphitic microcrystals, which is significant for preparing electrode materials. In practical operation, determining the optimal residence time requires careful consideration of feedstock characteristics, equipment energy consumption, and product quality requirements. For continuous microwave systems, precise control of residence time can be achieved by adjusting the material conveying speed. Such process optimization is a key factor in enhancing the economic efficiency of industrialized production.

Carbon materials for environmental remediation

Biochar with abundant porous structures has emerged as a multidisciplinary scientific and engineering research focus, owing to its multifunctional capabilities in carbon sequestration and emission reduction (CO_2 adsorption, Fig. 9a[162]), air purification (Volatile Organic Compounds (VOCs) adsorption, Fig. 9b[163]), pollution remediation (heavy metal ion removal in wastewater, Fig. 10a[164]), agricultural enhancement (soil fertility improvement, Fig. 10b[165]), industrial catalysis (catalyst support, Fig. 11a[166]), and construction applications (carbon sequestration implementation, Fig. 11b[167]). The pore structure of biochar exhibits significant correlations with its environmental functionalities. This correlation manifests through three key aspects: (1) microporous structure (< 2 nm) enhances gas adsorption via quantum confinement; (2) mesopores (2–50 nm) facilitate pollutant diffusion as transport channels; and (3) macropores (> 50 nm) provide microbial/catalytic reaction spaces. For instance, in CO_2 adsorption processes, strong van der Waals forces generated by micropores enable efficient capture at low temperatures, while mesopores ensure rapid gas mass transfer. Similarly, heavy metal ion removal relies on complexation with oxygen-containing functional groups on mesopore surfaces, whereas VOCs adsorption benefits from physical entrapment effects in hydrophobic macroporous structures. This hierarchical pore synergy makes biochar an ideal material for environmental remediation, though CP techniques struggle to precisely control pore hierarchical structures.

Pore structure constitutes a fundamental basis for its environmental functionalities. Among various biochar preparation methods, MAP is regarded as an exceptionally promising technology due to its unique advantage in constructing high SSA and well-developed pore structures. Compared to CP, MAP utilizes interactions between electromagnetic fields and material dipoles to achieve rapid and uniform volumetric heating. This heating mechanism generates internal heat sources through dipole rotation of polar molecules (e.g., water, lignin), avoiding temperature gradient issues caused by traditional external heating.

Fig. 9 (**a**) Schematic diagram of bamboo biochar modification for capturing CO_2 by lignin impregnation method and microwave irradiation method[162]. (**b**) Schematic diagram of the preparation of wheat straw-based microwave biochar catalyzed by granular activated carbon for adsorbing volatile organic compounds[163].

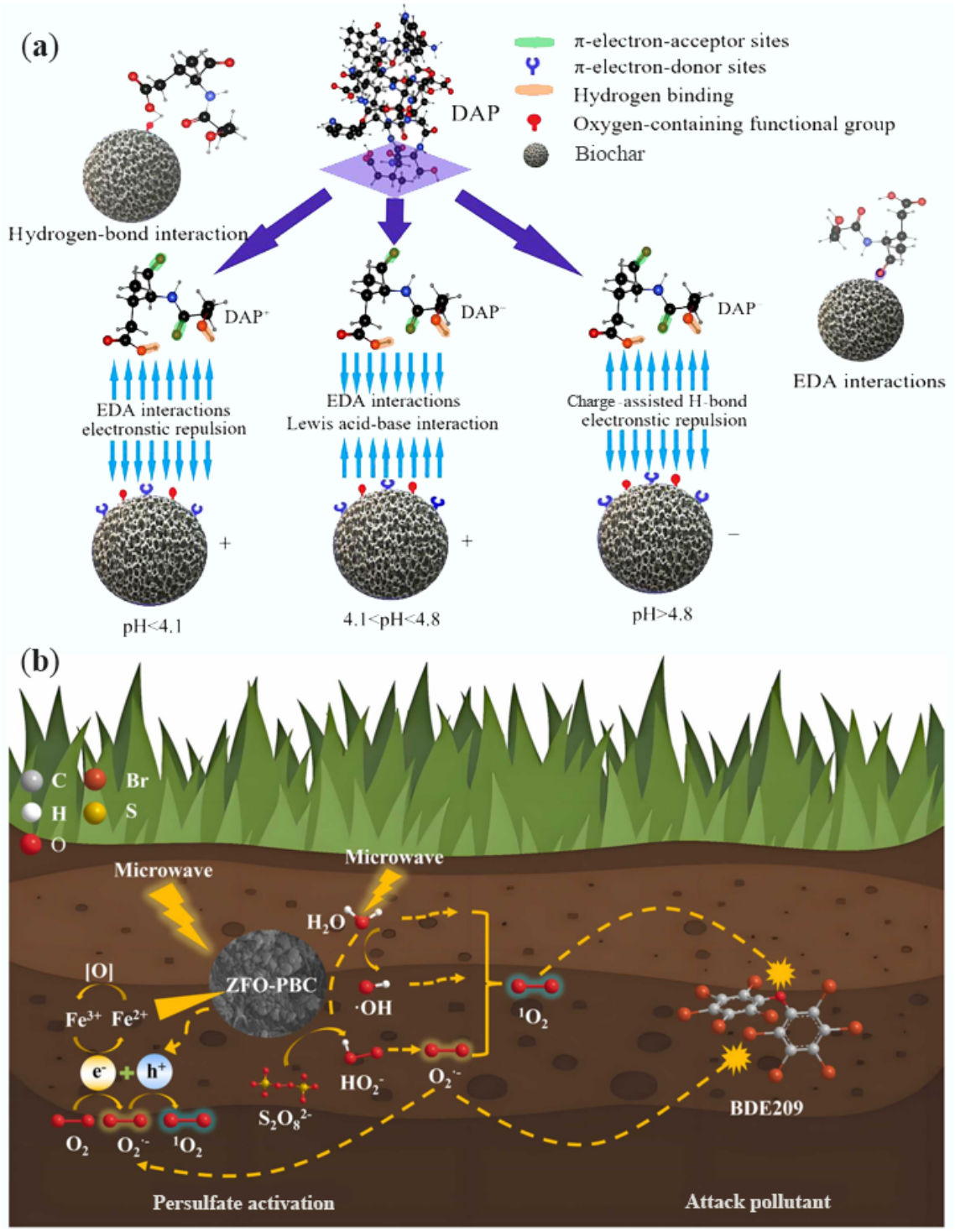

Fig. 10 (**a**) Mechanism of biochar adsorbing daptomycin[164]. (**b**) Mechanisms of persulfate system activation by the $ZnFe_2O_4$/phosphoric acid-modified architectural biochar/persulfate system[165].

Dynamic coupling between electromagnetic fields and biomass components also induces dielectric loss and space charge polarization, collectively promoting directional pore development. As shown in Fig. 12, specifically, cellulose undergoes selective depolymerization in microwave fields, forming regular microporous arrays. The thermoplastic behavior of lignin under alternating electric fields produces mesoporous templates while electromagnetic induction heating of ash minerals catalyzes macroporous structure formation. This not only significantly reduces energy consumption and shortens reaction time (e.g., from several hours to tens of minutes), but also provides more flexible pore regulation capabilities.

Studies demonstrate that biochar produced via MAP generally exhibits higher SSA and larger pore volume (PV), as shown in Fig. 13. For example, Huang et al.[177] prepared biochar through MAP of rice straw, achieving uniform pore size distribution and high SSA,

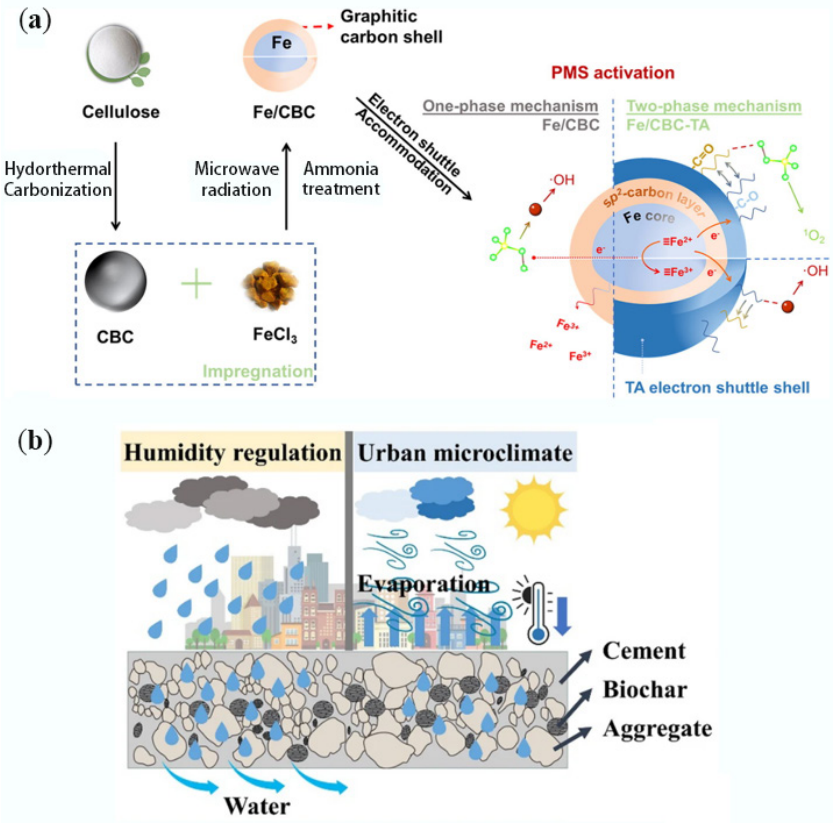

Fig. 11 (**a**) Schematic diagram of the catalytic mechanism of metal-biochar composites[166]. (**b**) Environmental and technical advantages of biochar composites: humidity regulation and urban microclimate[167].

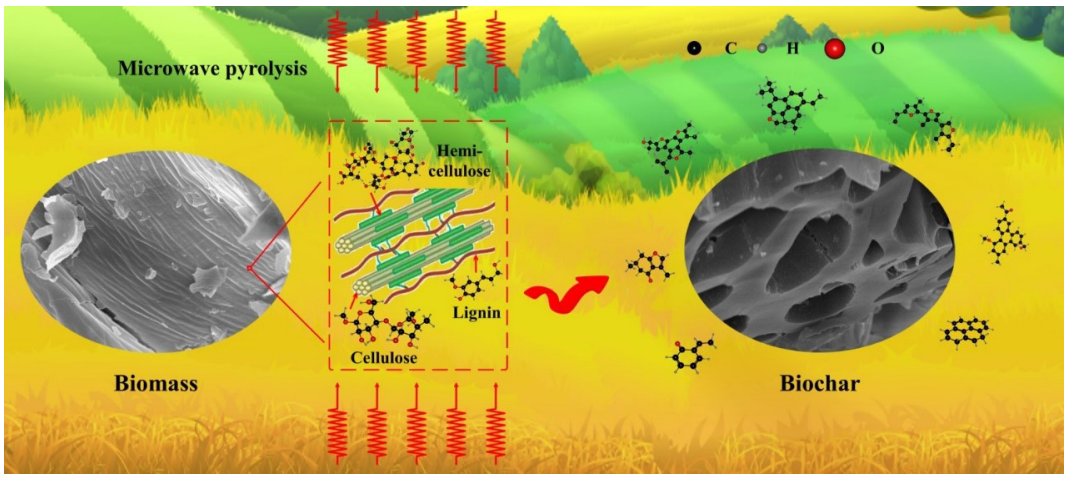

Fig. 12 Schematic diagram of biochar pore-forming mechanism[168].

attributed to microwave-induced directional cleavage of cellulose crystals and lignin melt reorganization. Its CO_2 adsorption capacity (80 mg/g) significantly outperformed conventional products, because microwave-specific hotspot effects promote the formation of ultra-micropore networks (< 0.7 nm) within biomass, perfectly matching the kinetic diameter of CO_2 (0.33 nm). Lin et al.[178] employed microwave-ferric chloride chemical activation to prepare hydrophobic porous biochar, discovering that ferric chloride forms nanoscale iron oxide clusters in microwave fields, acting as porogens to etch three-dimensional interconnected channels. With a heating time of merely 15 min (vs 120 min for conventional methods), SSA reached 455.90 m^2/g (vs 288.60 m^2/g for traditional method). This efficiency enhancement stems from non-thermal effects of microwaves on chemical activators, that is, electromagnetic oscillations accelerate Fe^{3+} to Fe^{2+} reduction, intensifying etching reaction kinetics. Adsorption capacities for benzene and toluene reached 136.60 and 94.60 mg/g, respectively, directly correlating with the volumetric proportion of 1–3 nm mesopores in the material. Microwave-specific selective heating enables lignin-derived carbon to form π-π conjugated structures, significantly enhancing affinity for aromatic compounds.

The advantages of MAP are also reflected in product characteristics. Brickler et al.[179] comparatively demonstrated that microwave-pyrolyzed biochars from switchgrass, biosolids, and water oak leaves

exhibit higher thermal stability, greater yield, and more diverse surface functional groups than conventional slow pyrolysis products. This discrepancy originates from non-thermal effects of microwave fields, where alternating electromagnetic forces directly act on molecular bonds, which induce selective cleavage of C=O and C–O–C bonds while simultaneously preserving thermally stable aromatic ring structures. Their nitrate-nitrogen (NO_3–N) adsorption capacity (13.30 mg/g) substantially exceeded that of slow-pyrolysis char (3.10 mg/g), attributable to microwave-induced nitrogen doping effects generating pyridinic-N and pyrrolic-N active sites within the carbon matrix. Furthermore, interfacial polarization effects generated during MAP facilitate the formation of abundant active sites within the material. This polarization induces localized charge separation at carbon layer edges, exposing coordinatively unsaturated carbon atoms. These sites significantly enhance adsorption performance by forming strong chemical bonds through electron cloud overlap with heavy metal ions. For instance, the Cr(VI) adsorption capacity (9.92 mg/g) of modified reed residue biochar prepared by Song et al.[180] was ascribed to Fenton-like reactive sites generated at microwave-activated Fe_3O_4/carbon interfaces. Wheat straw biochar pyrolyzed by Qi et al.[181] at 500 W microwave power exhibited Pb^{2+}, Cd^{2+}, and Cu^{2+} adsorption capacities of 139.44, 52.92, and 31.25 mg/g, respectively. This selective adsorption correlates with microwave-regulated sulfur doping levels—higher power promotes conversion of sulfur-containing groups in biomass into thiophenic-S, which demonstrates particular affinity for soft acid metals (Pb^{2+}). These results comprehensively illustrate that MAP constitutes an efficient and energy-saving advanced preparation method, with its core advantage residing in non-thermal interactions between electromagnetic fields and biomass components. These interactions effectively regulate biochar's pore structure and surface properties, thereby enhancing environmental application performance. Tailoring and optimizing pyrolysis operating conditions (such as pyrolysis temperature, microwave power, and residence time) according to specific biochar application scenarios is crucial for improving product quality and yield. For gas adsorption applications, a stepwise heating strategy should be employed where initial low temperatures (200–300 °C) help preserve oxygen-containing functional groups while subsequent high temperatures (600–700 °C) are crucial for developing microporous structures. Conversely, biochar intended for water treatment requires controlling microwave power within the 400–600 W range to balance meso-porosity with surface functional group density. Next, we will analyze the influences of pyrolysis temperature, microwave power, and residence time on biochar pore structure, with particular focus on structure-activity relationships between electromagnetic parameters and pore evolution.

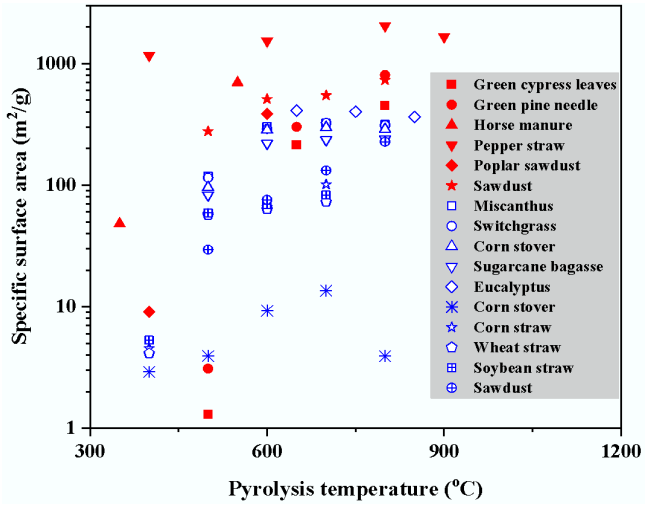

Fig. 13 Comparison of SSA of biochar produced from feedstocks under different pyrolysis temperatures. The red symbols are data obtained from microwave pyrolysis, and blue symbols are from conventional pyrolysis. Data has been surveyed from previous research[153,169–176].

It is worth emphasizing that the high SSA and PV values achieved via MAP, as compiled in Table 3, often surpass those attainable by CP or are achieved in a fraction of the time. For instance, achieving a comparable SSA to the pepper straw biochar (SSA > 2,000 m^2/g)[174] via CP would typically require much longer processing times and higher cumulative energy input. This direct comparison underscores MAP's superior efficiency in pore structure development. The pivotal role of pyrolysis temperature in pore structure evolution is evident from the data compiled in Table 3, which shows a marked increase in SSA and PV with temperature across various feedstocks[201–203]. During the low-temperature phase (200–400 °C), cellulose undergoes dehydration to form reactive intermediates that subsequently act as seeds for pore formation as temperatures rise, while hemicellulose undergoes rapid decomposition, with its degradation products forming initial pore networks within the material. When temperatures exceed 500 °C, lignin initiates complex molecular rearrangement and aromatization reactions. This process involves the conversion of sp^3-hybridized carbon to sp^2-hybridized carbon, generating a highly cross-linked porous carbon skeleton[204].

Continuous volatiles release and carbon structure reorganization collectively promote pore formation, particularly within the 500–700 °C range where aliphatic compounds and partial aromatic structures in biomass undergo cleavage, generating abundant micropores. Crucially, high-temperature treatment (> 700 °C) significantly alters biochar's microstructural characteristics through dual effects. First, disordered structures between carbon layers gradually transform into ordered microcrystalline arrangements, generating numerous uniform micropores through graphitization. Second, decomposition and gasification reactions of mineral components (e.g., K, Ca) ($C + CO_2 \rightarrow 2CO$) not only further enlarge pore dimensions but also leave unique mineral-templated pores within the carbon matrix[204]. These mineral-templated pores typically exhibit specific geometries and surface chemistries, providing additional adsorption active sites. Notably, MAP ensures more uniform temperature distribution due to its unique volumetric heating characteristics[205]. This uniformity enables synchronous pyrolysis throughout the biomass bulk, avoiding common issues in CP such as localized overheating and pore collapse. Simultaneously, the rapid heating feature of microwaves[25] effectively reduces tar deposition by shortening the residence time of tar precursors in intermediate temperature ranges, thereby better preserving pore structural integrity. Notably, exceptional pore performance (SSA > 2,000 m^2/g) can be achieved, as demonstrated by pepper straw biochar at 900 °C. This exceptional performance stems from sufficient graphitization of the carbon skeleton under high temperatures combined with microwave-induced uniform pore development. These results confirm the synergistic effect between high-temperature treatment and microwave technology, where high temperatures promote comprehensive carbon skeleton development and microwave heating simultaneously optimizes pore structure uniformity and accessibility through its unique non-thermal effects. The spatiotemporal distribution characteristics of temperature during MAP contribute distinctively to final pore structure formation.

Unlike conventional external heating, microwave heating achieves energy transfer through direct coupling between

Table 3 SSAs and PVs of biochars obtained under different microwave pyrolysis conditions

Feedstock	Pyrolysis condition	SSA (m^2/g)	PV (cm^3/g)	Ref.
Biosolids	400–800 °C	54.60–148.71	0.119–0.150	[182]
Corn stalk	700–900 °C	26.52–323.33	0.041–0.196	[168]
Green cypress leaves	500–800 °C	1.30–452.10	0.060–0.338	[173]
Green pine needle	500–800 °C	3.10–805.90	0.181–0.475	[173]
Horse manure	350–550 °C	48.30–698.40	0.047–0.302	[153]
Peanut shell	700–950 °C	10.76–67.29	0.011–0.084	[168]
Pepper straw	400–900 °C	1,162.68–2,038.61	0.470–0.870	[174]
Poplar sawdust	400–600 °C	9.10–385.00	0.040–0.200	[175]
Poplar wood chip	450–650 °C	47.43–71.30		[183]
Rice husk	700–900 °C	21.67–237.81	0.025–0.168	[168]
Sawdust	500–800 °C	276.30–729.20	0.126–0.361	[176]
Sludge	400–600 °C	12.58–99.07	0.037–0.182	[184]
Sludge + cotton stalk	400–600 °C	8.19–57.40	0.024–0.103	[184]
Solid digestate	300–500 °C	37.50–207.50	0.082–0.224	[185]
Sugar cane bagasse	350–550 °C	3.11–25.14	0.003–0.020	[186]
Waste crustaceous shell	400–800 °C	164.00–258.00	0.076–0.119	[187]
Activated sludge	400–1,000 W	167.00–323.00		[188]
Corn stalk	100–600 W	0.68–325.23	0.012–0.127	[111]
Corn stalk	400–600 W	97.22–296.76	0.096–0.202	[168]
Corn stover	500–1,800 W	0.59–43.18	0.003–0.017	[189]
Cow dung	300–1,000 W	50.58–126.99	0.045–0.119	[190]
Cow dung	300–1,000 W	18.13–113.81	0.000–0.082	[190]
Hemp stem	500–1,800 W	1.15–69.38	0.003–0.019	[189]
Palm kernel shell	550–750 W	100.00–270.00	0.030–0.110	[191]
Peanut shell	400–600 W	11.37–35.66	0.011–0.041	[168]
Rice husk	300–1,000 W	1.36–172.04	0.003–0.123	[192]
Rice husk	400–600 W	52.33–182.80	0.054–0.122	[168]
Rice straw	150–250 W	31.60–122.20	0.034–0.083	[177]
Waste bamboo chopsticks	200–450 W	166.00–414.00	0.008–0.120	[193]
Wheat straw	100–600 W	1.22–312.62	0.020–0.162	[163]
Wheat straw	100–600 W	13.47–190.35	0.002–0.131	[194]
Young durian fruit	450–800 W	6.66–19.33	0.017–0.038	[195]
Activated sludge	3–10 min	176.00–310.00		[188]
Biosolids	10–30 min	39.67–148.81	0.102–0.169	[182]
Canola seed	4–10 min	8.00–97.00		[196]
Corn stalk	60–180 min	28.31–268.78	0.070–0.188	[168]
Cow dung	5–20 min	2.22–50.58	0.000–0.045	[190]
Cow dung	5–20 min	71.51–113.81	0.067–0.082	[190]
Cow dung	5–20 min	74.10–95.50	0.065–0.081	[190]
Enteromorpha	10–30 min	473.44–693.65		[197]
Enteromorpha	10–30 min	995.69–1,403.83		[197]
Municipal sewage sludge	90–150 min	47.99–51.70		[160]
Peanut shell	60–180 min	4.68–26.70	0.008–0.030	[168]
Pulp and paper mill sludge	60–120 min	398.00–570.00		[198]
Reed canary grass	7–28 min	457.00–517.00		[199]
Rice husk	5–15 min	63.43–172.04	0.052–0.123	[192]
Rice husk	60–180 min	22.32–190.47	0.024–0.160	[168]
Spent brewery grain	20–30 min	1,011.00–1,072.00		[200]
Wheat straw	3–15 min	254.00–312.62		[163]

electromagnetic fields and polar molecules in biomass. This unique inside-out thermal gradient (as opposed to conventional heating), previously discussed, effectively prevents pore blockage and facilitates volatile escape. During heating, the differential coupling effects between microwave fields and biomass components (cellulose, hemicellulose, lignin) induce selective heating where strongly polar components (e.g., water, certain oxygen-containing functional groups) preferentially absorb microwave energy, which creates localized superheated regions that subsequently become pore-forming hotspots. When temperatures reach a critical point (~300 °C), biomass undergoes a fundamental transition in dielectric properties from insulator to semiconductor, significantly enhancing microwave absorption efficiency and accelerating pore development[205]. Particularly noteworthy is the microwave regulation of free radical reactions during carbonization where alternating electromagnetic fields promote directional movement and ordered recombination of free radicals, which ultimately lead to the formation of more regular pore structures. At high-temperature stages (> 700 °C), microwave penetration depth decreases, but the established conductive carbon network maintains high temperatures through resistive heating, ensuring final pore structure formation. Compared to CP, another advantage of MAP lies in its unique influence on mineral component behavior. That is, under alternating electromagnetic fields, metal mineral particles (e.g., K, Ca compounds) generate eddy currents, and their local heating accelerates the decomposition and volatilization of minerals, leaving more uniformly distributed mineral-templated pores in the carbon matrix[204]. Furthermore, plasma effects generated during MAP (especially at high temperatures) can further activate carbon surfaces, creating additional surface defects and edge sites that serve as both potential adsorption centers and anchor points for subsequent chemical modifications. Collectively, these characteristics endow microwave-pyrolyzed biochar with not only higher SSA and PV but also optimized pore size distribution and superior pore connectivity. These structural features directly determine performance in environmental applications. Therefore, precise control of pyrolysis temperature coupled with microwave heating advantages enables accurate regulation of biochar pore structure to meet specific material performance requirements across diverse application scenarios.

Microwave power plays a key regulatory role in the formation of biochar pore structure during MAP. Research has demonstrated that with variations in microwave power, the SSA and PV of biochar typically follow two distinct trends, either showing a monotonic decrease or exhibiting an initial increase followed by a decrease[159,206]. This difference primarily stems from the direct influence of microwave power on heating rate, which determines the efficiency of electromagnetic energy conversion into thermal energy by biomass and microwave absorbers[207,208]. Under lower power conditions, the interaction between microwaves and the material is weak, making it difficult to initiate significant molecular dissociation. When power is increased, enhanced electromagnetic energy input accelerates the dipole polarization rate of polar molecules within the biomass (such as water molecules and oxygen-containing functional groups), achieving a rapid temperature rise (up to 500 °C/min). This sharp temperature increase may skip certain low-temperature carbonization stages (such as the progressive deoxygenation process of lignin), forcing components like cellulose and hemicellulose to decompose violently within a shorter time. This promotes rapid escape of volatiles, reduces the formation of intermediate products like macromolecular tar, thereby avoiding pore clogging and facilitating direct micropore formation. Increasing microwave power also intensifies the endothermic differences among various components within the biomass, leading to localized thermal stress concentration. This stress prompts the carbon matrix to develop microcracks, forming an additional pore network. Notably, polar components in biomass, such as moisture and ash (containing metal salts), exhibit stronger microwave absorption capabilities. Under high-power conditions, these components are preferentially heated to high temperatures, triggering actions

such as steam activation and mineral-catalyzed gasification. Rapid vaporization of moisture generates high-pressure steam, physically stripping carbon layers to form meso/macroporous structures. Meanwhile, metals like K and Ca in the ash catalyze the gasification reaction of the carbon skeleton with CO_2 or steam ($C + H_2O \rightarrow CO + H_2$) at high temperatures, further enlarging pore size and generating new micropores[156]. Unlike conventional external heating methods, microwaves enable volumetric heating of materials. The enhanced microwave penetration capability under high power (related to frequency and material dielectric constant) allows larger volumes of biomass to be heated simultaneously, reducing temperature gradients. This avoids premature formation of an external carbonization layer that impedes internal volatile release, thereby significantly improving the uniformity of pore distribution. However, when microwave power exceeds a specific threshold (typically positively correlated with material dielectric loss), it may cause hotspot effects (localized overheating)[156,158]. On one hand, if the pyrolysis zone temperature reaches conditions for secondary cracking of tar (> 500 °C), residual tar is cracked into small-molecule gases (e.g., CH_4 and H_2), reducing pore blockage and further increasing SSA. On the other hand, excessive graphitization or melting may cause partial micropore merging or pore structure collapse, consequently reducing SSA. Therefore, preparing porous biochar via MAP requires optimization of power parameters. For the production of 3D porous carbon materials, MAP's efficiency and efficacy in pore structure development far surpass those of CP. Conventional pyrolysis requires up to 120 min to produce biochar with a specific surface area of 288.60 m^2/g, whereas MAP achieves a superior SSA of 455.90 m^2/g in a mere 15 min—an eightfold increase in efficiency accompanied by a nearly 60% larger surface area. In terms of energy consumption, MAP's volumetric heating and selective interaction with polar molecules lower the pyrolysis temperature range from the conventional 300–500 °C to 250–300 °C, increase heating rates to > 100 °C/min (3–5 times faster), and reduce activation energy by 40–150 kJ/mol. This faster, better, and cheaper characteristic, combined with its precise pore-tuning capability, solidifies MAP's significant advantage for the scaled-up production of high-performance porous carbons. For instance, Nazari et al.[189] reported optimal powers of 1,500 W for hemp stalks and corn stalks, while Minaei et al.[188] and Kuo et al.[192] determined optimal powers of 700 and 800 W, respectively, for activated sludge.

Residence time significantly influences the evolution of biochar pore structure, an effect that persists throughout all pyrolysis stages and is closely related to the thermochemical transformation behavior of biomass components. Research demonstrates that appropriately extending residence time facilitates complete pyrolysis of biomass components (cellulose, hemicellulose, and lignin)[196], attributable to significant kinetic differences in pyrolysis reactions among components, which require sufficient time to complete their respective transformation pathways. During the initial stage, short-term processing primarily releases low-boiling-point volatiles (e.g., moisture and light organic acids), whose escape leaves initial pore channels within the carbon matrix. As residence time extends, high-molecular-weight components (e.g., lignin-derived aromatic compounds) gradually undergo cracking. This cleavage process involves complex free radical reactions and molecular rearrangements, generating additional gases (CO, CH_4, etc.) and tar precursors. Continuous release of these volatiles not only enlarges existing micropores through physical etching but also promotes the formation of new micropores by facilitating carbon skeleton reorganization, thereby significantly increasing SSA[168]. Within microwave fields, prolonged residence time enables secondary cracking of formed tar (requiring high-temperature conditions). This secondary reaction converts large-molecule tar into small-molecule gases (e.g., H_2 and CO), reducing pore blockage risks while promoting further pore development through additional volatile generation. This minimizes condensate deposition within pores, effectively enhancing pore utilization efficiency[198], particularly improving connectivity in the mesoporous range. Notably, despite rapid heating in MAP, differences in dielectric properties among biomass components (e.g., moisture-rich vs dry zones) may cause localized thermal hysteresis. This non-uniform heating creates spatial variations in pyrolysis extent, affecting pore structure homogeneity. Appropriately extending residence time allows the material to reach global thermal equilibrium, ensuring all regions complete corresponding pyrolysis stages while avoiding uneven pore development due to localized incomplete pyrolysis, which is particularly critical for large-sized feedstocks or high-bulk-density reaction systems. However, excessively prolonged residence time leads to carbon skeleton sintering or thermal shrinkage. This sintering originates from fusion of carbon microcrystals and graphitization, causing pore structure collapse and SSA reduction[163,188]. Microwave-selective heating intensifies this process by enhancing localized thermal effects, that is, prolonging the residence time in the microwave fields increases the thermal stress on the carbon skeleton. This stress arises from non-uniform expansion due to dielectric heterogeneity across the carbon matrix, accelerating pore closure. Furthermore, prolonged high-temperature exposure promotes the transformation of amorphous carbon into ordered graphitic microcrystals. Though this structural ordering enhances electrical conductivity and thermal stability, it reduces surface defects and pore quantity[190,192,199], particularly micropores and mesopores contributed by amorphous carbon regions. Compared to conventional electric heating, microwave heating offers more precise residence time control due to its rapid heating characteristics. This precision stems from direct coupling between electromagnetic parameters (e.g., power, frequency) and material dielectric properties, facilitating easier regulation of pyrolysis kinetics. To achieve optimal pore structure preservation, residence time must be confined to the range where positive effects dominate. This optimal window depends on balancing feedstock type, microwave parameters, and desired pore characteristics. In practical applications, residence time should be dynamically adjusted according to feedstock properties and process parameters. Such dynamic control requires consideration of factors including moisture content, ash composition, and target pore characteristics to balance charring degree and pore development for optimized pore structure design. Particularly in continuous microwave systems, precise regulation of material conveying speed enables real-time adjustment of effective residence time, providing critical flexibility for pore structure control in industrial production. Simultaneously, complex interactions exist between residence time and other process parameters (e.g., temperature, microwave power), necessitating multi-parameter synergistic optimization strategies to fully leverage the unique advantages of MAP in pore structure regulation.

Carbon material used as a wave absorber

With the rapid advancement of electronic technology, issues stemming from excessive electromagnetic radiation in the microwave band have become increasingly severe, rendering electromagnetic pollution a global threat, such as electromagnetic interference (EMI), information leakage, and potential health risks (Fig. 14)[209–211]. Electromagnetic wave-absorbing materials play a crucial role in dissipating incident microwave energy, thereby suppressing electromagnetic noise, ensuring communication stability, protecting precision instruments, and enhancing military stealth capabilities[212,213].

Traditional absorbing materials, such as ferrites, metals, and their alloys, while possessing strong magnetic loss capabilities, suffer from disadvantages including high density, narrow absorption bandwidth, poor impedance matching, and insufficient environmental stability[214–216]. Consequently, the exploration of novel high-performance microwave absorbing materials is of paramount importance.

Biochar has emerged as a promising high-performance microwave absorbing material, distinguished by its renewability, low cost, lightweight nature, and unique structural tunability. Biomass precursors (e.g., agricultural waste) can be converted into porous carbon through carbonization, during which their inherent hierarchical pore structure is preserved and optimized, forming a high-surface-area mesoporous/microporous network[217–219]. This porous characteristic not only significantly reduces material density but also enhances electromagnetic wave energy dissipation through multiple scattering/reflection mechanisms, while simultaneously improving impedance matching and facilitating microwave penetration into the material interior[220]. As illustrated in Fig. 15, the microwave absorption performance of biochar primarily originates from its dielectric loss characteristics, including polarization relaxation[222–224], interfacial polarization[225–227], and conductive/resistive loss[220].

The interfacial polarization effect in these composites not only intensifies dielectric loss but also provides additional energy dissipation pathways through magnetic loss mechanisms (e.g., natural resonance, exchange resonance, and eddy current loss), achieving a wider effective absorption bandwidth (EAB) and stronger absorption intensity. The lightweight nature and structural tunability of biochar-based microwave absorbing materials confer broad application prospects in aerospace, electronic equipment, and military stealth fields. Compared to traditional microwave absorbers, biochar materials not only address weight issues but also achieve superior impedance matching and a wider EAB through porous structures and surface modifications[220]. Future research should further explore the structure-activity relationship between the microstructural regulation of biochar and its microwave absorption performance, develop more efficient and environmentally friendly preparation processes, and promote the practical application of biochar-based microwave absorbing materials.

The porous structure serves as the foundation for the microwave absorption performance of biochar. Carbon materials utilized for electromagnetic wave absorption and their corresponding performance parameters are listed in Table 4. A critical analysis of this survey reveals that materials derived from MAP, though fewer in number, frequently achieve top-tier performance. A prime example is the tremella-derived carbon[246] prepared via MAP, which exhibits an exceptional minimum reflection loss (RL_{min}) of –77.9 dB, outperforming many of the high-performing CP-derived absorbers listed in the same table, such as walnut shell biochar (RL_{min} = –67.6 dB)[247] and coconut shell biochar (RL_{min} = –48.9 dB)[233]. This demonstrates MAP's unique capability to create highly defective and porous structures that are paramount for superior microwave absorption.

Fig. 14 Electromagnetic radiation hazards and application of electromagnetic-wave absorption materials around daily life[209].

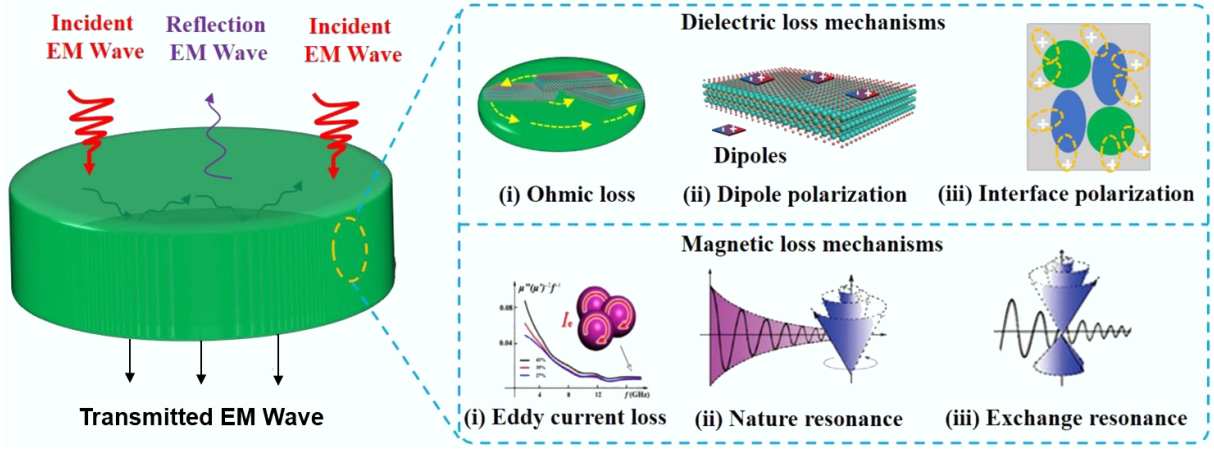

Fig. 15 Schematic diagram of electromagnetic wave absorption mechanisms[221].

Biochar preparation leverages a wide range of feedstock sources, including plant-derived, bacteria-derived, and animal-derived materials. Plant-derived biochar holds unique advantages in producing porous carbon by utilizing the natural water transport channels inherent in plant stems and leaves. For instance, Wu et al. successfully fabricated spinach-derived carbon-based materials with a porous layered structure via a one-step carbonization route, demonstrating excellent microwave absorption performance[255]. The orderly-channeled wood-derived biochar designed by Xi et al. confirmed that the parallel structure optimizes impedance matching[256]. Pore structure modulation is crucial for optimizing the microwave absorption performance of carbon materials, where micropores act as polarization centers, inducing dipole polarization, mesopores increase the SSA, triggering interfacial polarization, and macropores form conductive networks enhancing resistive loss[257]. For example, KOH-activated rice husk porous carbon achieved an RL_{min} of −47.46 dB and an EAB of 3.40 GHz. After loading nickel particles, the RL_{min} was further improved to −58.50 dB (EAB = 3.51 GHz)[258]. Furthermore, the rice husk-derived RPC@MoS_2 composite material developed by Yao et al. (Fig. 16a) formed a litchi-like porous structure through high-temperature carbonization and hydrothermal reaction. The three-dimensional carbon skeleton provided support for MoS_2 growth, achieving an RL_{min} of −50.69 dB at a thickness of 2.0 mm[259]. Aerogel structures, such as the wood-derived aerogel illustrated in Fig. 16b[260], prolong the microwave propagation path due to high porosity but require balancing mechanical strength and pore retention. Bacteria-derived biochar utilizes high-purity bacterial cellulose (BC) as the feedstock, characterized by high crystallinity, high hydrophilicity, and high SSA, making it suitable for designing carbon-based microwave absorbers. For instance, MXene/BC aerogels form multiple scattering interfaces through hydrogen bond cross-linking[261]. The ternary core-shell structure embedding Fe_7S_8 in BC (SdC@Fe/CBC) achieved strong attenuation through interfacial polarization[262]. Producers of animal-derived biochar recycle resources like livestock and poultry farming waste, relying on hollow pore structure design to obtain carbon-based microwave absorbers with exceptional electromagnetic protection performance. Examples include fish skin-derived co-doped 3D carbon foam (Fig. 17a) exhibiting high SSA and synergistic conductive/polarization/scattering effects[263], and gelatin-based hybrid carbon nanospheres (Fig. 17b) achieving RL_{min} = −50.9 dB and EAB = 3.5 GHz via tunable porosity[238]. The porous structure of biochar not only provides abundant interfacial polarization sites but also realizes multiple scattering and absorption of electromagnetic waves by constructing a hierarchical pore network. The special advantage of plant-derived biochar lies in its naturally occurring vascular bundle structure, which transforms into an ordered pore channel network during pyrolysis, offering an ideal scattering path for electromagnetic wave propagation. For example, corn stalk-derived hierarchical porous carbon materials exhibit excellent microwave absorption performance, attributed to their unique honeycomb-like pore channel structure[255]. Similarly, bamboo-derived biochar demonstrates superior dielectric properties due to its natural layered structure, which forms an interconnected conductive network after carbonization[256].

Precise regulation of the pore structure is vital for optimizing microwave absorption performance. Controlling pyrolysis temperature and activation conditions can modulate the pore size distribution and pore connectivity, thereby achieving fine-tuning of dielectric properties and impedance matching[257]. Introducing transition metal nanoparticles (e.g., Ni, Co) into biochar can significantly enhance its microwave absorption performance. These metal particles not only provide an additional magnetic loss mechanism but also strengthen the interfacial polarization effect through interactions with the carbon matrix[258]. The development of composites provides novel design strategies for biochar-based microwave absorbers. Combining biochar with two-dimensional materials (e.g., MoS_2, MXene) enables the construction of multi-component systems with synergistic effects, achieving a wider EAB and stronger absorption intensity[259]. Aerogel structures attract significant attention due to their ultra-high porosity and low density, but balancing the maintenance of high porosity with improved mechanical strength remains a challenge[260]. Bacterial cellulose-derived biochar possesses unique advantages owing to its high purity and well-defined nanofiber structure. These nanofibers form a continuous conductive network after carbonization, facilitating rapid dissipation of electromagnetic waves[261]. Incorporating magnetic components (e.g., Fe_7S_8) into bacterial cellulose-derived biochar can establish a magneto-dielectric synergistic loss mechanism. This ternary core-shell structure achieves superior microwave absorption performance through the combined action of interfacial polarization and magnetic loss[262]. The development of animal-derived biochar offers a new pathway for the resource utilization of waste biomass. These materials typically feature unique hollow pore structures and abundant heteroatom doping, characteristics beneficial for improving impedance matching and enhancing dielectric loss[263]. Gelatin-derived hybrid carbon nanospheres exhibit excellent microwave absorption performance due to their tunable pore structure and surface chemistry, offering novel concepts for designing lightweight and efficient microwave absorbing materials. Research on biochar-based microwave absorbing materials not only advances the development of high-performance electromagnetic protection materials but also provides new avenues for the resource utilization of biomass waste.

Table 4 Comparative study of biocarbon-based microwave absorption materials

Material	Pyrolysis condition	RL_{min} (dB)	EAB (GHz)	Ref.
Apple	600–900 °C, 2 h	−72.6	5.3	[228]
Bacterial cellulose	800 °C, 2 h	−53.3	4.2	[229]
Bamboo fiber	900 °C, 2 h	−75.2	4.6	[230]
Cellulose	640–700 °C, 2 h	−49.2	8.2	[231]
Cellulose dispersion	600–900 °C	−55.4	2.4	[232]
Coconut shell	450–650 °C	−48.9	7.9	[233]
Coconut shell	1,100 °C, 4 h	−54.2	4.2	[234]
Coffee grounds	650–800 °C, 1–4 h	−52.7	6.4	[235]
Cotton fiber	800 °C, 1 h	−60.9	6.1	[236]
Dried teak wood	800 °C, 2 h	−64.7	5.3	[237]
Gelatin	600–800 °C, 2 h	−50.9	3.5	[238]
Kelp	700 °C, 1 h	−75.0	4.8	[239]
Loofah sponges	600–900 °C, 2 h	−66.8	5.5	[240]
Peanut shell	1,100 °C, 2 h	−66.4	3.5	[241]
Pine needle	700–900 °C, 2 h	−56.3	3.4	[242]
Pine nut shell	170 °C, 14 h	−57.4	6.4	[243]
Rice husk	800 °C, 2 h	−68.1	5.0	[244]
Rose	1,000 °C, 1 h	−47.9	4.1	[245]
Tremella	600 °C, 1 h	−77.9	8.5	[246]
Walnut shell	750 °C, 2 h	−67.6	5.4	[247]
Water chestnut	600 °C, 2 h	−60.8	6.0	[248]
Wheat straw	800 °C, 1.5 h	−54.0	6.0	[249]
Almond wood shell	1,000 °C, 2 h	−37.9	7.0	[250]
Dried ballonflower	900 °C, 4 h	−47.0	5.5	[251]
Laver	650 °C, 2 h	−35.7	12.3	[252]
Soybean dregs	900 °C, 1 h	−18.5	4.8	[253]
Tremella	650 °C, 1 h	−34.6	8.8	[254]

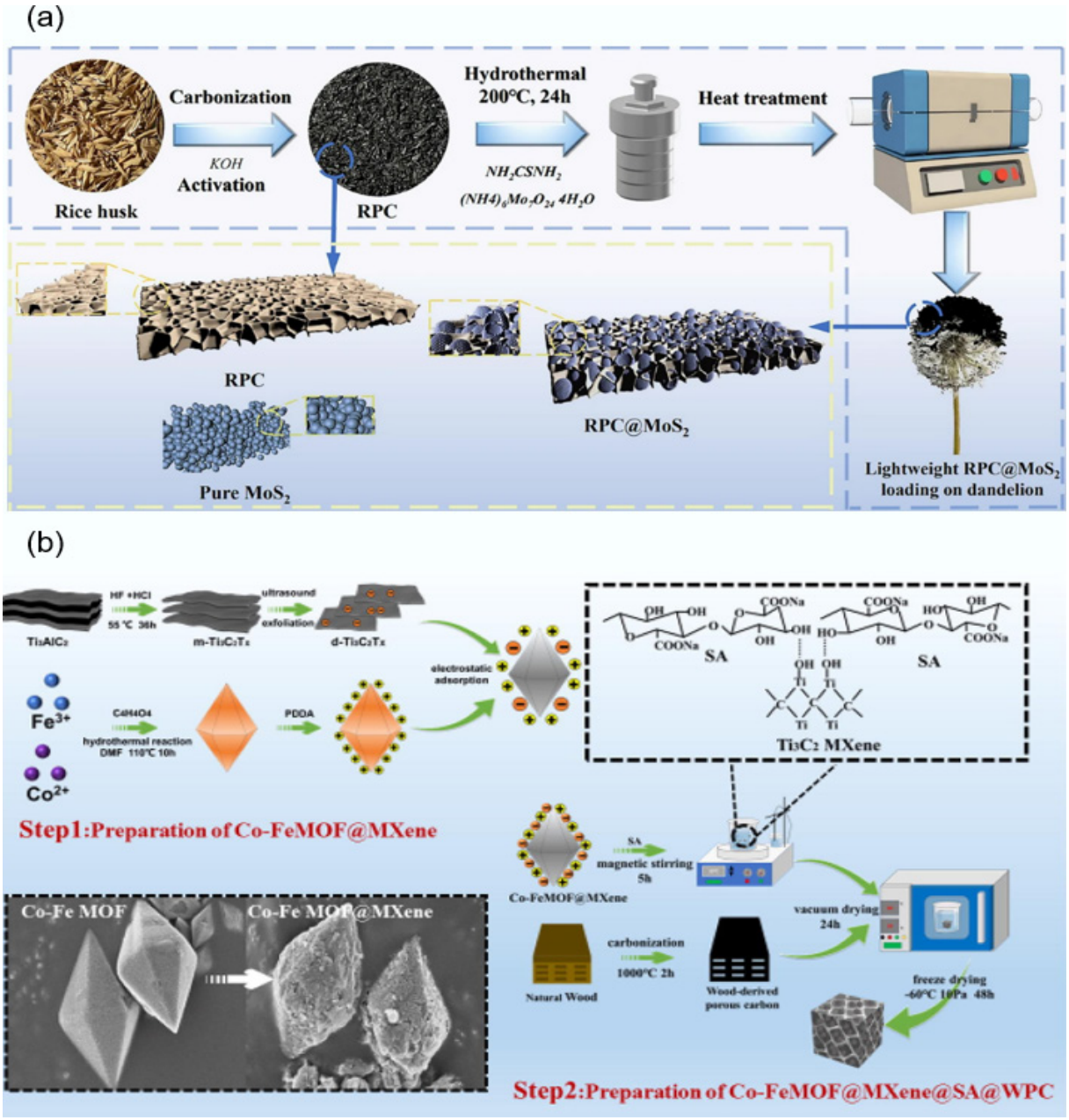

Fig. 16 (**a**) Schematic diagram of the synthesis process of RPC@MoS2 composite[261]. (**b**) Schematic diagram of the synthesis process of CoFe-MOF@Ti3C2TxMXene@SA@WPC[260].

Currently, CP methods are predominantly employed for biochar preparation but suffer from limitations such as high energy consumption and prolonged processing times. For plant-derived sources, rice husk carbonization requires thermal treatment at 650 °C[257], while wood-derived MOF composites necessitate carbonization at 900 °C[260]. Animal-derived gelatin carbonization demands precise temperature control to regulate crystallinity[238]. Although such processes can form a porous structure, pore development is constrained by heating uniformity. MAP, as an emerging technology, demonstrates significant potential for biochar preparation. MAP offers advantages including rapid heating, uniformity, and low energy consumption, enabling the production of biochar with more developed pore structures[264,265]. When activating waste textiles with ferric chloride, MAP achieved rapid and uniform heating while reducing energy consumption, resulting in more developed pore structures. Its self-activation mechanism utilizes pyrolysis gases (CO_2/H_2O) to simultaneously activate carbon, enhancing the SSA[200]. They further noted that, compared to CP, MAP yields solid products with higher PV values. Additionally, the presence of water induces significant microwave absorption, accelerating the heating rate and reaction kinetics of moist materials, thereby facilitating porous structure formation[266–268]. Moreover, MAP can reduce harmful gas emissions, increase product yield, and lower energy consumption. Consequently, MAP-produced biochar holds broad application prospects in microwave absorbing material fabrication. Pore development enhances multiple scattering and interfacial polarization in composites. For instance, conventional rice husk porous carbon exhibits an EAB of only 3.4 GHz[257], whereas microwave-activated textile-derived porous carbon demonstrates superior dynamic adsorption characteristics, indicating potential for

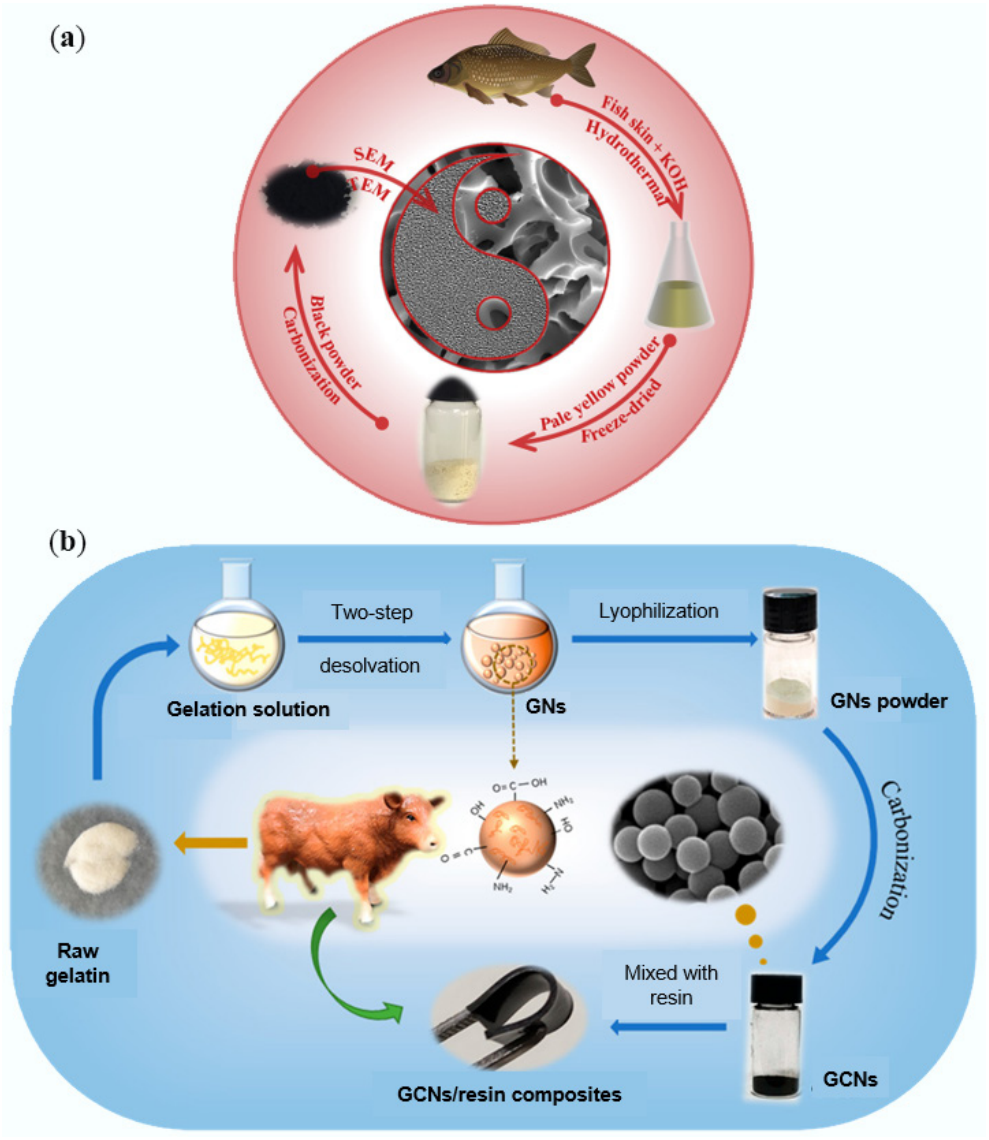

Fig. 17 (**a**) Synthesis of heteroatom doped biochar from fish skin[263]. (**b**) Schematic illustration of the preparation process of gelatin-based carbon nanospheres[238].

extended EAB. Furthermore, microwave's unique volumetric heating effect facilitates uniform heteroatom doping (e.g., phosphorus-doped lignin carbon achieved an RL_{min} improved to −59.8 dB[269]) and increases defect concentration (e.g., popcorn-derived biochar exhibited the highest ID/IG value at 800 °C[270]). Future research should delve into the pore structure-electromagnetic response correlation of microwave-pyrolyzed biochar, aiming to develop lightweight broadband absorbing materials while realizing the concept of green manufacturing[271]. The core advantage of MAP lies in its unique heating mechanism. This inside-out volumetric heating effectively overcomes temperature gradient issues inherent in CP, enabling more uniform pyrolysis of biomass feedstock[264]. Compared to traditional pyrolysis, the direct interaction between the electromagnetic field and the material during MAP not only enhances energy utilization efficiency but also promotes the formation of more complex pore structures. This pore structure optimization manifests primarily in three aspects. Firstly, microwave's selective heating preferentially targets polar components in biomass (e.g., lignin and hemicellulose), enabling effective pyrolysis and pore formation at lower temperatures[266]. Secondly, plasma effects generated within the microwave field can promote carbon skeleton reorganization, leading to more developed microporous and mesoporous structures. Thirdly, rapid heating during MAP effectively suppresses tar formation, reducing the risk of pore blockage[268]. These characteristics endow MAP-produced biochar with superior dielectric properties and impedance matching characteristics, offering new possibilities for developing high-performance microwave absorbing materials. Regarding microwave absorption performance, MAP-prepared biochar exhibits notable advantages. Compared to conventionally pyrolyzed counterparts, MAP can generate biochar with higher concentrations of structural defects and heteroatom doping. These features not only enhance the material's polarization relaxation loss but also improve its impedance matching characteristics[269]. For example, the unique electronic structure formed in phosphorus-doped lignin carbon under MAP conditions significantly boosts its dielectric loss capability[269]. Additionally, the distinct carbon microcrystalline structures formed during MAP facilitate the construction of three-dimensional conductive

networks. These network structures effectively dissipate electromagnetic wave energy through resistive loss mechanisms[270]. Notably, MAP-produced biochar often possesses more uniform elemental distribution and more controllable surface chemistry, features crucial for regulating the material's permittivity and permeability[271]. In practical applications, MAP-derived biochar-based composites have demonstrated excellent microwave absorption performance, with both EAB and RL_{min} outperforming materials prepared via CP[257,269]. Future research should prioritize optimizing MAP process parameters, particularly investigating the influence of microwave power, frequency, and treatment time on biochar pore structure and electromagnetic properties. This will provide theoretical guidance and technical support for developing the next generation of lightweight broadband microwave absorbing materials[271].

Carbon material used as energy storage and electrode materials

With the continuous growth of global energy demand and the increasingly severe issues of traditional fossil energy depletion and environmental pollution, the development of efficient and sustainable energy storage technologies has become an urgent priority[272,273]. Batteries and supercapacitors, as the core components of electrochemical energy storage systems, play an indispensable role in the effective utilization of renewable energy due to their excellent performance in energy density, power density, cycle life, and other aspects[274–276]. They not only balance the intermittency of renewable energy but also provide reliable power support for various application scenarios such as electronic products and electric vehicles. However, the performance bottlenecks of existing electrode materials severely constrain the development potential of batteries and supercapacitors. Therefore, exploring novel electrode materials has become a key breakthrough for enhancing the performance of energy storage devices.

Biochar, as a renewable material derived from biomass, has demonstrated great potential as an electrode material for batteries and supercapacitors after pyrolysis and activation treatments (Fig. 18)[277–279]. Its unique pore structure, high SSA, and tunable surface chemistry provide ideal conditions for rapid charge storage and release. Compared to traditional electrode materials like graphite and activated carbon, biochar can be prepared from various biomass resources, including agricultural and forestry waste[280]. This not only significantly reduces material costs but also enables resource recycling. Simultaneously, its preparation process is relatively simple, environmentally friendly, and effectively reduces CO_2 equivalent emissions, fully aligning with the strategic requirements of sustainable development[281]. More importantly, biochar electrodes exhibit excellent cycle stability and rate capability during charge-discharge processes, maintaining stable electrochemical performance even under high power output, which is decisive for improving the overall efficiency of energy storage systems. The performance advantages of biochar electrode materials are mainly reflected in their unique microstructural characteristics. Their hierarchical porous structure not only provides abundant ion transport channels but also enables efficient adsorption and rapid desorption of electrolyte ions through the regulation of surface functional groups. This structural characteristic allows biochar electrodes to demonstrate excellent rate performance in supercapacitor applications, maintaining high specific capacitance even under rapid charge-discharge conditions.

For battery applications, the three-dimensional conductive network structure of biochar provides continuous pathways for electron transport, while its rich surface defects and heteroatom doping significantly enhance the material's electrochemical activity[278]. These characteristics work synergistically, endowing biochar-based electrode materials with broad application prospects in energy storage systems such as lithium-ion batteries and sodium-ion batteries. Particularly noteworthy is that the surface chemical properties of biochar can be precisely regulated through precursor selection and pyrolysis conditions, providing an important means to optimize the reaction kinetics at the electrode/electrolyte interface[279]. For example, adjusting the pyrolysis temperature can alter the graphitization degree of biochar, thereby balancing the material's conductivity and the number of active sites. Introducing heteroatoms such as nitrogen and phosphorus can enhance the pseudocapacitive characteristics of the material. Physical or chemical activation can further expand the SSA and pore volume of the material[280]. These tunable properties enable biochar to adapt to the demands of different energy storage systems, providing new material choices for developing high-performance, low-cost energy storage devices.

From the perspective of sustainable development, the preparation process of biochar electrode materials offers significant environmental advantages. Traditional electrode materials like graphite often require high-temperature treatment and strong acid activation for production, resulting in high energy consumption and substantial pollutant generation. In contrast, biochar can be obtained under relatively mild pyrolysis conditions, and its raw materials are widely available, including renewable resources such as crop straws, fruit shells, and wood processing waste[281]. This 'turning waste into treasure' production model not only achieves high-value utilization of biomass resources but also reduces the environmental pressure associated with the disposal of agricultural and forestry waste. Furthermore, by-products generated during biochar preparation, such as bio-oil and syngas, can be utilized as energy or chemical feedstocks, further improving the resource utilization efficiency of the entire production process. From a life cycle assessment perspective, the carbon footprint of biochar electrode materials are significantly lower than that of traditional electrode materials, which are crucial for achieving carbon neutrality goals. In practical applications, biochar-based electrode materials have demonstrated excellent performance in various energy storage systems. In the field of supercapacitors, the high SSA and well-developed pore structure of biochar enables the storage of large amounts of charge, while its good electrical conductivity ensures rapid charge transfer. In the field of lithium-ion batteries, biochar can serve as an anode material, its porous structure effectively alleviating volume changes during charge-discharge cycles and enhancing cycling stability. In emerging energy storage systems such as sodium-ion batteries and potassium-ion batteries, the interlayer spacing and surface chemistry of biochar can be tuned to optimize ion storage performance, offering new solutions to electrode material challenges in these systems. Particularly noteworthy is that biochar materials can also be composited with other functional materials. For example, compositing with transition metal oxides can combine the advantages of electric double-layer capacitance (EDLC) and pseudo capacitance, while compositing with conductive polymers can improve the flexibility and processability of the material[278,279]. These composite material design strategies further expand the application scope of biochar in the energy storage field. Future research should focus on the structure-performance relationship between the microstructure and electrochemical properties of biochar, developing more precise preparation methods, and promoting its practical application in large-scale energy storage systems.

Biochar's performance as an electrode material hinges on the regulation of its pore structure and surface chemistry. A survey of

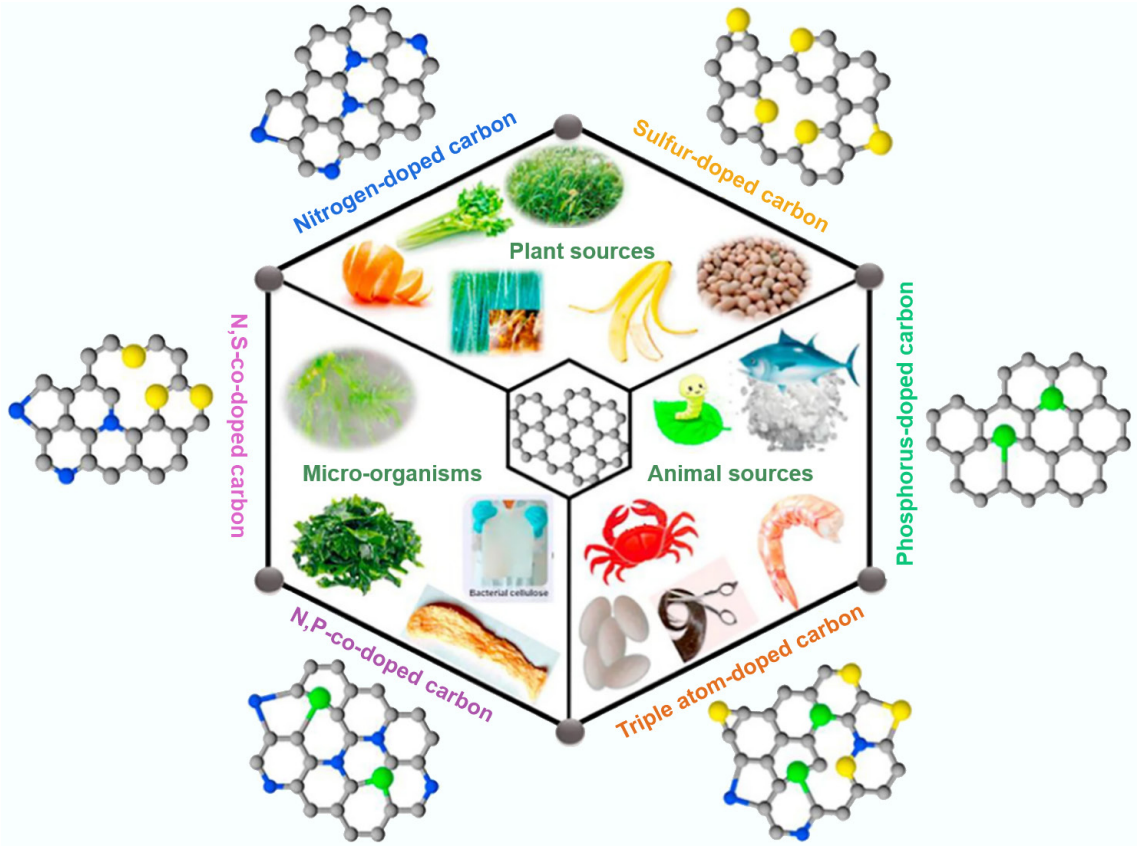

Fig. 18 Various self-doped biomass-derived carbon materials as a supercapacitor electrode[277].

representative materials, their preparation conditions, and key electrochemical parameters is presented in Table 5. Biochar electrodes derived from diverse precursors, such as aloe vera, crab shells, and lotus leaves, can achieve high SSA (up to 3,557 m^2/g) and remarkable specific capacitance (exceeding 500 F/g in some cases)[307–310]. It should be noted that the exceptionally high capacitance of 1,214 F/g originates from a Ni-Al layered double hydroxide/carbon fiber composite[293], rather than a pure porous carbon, highlighting the performance gain achievable through strategic material hybridization. The working mechanism of biochar electrodes combines EDLC with pseudocapacitive effects (Fig. 19)[311,312], where EDLC relies on ion adsorption at electrode/electrolyte interfaces while pseudo capacitance arises from surface redox reactions or heteroatom doping. Magnetic biochar-polyaniline composites using durian peel precursors exhibit an SSA of 835 m^2/g after pyrolysis at 800 °C, with the final composite achieving an ultra-high specific capacitance of 615 F/g[313]. Electrochemical performance is co-regulated by pore structure and surface chemistry. Micropores (< 2 nm) provide charge storage sites but limit ion diffusion, whereas mesopores (2–50 nm) significantly enhance transport kinetics. For instance, cotton-based porous carbon with an SSA of 1,508 m^2/g and mesoporous structure (9.18 nm) delivers specific capacitances of 278 and 208 F/g at current densities of 1 and 100 A/g, respectively[314]. Surface heteroatom doping (N/O/S) enhances wettability and introduces pseudo capacitance, though excessive doping increases leakage currents and accelerates self-discharge[315]. This reflects the synergistic balance between pore structure optimization and surface chemical modification in electrode material design. Performance optimization of biochar electrodes requires not only rational pore design but also precise regulation of surface chemistry. The latter, in particular, is governed by preparation parameters such as pyrolysis temperature, activator type, and doping methods, which significantly influence the final performance. For example, biochar pyrolyzed at lower temperatures typically retains more oxygen-containing functional groups, enhancing material wettability and pseudocapacitive contributions, while high-temperature treatment facilitates more developed graphitic structures and conductive networks[307]. The activation process critically impacts electrode performance. KOH activation is widely adopted for its exceptional pore-forming efficacy, though its negative effects on mechanical strength must be considered[310]. Furthermore, precursor selection directly determines microstructural and surface properties, with lignocellulosic feedstocks tending to form more ordered pore channels while protein-rich materials readily generate abundant nitrogen-doped sites[308]. In practical applications, electrolyte systems substantially influence biochar electrode performance. Aqueous electrolytes are widely used in supercapacitors for their safety and low cost, but organic electrolytes enable wider electrochemical windows for higher energy density[311]. Though expensive, ionic liquid electrolytes offer unique advantages in high-performance systems due to their exceptional electrochemical stability and wide voltage windows[312]. Electrode/electrolyte interfacial interaction mechanisms also critically affect performance, where appropriate interfacial wettability ensures full contact between electrolyte ions and active sites, while excessive interactions may cause irreversible side reactions[313]. At the device level, optimizing biochar-based supercapacitors require coordinated consideration of multiple components, including electrode materials, electrolytes, separators, and current collectors. For instance, developing flexible supercapacitors demand biochar electrodes with excellent

Table 5 Preparation methods of biochar, electrolyte, and application in supercapacitors

Raw material	Preparation condition	SSA (m^2/g)	Current density (A/g)	Capacitance (F/g)	Ref.
Aloe vera	700 °C, 1 h	1,890	0.5	410	[282]
Anthracite	900 °C, 2 h	2,814	0.5	325	[283]
Castor shell	800 °C, 4 h	1,527	1	365	[284]
Cellulose	650 °C, 2.5 h	1,588	0.5	288	[285]
Chili straw	800 °C, 1 h	2,768.5	1	352	[24]
Crab shells/ rice husks	700 °C, 3 h	3,557	0.5	474	[286]
Crop straw	800 °C, 1 h	1,058.4	1	317	[287]
Corn gluten meal	500 °C	3,353	0.5	488	[288]
Corn stalk	800 °C, 2 h	2,054	0.5	461	[289]
Corn stover	820 °C, 1 h	1,432.9	0.1	246	[290]
Cotton seed husk	700 °C, 1 h	1,694.1	0.5	238	[291]
Cotton stalk	800 °C, 2 h	1,964.5	0.2	254	[292]
Cotton stalk	1,000 °C	327	1	1,214	[293]
Kapok wood	700 °C, 1 h	2,909.8	0.2	380	[294]
Moringa leaves	800 °C, 2 h	1,327	50	234	[295]
Peanut shell	800 °C, 1 h	1,138	0.2	447	[296]
Rice husk	800 °C, 2 h	3,263	0.5	315	[297]
Rice straw	700 °C, 1 h	3,333	0.1	400	[298]
Rice straw	850 °C, 2 h	2,537	0.5	324	[299]
Sargassum	800 °C, 20 min	1,367.6	1.0	531	[26]
Shaddock endotheliums	750 °C, 1 h	1,265	0.2	550	[300]
Sisal	750 °C	2,289	0.5	415	[301]
Bagasse	700 °C, 1 h	2,296	0.5	180	[302]
Rice husk	600 °C, 1 h	454.6	0.5	130.3	[303]
Sword bean shell	700 °C, 2 h	2,282	1.0	264	[304]
Tea leaves	1,200 °C	911.9	1	167	[305]
Withered rose	800 °C, 1.5 h	1,911	0.5	208	[306]

mechanical flexibility and structural stability to meet requirements in wearable electronics[308]. Design strategies differ between symmetric supercapacitors (typically using identical biochar for both electrodes) and asymmetric configurations (requiring electrodes with matched potential windows)[314]. Additionally, scalable fabrication processes and cost control significantly impact practical implementation, necessitating balanced consideration of performance and economic feasibility[315]. Future research should emphasize deeper understanding of structure-performance relationships, employing advanced characterization combined with theoretical computations to elucidate connections between microstructural features and macroscopic electrochemical properties. Concurrently, developing greener and more efficient preparation processes to advance biochar electrodes from laboratory research toward industrial applications represents a crucial direction. Through interdisciplinary integration, biochar electrode materials hold promise to play increasingly important roles in next-generation energy storage systems, offering innovative solutions to energy and environmental challenges.

Traditional pyrolysis methods face bottlenecks such as high energy consumption and limited structural control in preparing biochar electrodes. For instance, walnut shell carbonization requires high-temperature activation at 800 °C to achieve a high SSA of 3,577 m^2/g, yet excessive micropore proportion severely restricts ion transport efficiency[315]. The dual-stage activation process for cotton stalks relies on strong oxidizing agents like $KMnO_4$/KOH, complicating preparation and increasing environmental burdens[316]. In contrast, MAP demonstrates significant advantages in energy efficiency, high productivity, and environmental friendliness due to its unique energy conversion mechanism (as shown in Fig. 20a and b)[317,319], enabling effective optimization of pore structure distribution. Studies reveal that under 700 W microwave power, bagasse pyrolysis yields an optimal structure with an SSA of 764 m^2/g and a mesopore proportion of 64%. Electrodes fabricated from this material exhibit an electro-sorption capacity of 11.4 mg/g at 1.2 V potential[320]. After HCl/HF acid pretreatment, microwave-induced carbonization of cumin waste produces activated carbon with a specific capacitance increase from 117 to 155 F/g. This improvement stems from the porous microstructure formed after acid-wash impurity removal, facilitating rapid ion diffusion and double-layer reorganization[321]. Microwave-treated biochar electrodes show broad prospects in energy and environmental fields. Liu et al.[322] prepared porous carbon spheres via microwave-assisted reactions, achieving an SSA of 1,321 m^2/g, PV of 0.59 cm^3/g, specific capacitance of 243.13 F/g, and electro-sorption capacity of 5.81 mg/g. Adorna et al.[323] composited manganese dioxide with activated biochar from waste coconut shells. The nanocomposite prepared by indirect co-precipitation combines high SSA with mesoporous structure, demonstrating a specific capacitance of 410–523 F/g at 5 mV/s, and electro-sorption capacity of 33.9–68.4 mg/g. Notably, porous carbon derived from the MAP of waste palm not only features hierarchical meso/microporous structures

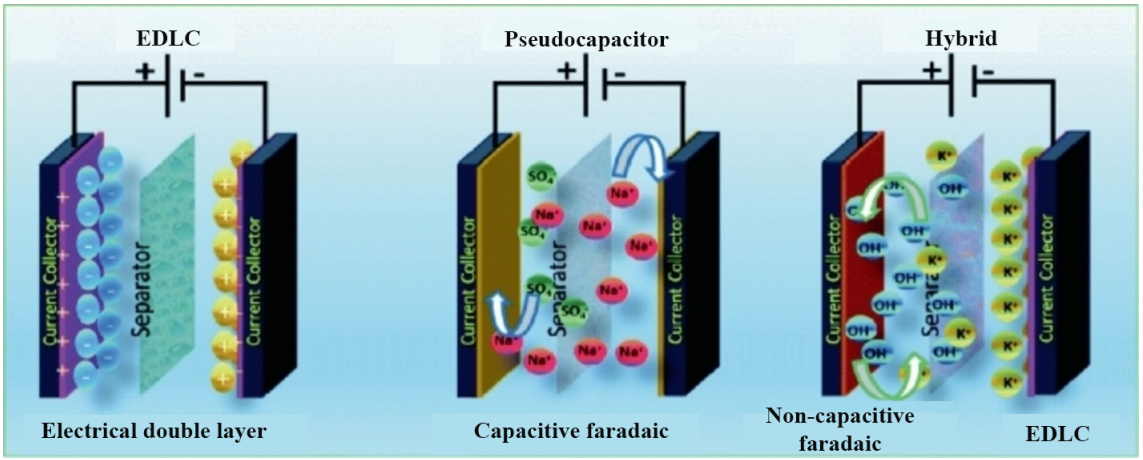

Fig. 19 Types of supercapacitors - EDLC, pseudo capacitor, hybrid[311].

promoting ion diffusion but also exhibits surface oxygen heteroatoms that significantly enhance wettability. This enables the electrode to maintain a specific capacitance of 164.8 F/g at 0.5 A/g, while achieving over 92% capacity retention after 2,000 cycles[324]. Future research priorities are as follows: (1) integrating hydrothermal pretreatment to decompose biomass cross-linked structures (e.g., achieving 299.3 F/g at 0.5 A/g via KOH activation after hydrothermal carbonization of tremella[325]); (2) developing mesopore-oriented processes to balance SSA utilization with ion diffusion rates; and (3) designing composite electrodes such as MnO_2-intercalated nitrogen-doped carbon (e.g., the MnO_2@N-APC system reaching 28 W·h/kg energy density[326]) to enhance capacity and cycling stability through synergistic effects. With the increasing standardization of microwave processes, this approach will provide crucial technical support for the green manufacturing of energy storage devices under dual carbon goals. The core advantage of MAP technology lies in its unique heating mechanism. This inside-out volumetric heating approach effectively overcomes temperature gradient issues in CP, enabling more uniform biomass decomposition[318]. Compared with traditional pyrolysis, direct electromagnetic interaction with materials, during MAP, not only improves energy utilization efficiency but also promotes more complex pore structure formation. This pore structure optimization manifests in three aspects. First, microwave's selective heating preferentially targets polar components (e.g., lignin and hemicellulose) in biomass, achieving effective pyrolysis and pore formation at lower temperatures[320]. Second, plasma effects generated in microwave fields facilitate carbon skeleton reorganization, forming more developed micro/mesoporous structures[321]. Third, rapid heating during MAP effectively suppresses tar formation, reducing pore-clogging risks[324]. These characteristics endow microwave-pyrolyzed biochar with superior dielectric properties and impedance

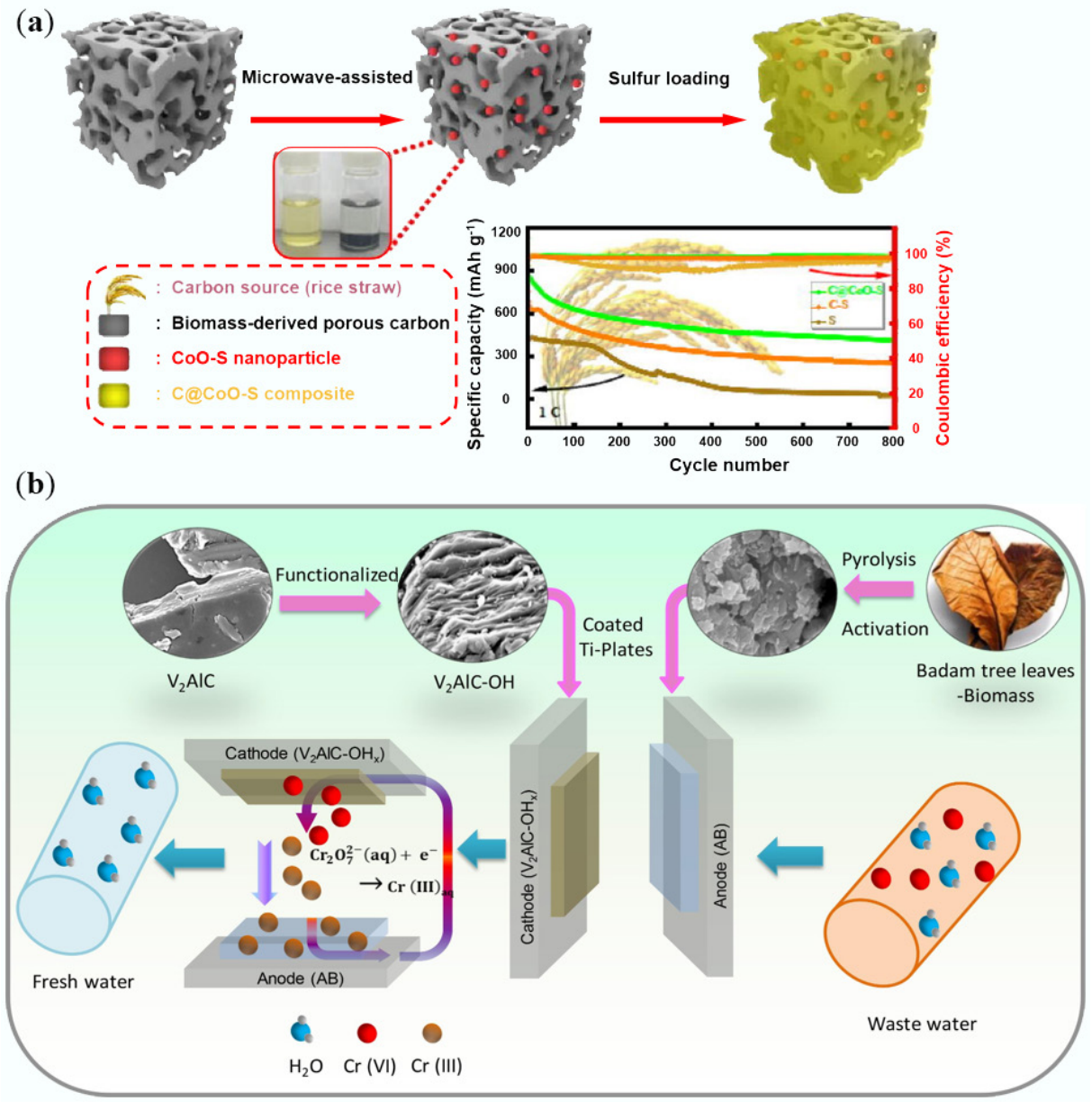

Fig. 20 (**a**) Schematic diagram of the preparation of biochar electrodes modified by sulfur/CoO nanoparticles[318]. (**b**) Schematic illustration of the asymmetric CDI setup, and the Cr(VI) reduction mechanism using AB/V_2AlC-OHx electrodes[319].

matching, offering new possibilities for high-performance microwave absorption materials. Regarding microwave absorption performance, microwave-pyrolyzed biochar demonstrates significant advantages. Compared to CP, MAP generates higher concentrations of structural defects and heteroatom doping, which not only enhance polarization relaxation losses, but also improves impedance matching[322]. For example, phosphorus-doped lignin carbon formed under MAP conditions exhibits significantly improved dielectric loss capabilities due to its unique electronic structure[323]. Furthermore, the distinct carbon microcrystalline structures formed during MAP facilitate the construction of three-dimensional conductive networks that effectively dissipate electromagnetic wave energy through resistive loss mechanisms[324].

Notably, microwave-pyrolyzed biochar often features more uniform element distribution and tunable surface chemistry, characteristics crucial for regulating dielectric constant and magnetic permeability[325]. In practical applications, biochar-based composites prepared via MAP already demonstrate excellent microwave absorption performance, outperforming traditionally pyrolyzed materials in EAB and RL_{min}[316,326]. Future research should prioritize optimizing MAP parameters (particularly microwave power, frequency, and processing time) to understand their effects on biochar pore structures and electromagnetic properties, providing theoretical guidance and technical support for developing next-generation lightweight broadband microwave absorbers.

Conclusions and outlook

This comprehensive review highlights the transformative potential of MAP as a sustainable, efficient, and highly controllable technology for producing advanced carbon materials from diverse waste feedstocks such as biomass, municipal solid waste, and industrial exhaust gases. A critical analysis of multidimensional carbon materials, including 1D nanotubes and nanofibers, 2D graphene, and 3D porous carbons demonstrates that MAP consistently surpasses CP in energy efficiency, reaction kinetics, product performance, and environmental impact, making it a key technology for achieving carbon neutrality goals. The inherent advantages of microwave heating, such as volumetric energy transfer, selective molecular activation, rapid heating rates exceeding 100 °C/min, and the elimination of thermal gradients, provide unmatched control over material microstructure and functionality.

In the realm of 1D carbon nanomaterials, microwave CVD dramatically shortens synthesis time by over 90% and favors the formation of defect-rich, brush-like multi-walled CNTs, which are particularly suitable for applications like field emission and supercapacitors, despite conventional CVD producing longer SWCNTs. For 2D graphene, microwave reduction achieves rapid deoxygenation within seconds, bypassing the lengthy processes of traditional methods. The core advantage lies in the restoration of the sp^2 carbon network with minimal defects, leading to exceptionally high electrical conductivity and excellent performance in flexible electronics and energy storage devices. Regarding 3D carbon materials, MAP consistently outperforms CP in enhancing fuel properties (HHV), developing sophisticated porous architectures (SSA and PV), and tailoring functional performance for applications in adsorption, wave absorption, and energy storage. As electromagnetic wave absorbers, microwave-pyrolyzed biochar leverages its tunable pore hierarchy and defect density to achieve exceptional performance. In energy storage, MAP-synthesized electrodes deliver superior electrochemical metrics due to enhanced ion diffusion and pseudocapacitance. Acid-pretreated cumin waste activated via MAP attains a specific capacitance of 155 F/g, which is 33% higher than conventional equivalents. KOH-activated lotus leaf biochar achieves an ultrahigh SSA of 2,350.8 m^2/g and PV of 1.37 cm^3/g, yielding 478 F/g at 1 A/g with 89.1% retention after 5,000 cycles. These results starkly contrast with CP electrodes, where excessive micropores or complex activation limit performance and scalability.

This review clearly demonstrates that microwave technology surpasses conventional pyrolysis by enabling precise microstructure control, reducing energy consumption by 30%–50%, shortening processing times by 60%–90%, and enhancing key functional properties including SSA by 40–60%, adsorption capacity by 30%–50%, electrochemical capacitance by 20%–40%, and microwave absorption intensity by 20–30 dB. These advances stem from microwave-specific mechanisms such as volumetric heating, non-thermal molecular activation, and dielectric-loss-driven pore engineering, confirming MAP as the leading green technology for scalable, high-performance carbon material production that directly contributes to sustainable energy and environmental solutions.

However, despite these promising advancements, several challenges and limitations remain in the microwave preparation of sustainable carbon materials. Firstly, the cost of microwave equipment and the need for specialized knowledge for its operation may hinder widespread adoption, particularly in developing countries. Secondly, the optimization of microwave process parameters, such as power, temperature, and residence time, requires further in-depth study to achieve consistent and reproducible material properties. Additionally, the scalability of MAP for large-scale industrial production remains an area of concern, as scaling up may introduce new challenges related to heat distribution and material handling. Future research should focus on addressing these challenges. Cost-effective and user-friendly microwave systems need to be developed to broaden their applicability. Furthermore, advanced computational models and artificial intelligence techniques can be employed to optimize microwave process parameters, ensuring precise control over material properties. Exploring hybrid microwave-conventional methods may also provide a balanced approach, combining the efficiency of microwave heating with the scalability of conventional techniques. Lastly, the integration of MAP with other sustainable technologies, such as circular economy practices and waste-to-energy systems, holds potential for realizing a truly sustainable future. By addressing these challenges and exploring new opportunities, the microwave preparation of sustainable carbon materials stands to play a pivotal role in achieving global carbon neutrality goals.

Beyond process parameter optimization, the design of the microwave reactor itself is a critical factor governing the scalability and commercialization of MAP technology. Laboratory-scale systems predominantly employ single-mode cavities, which provide precise field control and high efficiency for fundamental studies but are limited by small processing volumes. For industrial translation, continuous or large-scale multi-mode reactors are essential, yet they face challenges in maintaining field uniformity, which can lead to uneven heating and product inconsistency (e.g., localized hotspots causing pore structure heterogeneity). Future reactor designs must integrate multi-physics modeling (coupling electromagnetism, heat transfer, and reaction kinetics) with intelligent systems. This includes implementing dynamic impedance matching, incorporating fiber-optic temperature sensors for real-time monitoring, and developing modular, scalable cavity geometries that can process diverse feedstock forms (e.g., powders, pellets, slurries) efficiently. Overcoming these engineering hurdles is paramount to achieving the reproducible, large-volume production of high-quality carbon materials required for industrial applications. Furthermore, a thorough techno-economic analysis is imperative to assess the real-world

viability of MAP. While the operational benefits—such as reduced energy consumption (30%–50%), shorter processing times (60%–90%), and higher product value—are clear from laboratory data, the initial capital investment for industrial-scale microwave systems remains substantially higher than for conventional pyrolysis furnaces. The economic calculus must also account for the cost of raw material pretreatment, such as drying to an optimal moisture content and the potential need for microwave susceptors (e.g., activated carbon, SiC) to process low-dielectric feedstocks. Future life-cycle assessment and techno-economic studies are needed to quantify the trade-offs between the superior product performance, potential revenue from high-value carbon materials, and the associated capital and operational expenditures. Government policies supporting carbon-neutral technologies could provide a decisive economic incentive, improving the return on investment and accelerating the adoption of MAP for sustainable carbon material production.

Author contributions

The authors confirm their contributions to the paper as follows: study conception and design were performed by Tianhao Qiu and Yaning Zhang; data collection was performed by Tianhao Qiu, Kaihan Xie, Chaoyue Liu, and Faizan Ahmad; analysis and interpretation of results were performed by Tianhao Qiu, Kaihan Xie, and Chaoyue Liu; draft manuscript preparation was performed by Tianhao Qiu, Wenke Zhao, Müslüm Arıcı, and Yaning Zhang. All authors reviewed the results and approved the final version of the manuscript.

Data availability

The datasets used or analyzed during the current study are available from the corresponding author upon reasonable request.

Fundings

This work was supported by the National Natural Science Foundation of China (Grant No. 52476005) and Heilongjiang Provincial Key R&D Program 'Unveiling the Leader' Project (Grant No. 2023ZXJ02C04).

Declarations

Competing interests

All authors declare that there are no competing interests.

Author details

[1]School of Energy Science and Engineering, Harbin Institute of Technology (HIT), Harbin 150001, China; [2]Mechanical Engineering Department, Engineering Faculty, Kocaeli University, Kocaeli 41001, Turkey

References

[1] Prabowo J, Lai L, Wang Y, Wu R, Chen Y. 2025. Sustainable carbon materials from methane pyrolysis for energy applications. *Current Opinion in Green and Sustainable Chemistry* 52:101004

[2] Hegde SS, Bhat BR. 2024. Impact of electrolyte concentration on electrochemical performance of Cocos nucifera Waste-Derived High-Surface carbon for green energy storage. *Fuel* 371(A):131999

[3] Li X, Yu Y, Zhang Y, Wang J, She D. 2024. Synergistic effects of modified biochar and selenium on reducing heavy metal uptake and improving pakchoi growth in Cd, Pb, Cu, and Zn–contaminated soil. *Journal of Environmental Chemical Engineering* 12(4):113170

[4] Yang H, Zhang B, Sun J, Su X, Huo S, et al. 2024. Efficient Fe_3O_4@porous carbon microwave absorber constructed from cotton cellulose nanofibers hydrogel. *Journal of Alloys and Compounds* 997:174956

[5] Zhang Z, Kang J, Liu R, Sun Z, Feng L, et al. 2024. Microwave photonic mixing approach to doppler frequency shift measurement. *IEEE Transactions on Instrumentation and Measurement* 73:1008508

[6] Sun Y, Chen Y, Tang L, Jia X, Ma H, et al. 2025. A submicrosecond-response ultrafast microwave ranging method based on optically generated frequency-modulated pulses. *Sensors* 25(1):58

[7] Yu B, Wang HQ, Ju L, Hou KX, Xiao ZD, et al. 2025. A bio-inspired microwave wireless system for constituting passive and maintenance-free IoT networks. *National Science Review* 12(2):nwae435

[8] Gong C, Ding J, Wang C, Zhang Y, Guo Y, et al. 2023. Defect-induced dipole polarization engineering of electromagnetic wave absorbers: insights and perspectives. *Composites Part B: Engineering* 252:110479

[9] Zhao B, Yan Z, Li D, Zhou X, Du Y, et al. 2023. Hierarchical flower-like sulfides with increased entropy for electromagnetic wave absorption. *ACS Applied Materials & Interfaces* 15(51):59618–29

[10] Nagashima I, Sugiyama J, Shimizu H. 2023. Study of 400 MHz microwave conduction loss effect for a hydrolysis reaction by thermostable β-glucosidase HT1. *Bioscience, Biotechnology, and Biochemistry* 87(2):158–162

[11] Duan L, Zhou J, Yan Y, Tao J, Liu Y, et al. 2025. Electron migratory polarization of interfacial electric fields facilitates efficient microwave absorption. *Advanced Functional Materials* 35(10):2416727

[12] Sun J, Huang X, Liu Y, Zhang K, Yan Y, et al. 2023. Enhanced microwave absorption performance originated from interface and unrivaled impedance matching of SiO_2/carbon fiber. *Applied Surface Science* 623:157029

[13] Tian W, Li Z, Wu L. 2020. Experimental demonstration of a microwave non-thermal effect in DMSO-NaCl aqueous solution. *Chemical Physics* 528:110523

[14] Guo L, Lan J, Du Y, Zhang TC, Du D. 2020. Microwave-enhanced selective leaching of arsenic from copper smelting flue dusts. *Journal of Hazardous Materials* 386:121964

[15] Zhang Y, Chen P, Liu S, Peng P, Min M, et al. 2017. Effects of feedstock characteristics on microwave-assisted pyrolysis – a review. *Bioresource Technology* 230:143–151

[16] Qiu T, Liu C, Cui L, Liu H, Muhammad K, et al. 2023. Comparison of corn straw biochars from electrical pyrolysis and microwave pyrolysis. *Energy Sources, Part A: Recovery, Utilization, and Environmental Effects* 45(1):636–649

[17] Qiu T, Cao W, Xie K, Ahmad F, Zhao W, et al. 2025. CO_2 capture performances of H_3PO_4/KOH activated microwave pyrolyzed porous biochar. *Sustainable Carbon Materials* 1:e004

[18] Salakhi M, Thomson MJ. 2025. A particle-scale study showing microwave energy can effectively decarbonize process heat in fluidization industry. *iScience* 28(2):111732

[19] Nilova LP, Ikramov RA, Malyutenkova SM, Chunin SA, Lu W, et al. 2020. High-speed infrared photography in the study of thermophysical processes in the manufacture of jelly products. *IOP Conference Series: Materials Science and Engineering* 940:012083

[20] Zhang Y, Ke C, Fu W, Cui Y, Rehan MA, et al. 2020. Simulation of microwave-assisted gasification of biomass: a review. *Renewable Energy* 154:488–496

[21] Zhang Y, Luo H, Kong L, Zhao X, Miao G, et al. 2020. Highly efficient production of lactic acid from xylose using Sn-beta catalysts. *Green Chemistry* 22(21):7333–736

[22] Zhang Y, Liu S, Fan L, Zhou N, Omar MM, et al. 2018. Oil production from microwave-assisted pyrolysis of a low rank American brown coal. *Energy Conversion and Management* 159:76–84

[23] Ellison C, Abdelsayed V, Smith MW. 2023. Analysis of char structure and composition from microwave and conventional pyrolysis/gasification of low and middle rank coals. *Fuel* 354:129301

[24] Zhang X, Ma X, Yu Z, Yi Y, Huang Z, et al. 2022. Preparation of high-value porous carbon by microwave treatment of chili straw pyrolysis residue. *Bioresource Technology* 360:127520

[25] Jankovská Z, Matějová L, Tokarský J, Peikertová P, Dopita M, et al. 2024. Microporous carbon prepared by microwave pyrolysis of scrap tyres and the effect of K^+ in its structure on xylene adsorption. *Carbon* 216:118581

[26] Huang H, Chen Y, Ma R, Luo J, Sun S, et al. 2023. Preparation of high performance porous carbon by microwave synergistic nitrogen/phosphorus doping for efficient removal of Cu^{2+} via capacitive deionization. *Environmental Research* 222:115342

[27] Fan YY, Cheng HM, Wei YL, Su G, Shen ZH. 2000. Tailoring the diameters of vapor-grown carbon nanofibers. *Carbon* 38(6):921–927

[28] Merkulov VI, Melechko AV, Guillorn MA, Lowndes DH, Simpson ML. 2002. Effects of spatial separation on the growth of vertically aligned carbon nanofibers produced by plasma-enhanced chemical vapor deposition. *Applied Physics Letters* 80(3):476–478

[29] Kim HI, Wang M, Lee SK, Kang J, Nam JD, et al. 2017. Tensile properties of millimeter-long multi-walled carbon nanotubes. *Scientific Reports* 7:9512

[30] Chen K, Gao W, Emaminejad S, Kiriya D, Ota H, et al. 2016. Printed carbon nanotube electronics and sensor systems. *Advanced Materials* 28(22):4397–4414

[31] Farrera C, Andón FT, Feliu N. 2017. Carbon nanotubes as optical sensors in biomedicine. *ACS Nano* 11(11):10637–10643

[32] Hone J, Llaguno MC, Biercuk MJ, Johnson AT, Batlogg B, et al. 2002. Thermal properties of carbon nanotubes and nanotube-based materials. *Applied Physics A* 74(3):339–343

[33] Zheng Q, Cao WQ, Zhai H, Cao MS. 2023. Tailoring carbon-based nanofiber microstructures for electromagnetic absorption, shielding, and devices. *Materials Chemistry Frontiers* 7(9):1737–1759

[34] Zhou X, Wang Y, Gong C, Liu B, Wei G. 2020. Production, structural design, functional control, and broad applications of carbon nanofiber-based nanomaterials: a comprehensive review. *Chemical Engineering Journal* 402:126189

[35] Feng S, Li K, Hu P, Cai C, Liu J, et al. 2023. Solvent-free synthesis of hollow carbon nanostructures for efficient sodium storage. *ACS Nano* 17(22):23152–23159

[36] Zhang L, Zhang H, Liu K, Hou J, Badamdorj B, et al. 2023. In-situ synthesis of –P=N-doped carbon nanofibers for single-atom catalytic hydrosilylation. *Advanced Materials* 35(15):e2209310

[37] Smolka W, Dlugon E, Jelen P, Niemiec W, Panek A, et al. 2019. Carbon nanofibers coated with silicon/calcium-based compounds for medical application. *Journal of Nanomaterials* 2019:7172641

[38] Wang S, Zhao X, Yin X, Yu J, Ding B. 2016. Electret polyvinylidene fluoride nanofibers hybridized by polytetrafluoroethylene nanoparticles for high-efficiency air filtration. *ACS Applied Materials & Interfaces* 8(36):23985–23994

[39] Lavagna L, Bartoli M, Musso S, Suarez-Riera D, Tagliaferro A, et al. 2022. A first assessment of carbon nanotubes grown on oil-well cement via chemical vapor deposition. *Nanomaterials* 12(14):2346

[40] Ando Y, Zhao X, Sugai T, Kumar M. 2004. Growing carbon nanotubes. *Materials Today* 7(10):22–29

[41] Chrzanowska J, Hoffman J, Małolepszy A, Mazurkiewicz M, Kowalewski TA, et al. 2015. Synthesis of carbon nanotubes by the laser ablation method: effect of laser wavelength. *Physica Status Solidi B* 252(8):1860–1867

[42] Arenal R, Lopez-Bezanilla A. 2014. *In situ* formation of carbon nanotubes encapsulated within boron nitride nanotubes *via* electron irradiation. *ACS Nano* 8(8):8419–8425

[43] Lin CC, Lin YW. 2015. Synthesis of carbon nanotube/graphene composites by one-step chemical vapor deposition for electrodes of electrochemical capacitors. *Journal of Nanomaterials* 2015:741928

[44] Liu Y, Guo N, Yin P, Zhang C. 2019. Facile growth of carbon nanotubes using microwave ovens: the emerging application of highly efficient domestic plasma reactors. *Nanoscale Advances* 1(12):4546–4559

[45] Druzhinina T, Weltjens W, Hoeppener S, Schubert US. 2009. The selective heating of iron nanoparticles in a single-mode microwave for the patterned growths of carbon nanofibers and nanotubes. *Advanced Functional Materials* 19(8):1287–1292

[46] Yoon DM, Yoon BJ, Lee KH, Kim HS, Park CG. 2006. Synthesis of carbon nanotubes from solid carbon sources by direct microwave irradiation. *Carbon* 44(7):1339–1343

[47] Nie H, Cui M, Russell TP. 2013. A route to rapid carbon nanotube growth. *Chemical Communications* 49(45):5159–5161

[48] Mahar B, Laslau C, Yip R, Sun Y. 2007. Development of carbon nanotube-based sensors—a review. *IEEE Sensors Journal* 7(1–2):266–284

[49] Avraham ES, Westover AS, Girshevitz O, Pint CL, Nessim GD. 2019. Modulating the height of carbon nanotube forests by controlling the molybdenum thin film reservoir thickness. *Nanoscale* 11(4):1929–1936

[50] Liu C, Li S, Wu Z, Yang J, Qin J, et al. 2025. Microwave-assisted catalytic upcycling of plastic wastes over heterojunction-structured layered triple oxides. *ACS Applied Materials & Interfaces* 17(19):28188–28198

[51] Lee BS, Yang HS, Yu WR. 2014. Fabrication of double-tubular carbon nanofibers using quadruple coaxial electrospinning. *Nanotechnology* 25(46):465602

[52] Aboagye A, Elbohy H, Kelkar AD, Qiao Q, Zai J, et al. 2015. Electrospun carbon nanofibers with surface-attached platinum nanoparticles as cost-effective and efficient counter electrode for dye-sensitized solar cells. *Nano Energy* 11:550–556

[53] Li W, Li M, Wang M, Zeng L, Yu Y. 2015. Electrospinning with partially carbonization in air: highly porous carbon nanofibers optimized for high-performance flexible lithium-ion batteries. *Nano Energy* 13:693–701

[54] Simon A, Seyring M, Kämnitz S, Richter H, Voigt I, et al. 2015. Carbon nanotubes and carbon nanofibers fabricated on tubular porous Al_2O_3 substrates. *Carbon* 90:25–33

[55] Xing Y, Wang Y, Zhou C, Zhang S, Fang B. 2014. Simple synthesis of mesoporous carbon nanofibers with hierarchical nanostructure for ultrahigh lithium storage. *ACS Applied Materials & Interfaces* 6(4):2561–2567

[56] Ren J, Li FF, Lau J, González-Urbina L, Licht S. 2015. One-pot synthesis of carbon nanofibers from CO_2. *Nano Letters* 15(9):6142–6148

[57] Mori S, Suzuki M. 2009. Catalyst-free low-temperature growth of carbon nanofibers by microwave plasma-enhanced CVD. *Thin Solid Films* 517(14):4264–4267

[58] Bigdeli S, Fatemi S. 2015. Fast carbon nanofiber growth on the surface of activated carbon by microwave irradiation: a modified nano-adsorbent for deep desulfurization of liquid fuels. *Chemical Engineering Journal* 269:306–315

[59] Gupta VK, Agarwal S, Tyagi I, Sohrabi M, Fakhri A, et al. 2016. Microwave-assisted hydrothermal synthesis and adsorption properties of carbon nanofibers for methamphetamine removal from aqueous solution using a response surface methodology. *Journal of Industrial and Engineering Chemistry* 41:158–164

[60] Deeney C, McKiernan EP, Belhout SA, Rodriguez BJ, Redmond G, et al. 2019. Template-assisted synthesis of luminescent carbon nanofibers from beverage-related precursors by microwave heating. *Molecules* 24(8):1455

[61] Li Z, Chen L, Meng S, Guo L, Huang J, et al. 2015. Field and temperature dependence of intrinsic diamagnetism in graphene: theory and experiment. *Physical Review B* 91(9):094429

[62] Novoselov KS, Geim AK, Morozov SV, Jiang D, Zhang Y, et al. 2004. Electric field effect in atomically thin carbon films. *Science* 306(5696):666–669

[63] Ding J, Rahman OU, Peng W, Dou H, Yu H. 2018. A novel hydroxyl epoxy phosphate monomer enhancing the anticorrosive performance of waterborne Graphene/Epoxy coatings. *Applied Surface Science* 427:981–991

[64] Lee D, Lee B, Park KH, Ryu HJ, Jeon S, et al. 2015. Scalable exfoliation process for highly soluble boron nitride nanoplatelets by hydroxide-assisted ball milling. *Nano Letters* 15(2):1238–1244

[65] Novoselov KS, Fal'ko VI, Colombo L, Gellert PR, Schwab MG, et al. 2012. A roadmap for graphene. *Nature* 490(7419):192–200

[66] Balandin AA, Ghosh S, Bao W, Calizo I, Teweldebrhan D, et al. 2008. Superior thermal conductivity of single-layer graphene. *Nano Letters* 8(3):902–907

[67] Lee JU, Yoon D, Cheong H. 2012. Estimation of Young's modulus of graphene by Raman spectroscopy. *Nano Letters* 12(9):4444–4448
[68] Zhu Y, Murali S, Cai W, Li X, Suk JW, et al. 2010. Graphene and graphene oxide: synthesis, properties, and applications. *Advanced Materials* 22(35):3906–3924
[69] Lu SY, Jin M, Zhang Y, Niu YB, Gao J, et al. 2018. Chemically exfoliating biomass into a graphene-like porous active carbon with rational pore structure, good conductivity, and large surface area for high-performance supercapacitors. *Advanced Energy Materials* 8(11):1702545
[70] Jiang MJ, Zhang Y, Wu G, Chen SC, Chen L, et al. 2019. NIR light manipulated "paper art" for customizing devices with sophisticated structure from DA-epoxy/graphene composites. *Composites Part B: Engineering* 177:107369
[71] Pandey S, Karakoti M, Surana K, Dhapola PS, SanthiBhushan B, et al. 2021. Graphene nanosheets derived from plastic waste for the application of DSSCs and supercapacitors. *Scientific Reports* 11(1):3916
[72] Kittusamy RK, Rajagopal V, Felix PG. 2023. Numerical and experimental investigation on the melting heat transfer of nanographene-enhanced phase change material composites for thermal energy storage applications. *International Journal of Heat and Mass Transfer* 206:123940
[73] He G, Huang S, Villalobos LF, Zhao J, Mensi M, et al. 2019. High-permeance polymer-functionalized single-layer graphene membranes that surpass the postcombustion carbon capture target. *Energy & Environmental Science* 12(11):3305–3312
[74] Seo DH, Pineda S, Woo YC, Xie M, Murdock AT, et al. 2018. Anti-fouling graphene-based membranes for effective water desalination. *Nature Communications* 9:683
[75] Hashmi A, Nayak V, Singh KR, Jain B, Baid M, et al. 2022. Potentialities of graphene and its allied derivatives to combat against SARS-CoV-2 infection. *Materials Today Advances* 13:100208
[76] Jirimali H, Singh J, Boddula R, Lee JK, Singh V. 2022. Nano-structured carbon: its synthesis from renewable agricultural sources and important applications. *Materials* 15(11):3969
[77] Poorna A, Saravanathamizhan R, Balasubramanian N. 2021. Graphene and graphene-like structure from biomass for Electrochemical Energy Storage application - a review. *Electrochemical Science Advances* 1(3):e2000028
[78] Qiu S, Li W, Zheng W, Zhao H, Wang L. 2017. Synergistic effect of polypyrrole-intercalated graphene for enhanced corrosion protection of aqueous coating in 3.5% NaCl solution. *ACS Applied Materials & Interfaces* 9(39):34294–34304
[79] Chen K, Shi L, Zhang Y, Liu Z. 2018. Scalable chemical-vapour-deposition growth of three-dimensional graphene materials towards energy-related applications. *Chemical Society Reviews* 47(9):3018–3036
[80] Song M, Kitipornchai S, Yang J. 2017. Free and forced vibrations of functionally graded polymer composite plates reinforced with graphene nanoplatelets. *Composite Structures* 159:579–588
[81] Bhattacharjee S, MacIntyre CR, Wen X, Bahl P, Kumar U, et al. 2020. Nanoparticles incorporated graphene-based durable cotton fabrics. *Carbon* 166:148–163
[82] Ren PG, Yan DX, Ji X, Chen T, Li ZM. 2011. Temperature dependence of graphene oxide reduced by hydrazine hydrate. *Nanotechnology* 22(5):055705
[83] Zhang J, Yang H, Shen G, Cheng P, Zhang J, et al. 2010. Reduction of graphene oxide *via* L-ascorbic acid. *Chemical Communications* 46(7):1112–1114
[84] Calderon-Ayala G, Cortez-Valadez M, Mani-Gonzalez PG, Britto Hurtado R, Contreras-Rascon JI, et al. 2017. Green synthesis of reduced graphene oxide using ball milling. *Carbon Letters* 21(1):93–97
[85] De Silva KKH, Huang HH, Joshi R, Yoshimura M. 2020. Restoration of the graphitic structure by defect repair during the thermal reduction of graphene oxide. *Carbon* 166:74–90
[86] Lyu J, Mayyas M, Salim O, Zhu H, Chu D, et al. 2019. Electrochemical performance of hydrothermally synthesized rGO based electrodes. *Materials Today Energy* 13:277–284
[87] Tan H, Wang D, Guo Y. 2018. Thermal growth of graphene: a review. *Coatings* 8(1):40
[88] Kumar PV, Bardhan NM, Chen GY, Li Z, Belcher AM, et al. 2016. New insights into the thermal reduction of graphene oxide: impact of oxygen clustering. *Carbon* 100:90–98
[89] Toh SY, Loh KS, Kamarudin SK, Daud WRW. 2014. Graphene production *via* electrochemical reduction of graphene oxide: synthesis and characterisation. *Chemical Engineering Journal* 251:422–434
[90] Marrani AG, Motta A, Schrebler R, Zanoni R, Dalchiele EA. 2019. Insights from experiment and theory into the electrochemical reduction mechanism of graphene oxide. *Electrochimica Acta* 304:231–238
[91] Marrani AG, Coico AC, Giacco D, Zanoni R, Scaramuzzo FA, et al. 2018. Integration of graphene onto silicon through electrochemical reduction of graphene oxide layers in non-aqueous medium. *Applied Surface Science* 445:404–414
[92] Aunkor MTH, Mahbubul IM, Saidur R, Metselaar HSC. 2016. The green reduction of graphene oxide. *RSC Advances* 6(33):27807–27828
[93] Zhang Y, Hao H, Wang L. 2016. Effect of morphology and defect density on electron transfer of electrochemically reduced graphene oxide. *Applied Surface Science* 390:385–392
[94] Mohandoss M, Gupta SS, Nelleri A, Pradeep T, Maliyekkal SM. 2017. Solar mediated reduction of graphene oxide. *RSC Advances* 7(2):957–963
[95] Todorova N, Giannakopoulou T, Boukos N, Vermisoglou E, Lekakou C, et al. 2017. Self-propagating solar light reduction of graphite oxide in water. *Applied Surface Science* 391:601–608
[96] Han DD, Zhang YL, Jiang HB, Xia H, Feng J, et al. 2015. Moisture-responsive graphene paper prepared by self-controlled photoreduction. *Advanced Materials* 27(2):332–338
[97] Schwenke AM, Hoeppener S, Schubert US. 2015. Synthesis and modification of carbon nanomaterials utilizing microwave heating. *Advanced Materials* 27(28):4113–4141
[98] Li Z, Yao Y, Lin Z, Moon KS, Lin W, et al. 2010. Ultrafast, dry microwave synthesis of graphene sheets. *Journal of Materials Chemistry* 20(23):4781–4783
[99] Voiry D, Yang J, Kupferberg J, Fullon R, Lee C, et al. 2016. High-quality graphene *via* microwave reduction of solution-exfoliated graphene oxide. *Science* 353(6306):1413–1416
[100] Jiang WS, Yang C, Chen GX, Yan XQ, Chen SN, et al. 2018. Preparation of high-quality graphene using triggered microwave reduction under an air atmosphere. *Journal of Materials Chemistry C* 6(7):1829–1835
[101] Wan J, Huang L, Wu J, Xiong L, Hu Z, et al. 2018. Microwave combustion for rapidly synthesizing pore-size-controllable porous graphene. *Advanced Functional Materials* 28(22):1800382
[102] Zhao Y, He J. 2019. Novel template-assisted microwave conversion of graphene oxide to graphene patterns: a reduction transfer mechanism. *Carbon* 148:159–163
[103] Han HJ, Chen YN, Wang ZJ. 2015. Effect of microwave irradiation on reduction of graphene oxide films. *RSC Advances* 5(113):92940–92946
[104] Zedan AF, Sappal S, Moussa S, El-Shall MS. 2010. Ligand-controlled microwave synthesis of cubic and hexagonal CdSe nanocrystals supported on graphene photoluminescence quenching by graphene. *The Journal of Physical Chemistry C* 114(47):19920–19927
[105] Kumar D, Raghavan CM, Sridhar C, Shin JH, Ryu SH, et al. 2015. Microwave-assisted synthesis, characterization of reduced graphene oxide, and its antibacterial activity. *Bulletin of the Korean Chemical Society* 36(8):2034–2038
[106] Wu W, Liu M, Gu Y, Guo B, Ma H, et al. 2020. Fast chemical exfoliation of graphite to few-layer graphene with high quality and large size via a two-step microwave-assisted process. *Chemical Engineering Journal* 381:122592
[107] Eswaraiah V, Aravind SSJ, Ramaprabhu S. 2011. Top down method for synthesis of highly conducting graphene by exfoliation of graphite oxide using focused solar radiation. *Journal of Materials Chemistry* 21(19):6800–6803
[108] Mohanapriya K, Ghosh G, Jha N. 2016. Solar light reduced graphene as high energy density supercapacitor and capacitive deionization electrode. *Electrochimica Acta* 209:719–729

[109] Liu Z, Niu W, Chu H, Zhou T, Niu Z. 2018. Effect of the carbonization temperature on the properties of biochar produced from the pyrolysis of crop residues. *BioResources* 13(2):3429–3446

[110] Wu Z, Huang X, Chen R, Mao X, Qi X. 2022. The United States and China on the paths and policies to carbon neutrality. *Journal of Environmental Management* 320:115785

[111] Xiang W, Zhang X, Cao C, Quan G, Wang M, et al. 2022. Microwave-assisted pyrolysis derived biochar for volatile organic compounds treatment: characteristics and adsorption performance. *Bioresource Technology* 355:127274

[112] Gu X, Ma X, Li L, Liu C, Cheng K, et al. 2013. Pyrolysis of poplar wood sawdust by TG-FTIR and Py–GC/MS. *Journal of Analytical and Applied Pyrolysis* 102:16–23

[113] So CL, Eberhardt TL. 2018. FTIR-based models for assessment of mass yield and biofuel properties of torrefied wood. *Wood Science and Technology* 52(1):209–227

[114] Balat M. 2008. Mechanisms of thermochemical biomass conversion processes. Part 1: reactions of pyrolysis. *Energy Sources, Part A: Recovery, Utilization and Environmental Effects* 30(7):620–635

[115] Li Y, Liu H, Xiao K, Liu X, Hu H, et al. 2019. Correlations between the physicochemical properties of hydrochar and specific components of waste lettuce: influence of moisture, carbohydrates, proteins and lipids. *Bioresource Technology* 272:482–488

[116] Shahbeik H, Peng W, Panahi HKS, Dehhaghi M, Guillemin GJ, et al. 2022. Synthesis of liquid biofuels from biomass by hydrothermal gasification: a critical review. *Renewable and Sustainable Energy Reviews* 167:112833

[117] Zhang W, Chen Q, Chen J, Xu D, Zhan H, et al. 2023. Machine learning for hydrothermal treatment of biomass: a review. *Bioresource Technology* 370:128547

[118] Funke A, Ziegler F. 2010. Hydrothermal carbonization of biomass: a summary and discussion of chemical mechanisms for process engineering. *Biofuels Bioproducts and Biorefining* 4(2):160–177

[119] Chen C, Fan D, Ling H, Huang X, Yang G, et al. 2022. Microwave catalytic co-pyrolysis of *Chlorella vulgaris* and high density polyethylene over activated carbon supported monometallic: characteristics and bio-oil analysis. *Bioresource Technology* 363:127881

[120] Ke C, Zhang Y, Gao Y, Pan Y, Li B, et al. 2019. Syngas production from microwave-assisted air gasification of biomass: part 1 model development. *Renewable Energy* 140:772–778

[121] Zhang Y, Ke C, Gao Y, Liu S, Pan Y, et al. 2019. Syngas production from microwave-assisted air gasification of biomass: part 2 model validation. *Renewable Energy* 140:625–632

[122] Fodah AEM, Ghosal MK, Behera D. 2021. Quality assessment of bio-oil and biochar from microwave-assisted pyrolysis of corn stover using different adsorbents. *Journal of the Energy Institute* 98:63–76

[123] Fan S, Cui L, Li H, Guang M, Liu H, et al. 2023. Value-added biochar production from microwave pyrolysis of peanut shell. *International Journal of Chemical Reactor Engineering* 21(8):1035–1046

[124] Aniza R, Chen WH, Yang FC, Pugazhendh A, Singh Y. 2022. Integrating Taguchi method and artificial neural network for predicting and maximizing biofuel production *via* torrefaction and pyrolysis. *Bioresource Technology* 343:126140

[125] Gronnow MJ, Budarin VL, Mašek O, Crombie KN, Brownsort PA, et al. 2013. Torrefaction/biochar production by microwave and conventional slow pyrolysis–comparison of energy properties. *GCB Bioenergy* 5(2):144–152

[126] Selvam SM, Paramasivan B. 2022. Microwave assisted carbonization and activation of biochar for energy-environment nexus: a review. *Chemosphere* 286(1):131631

[127] Li M, Li Y, Lu C, Wei T, Ahmed M, et al. 2025. Microwave pyrolysis of rapeseed straw for low sulfur content and high heating value (HHV) solid fuel production: transformation mechanism and form of sulfur in biochar during the pyrolysis process. *Energy* 326:136381

[128] Huang YF, Sung HT, Chiueh PT, Lo SL. 2017. Microwave torrefaction of sewage sludge and leucaena. *Journal of the Taiwan Institute of Chemical Engineers* 70:236–243

[129] Zhang J, Zuo W, Tian Y, Chen L, Yin L, et al. 2017. Sulfur transformation during microwave and conventional pyrolysis of sewage sludge. *Environmental Science & Technology* 51(1):709–717

[130] Gómez N, Banks SW, Nowakowski DJ, Rosas JG, Cara J, et al. 2018. Effect of temperature on product performance of a high ash biomass during fast pyrolysis and its bio-oil storage evaluation. *Fuel Processing Technology* 172:97–105

[131] Reza MT, Lynam JG, Uddin MH, Coronella CJ. 2013. Hydrothermal carbonization: fate of inorganics. *Biomass and Bioenergy* 49:86–94

[132] Lin Y, Ge Y, He Q, Chen P, Xiao H. 2022. The redistribution and migration mechanism of chlorine during hydrothermal carbonization of waste biomass and fuel properties of hydrochars. *Energy* 244:122578

[133] Chu G, Zhao J, Chen F, Dong X, Zhou D, et al. 2017. Physi-chemical and sorption properties of biochars prepared from peanut shell using thermal pyrolysis and microwave irradiation. *Environmental Pollution* 227:372–379

[134] Parvez AM, Afzal MT, Jiang P, Wu T. 2020. Microwave-assisted biomass pyrolysis polygeneration process using a scaled-up reactor: product characterization, thermodynamic assessment and bio-hydrogen production. *Biomass and Bioenergy* 139:105651

[135] Nzediegwu C, Arshad M, Ulah A, Naeth MA, Chang SX. 2021. Fuel, thermal and surface properties of microwave-pyrolyzed biochars depend on feedstock type and pyrolysis temperature. *Bioresource Technology* 320:124282

[136] Fodah AEM, Ghosal MK, Behera D. 2021. Bio-oil and biochar from microwave-assisted catalytic pyrolysis of corn stover using sodium carbonate catalyst. *Journal of the Energy Institute* 94:242–251

[137] Liew RK, Nam WL, Chong MY, Phang XY, Su MH, et al. 2018. Oil palm waste: an abundant and promising feedstock for microwave pyrolysis conversion into good quality biochar with potential multi-applications. *Process Safety and Environmental Protection* 115:57–69

[138] Kumar NV, Sawargaonkar GL, Rani CS, Singh A, Prakash TR, et al. 2023. Comparative analysis of pigeonpea stalk biochar characteristics and energy use under different biochar production methods. *Sustainability* 15(19):1–17

[139] Lin YL, Zheng NY, Cheng HJ, Chang CC. 2024. Blending *Saccharum* bagasse and waste cooking oil for biofuel production via microwave co-torrefaction process. *Fuel* 367:131349

[140] Zhou J, Liu S, Zhou N, Fan L, Zhang Y, et al. 2018. Development and application of a continuous fast microwave pyrolysis system for sewage sludge utilization. *Bioresource Technology* 256:295–301

[141] Ali BM, Salih MI, Abdulqader MA, Bakthavatchalam B, Hussein OA. 2024. Dehydration and decarboxylation *via* pyrolysis process of waste oily sludge accumulated at North Refineries Company Baiji for use as a pyro-fuel. *Desalination and Water Treatment* 318:100330

[142] Foong SY, Latiff NSA, Liew RK, Yek PNY, Lam SS. 2020. Production of biochar for potential catalytic and energy applications *via* microwave vacuum pyrolysis conversion of cassava stem. *Materials Science for Energy Technologies* 3:728–733

[143] Salema AA, Afzal MT, Bennamoun L. 2017. Pyrolysis of corn stalk biomass briquettes in a scaled-up microwave technology. *Bioresource Technology* 233:353–362

[144] Rajasekhar Reddy B, Vinu R. 2018. Microwave-assisted co-pyrolysis of high ash Indian coal and rice husk: product characterization and evidence of interactions. *Fuel Processing Technology* 178:41–52

[145] Ge S, Foong SY, Ma NL, Liew RK, Wan Mahari WA, et al. 2020. Vacuum pyrolysis incorporating microwave heating and base mixture modification: an integrated approach to transform biowaste into eco-friendly bioenergy products. *Renewable and Sustainable Energy Reviews* 127:109871

[146] Nhuchhen DR, Afzal MT, Dreise T, Salema AA. 2018. Characteristics of biochar and bio-oil produced from wood pellets pyrolysis using a bench scale fixed bed, microwave reactor. *Biomass and Bioenergy* 119:293–303

[147] Zhang C, Wang C, Cao G, Chen WH, Ho SH. 2019. Comparison and characterization of property variation of microalgal biomass with non-oxidative and oxidative torrefaction. *Fuel* 246:375–385

[148] Chen WH, Arpia AA, Chang JS, Kwon EE, Park YK, et al. 2022. Catalytic microwave torrefaction of microalga *Chlorella vulgaris* FSP-E with magnesium oxide optimized *via* taguchi approach: a thermo-energetic analysis. *Chemosphere* 290:133374

[149] Shakiba A, Aliasghar A, Moazeni K, Pazoki M. 2023. Hydrothermal carbonization of sewage sludge with sawdust and corn stalk: optimization of process parameters and characterization of hydrochar. *Bioenergy Research* 16(4):2386–2397
[150] Arpia AA, Chen WH, Ubando AT, Tabatabaei M, Lam SS, et al. 2021. Catalytic microwave-assisted torrefaction of sugarcane bagasse with calcium oxide optimized *via* Taguchi approach: product characterization and energy analysis. *Fuel* 305:121543
[151] Idris R, Chong WWF, Ali A, Idris S, Hasan MF, et al. 2021. Phenol-rich bio-oil derivation *via* microwave-induced fast pyrolysis of oil palm empty fruit bunch with activated carbon. *Environmental Technology & Innovation* 21:101291
[152] Zhou C, Zhang Y, Liu Y, Deng Z, Li X, et al. 2021. Co-pyrolysis of textile dyeing sludge and red wood waste in a continuously operated auger reactor under microwave irradiation. *Energy* 218:119398
[153] Mong GR, Chong CT, Ng JH, Chong WWF, Lam SS, et al. 2020. Microwave pyrolysis for valorisation of horse manure biowaste. *Energy Conversion and Management* 220:113074
[154] Haeldermans T, Claesen J, Maggen J, Carleer R, Yperman J, et al. 2019. Microwave assisted and conventional pyrolysis of MDF–characterization of the produced biochars. *Journal of Analytical and Applied Pyrolysis* 138:218–230
[155] Ellison CR, Hoff R, Mărculescu C, Boldor D. 2020. Investigation of microwave-assisted pyrolysis of biomass with char in a rectangular waveguide applicator with built-in phase-shifting. *Applied Energy* 259:114217
[156] Lin J, Sun S, Xu D, Cui C, Ma R, et al. 2022. Microwave directional pyrolysis and heat transfer mechanisms based on multiphysics field stimulation: design porous biochar structure via controlling hotspots formation. *Chemical Engineering Journal* 429:132195
[157] Foong SY, Liew RK, Yang Y, Cheng YW, Yek PNY, et al. 2020. Valorization of biomass waste to engineered activated biochar by microwave pyrolysis: progress, challenges, and future directions. *Chemical Engineering Journal* 389:124401
[158] Kumar NS, Grekov D, Pré P, Alappat BJ. 2020. Microwave mode of heating in the preparation of porous carbon materials for adsorption and energy storage applications–an overview. *Renewable and Sustainable Energy Reviews* 124:109743
[159] Arpia AA, Chen WH, Lam SS, Rousset P, de Luna MDG. 2021. Sustainable biofuel and bioenergy production from biomass waste residues using microwave-assisted heating: a comprehensive review. *Chemical Engineering Journal* 403:126233
[160] Fang Z, Liu F, Li Y, Li B, Yang T, et al. 2021. Influence of microwave-assisted pyrolysis parameters and additives on phosphorus speciation and transformation in phosphorus-enriched biochar derived from municipal sewage sludge. *Journal of Cleaner Production* 287:125550
[161] Duarah P, Debnath B, Purkait MK. 2024. Synthesis of antibacterial fluorescent carbon dots and green coal-like hydrochar from tea Industry byproducts *via* hydrothermal carbonization. *Industrial Crops and Products* 221:119364
[162] Zhang X, Xu H, Xiang W, You X, Dai H, et al. 2024. Lignin-impregnated biochar assisted with microwave irradiation for CO_2 capture: adsorption performance and mechanism. *Biochar* 6(1):22
[163] Zhang X, Xiang W, Miao X, Li F, Qi G, et al. 2022. Microwave biochars produced with activated carbon catalyst: characterization and sorption of volatile organic compounds (VOCs). *Science of The Total Environment* 827:153996
[164] Zhang L, Ai T, Tian X, Xu C, Wu Y, et al. 2022. Microwave-assisted preparation of Ag/Fe magnetic biochar from clivia leaves for adsorbing daptomycin antibiotics. *Open Chemistry* 20(1):388–400
[165] Luo Y, Lin Q, Liu Y, Zheng J, Zeng C, et al. 2025. Construction of waste-modified biochar as a means for the efficient removal of BDE209 from soil *via* microwaves: a novel low-toxicity degradation pathway. *Journal of Environmental Chemical Engineering* 13(3):116173
[166] Wan Z, Sun Y, Tsang DCW, Xu Z, Khan E, et al. 2020. Sustainable impact of tartaric acid as electron shuttle on hierarchical iron-incorporated biochar. *Chemical Engineering Journal* 395:125138
[167] Zhang Y, He M, Wang L, Yan J, Ma B, et al. 2022. Biochar as construction materials for achieving carbon neutrality. *Biochar* 4(1):59
[168] Qiu T, Li C, Zhao W, Naz MY, Zhang Y. 2025. Microwave-assisted pyrolysis of biomass: influence of feedstock and pyrolysis parameters on porous biochar properties. *Biomass and Bioenergy* 193:107583
[169] Chatterjee R, Sajjadi B, Chen WY, Mattern DL, Hammer N, et al. 2020. Effect of pyrolysis temperature on PhysicoChemical properties and acoustic-based amination of biochar for efficient CO_2 adsorption. *Frontiers in Energy Research* 8:85
[170] Fernandes BCC, Mendes KF, Tornisielo VL, Teófilo TMS, Takeshita V, et al. 2022. Effect of pyrolysis temperature on eucalyptus wood residues biochar on availability and transport of hexazinone in soil. *International Journal of Environmental Science and Technology* 19(1):499–514
[171] Hu E, Tian Y, Yang Y, Dai C, Li M, et al. 2022. Pyrolysis behaviors of corn stover in new two-stage rotary kiln with baffle. *Journal of Analytical and Applied Pyrolysis* 161:105398
[172] Hu E, Shang S, Wang N, Nan X, Zhong S, et al. 2019. Influence of the pyrolytic temperature and feedstock on the characteristics and naphthalene adsorption of crop straw-derived biochars. *BioResources* 14(2):2885–2902
[173] Chen Y, Li C, Zhang L, Zhang S, Wang Y, et al. 2025. Inherent water in green pine needles and cypress leaves induces self-activation in microwave pyrolysis. *Fuel* 379:133101
[174] Hu J, Mi B, Chen L, Yuan Y, Zhang J, et al. 2024. An economical preparation strategy of magnetic biochar with high specific surface area for efficient removal of methyl orange. *International Journal of Biological Macromolecules* 276(1):134156
[175] Jiang Y, Zhang K, Li C, Shao Y, Zhang L, et al. 2024. Investigation of interactions of nickel with pyrolytic products in pyrolysis of poplar with nickel acetate via furnace or microwave heating. *Journal of Industrial and Engineering Chemistry* 134:123–36
[176] Charmas B, Wawrzaszek B, Jedynak K. 2024. Effect of pyrolysis temperature and hydrothermal activation on structure, physicochemical, thermal and dye adsorption characteristics of the biocarbons. *Chemphyschem* 25(4):e202300773
[177] Huang YF, Chiueh PT, Shih CH, Lo SL, Sun L, et al. 2015. Microwave pyrolysis of rice straw to produce biochar as an adsorbent for CO_2 capture. *Energy* 84:75–82
[178] Lin J, Xu Z, Zhang Q, Cao Y, Mašek O, et al. 2024. Enhanced adsorption of aromatic VOCs on hydrophobic porous biochar produced *via* microwave rapid pyrolysis. *Bioresource Technology* 393:130085
[179] Brickler CA, Wu Y, Li S, Anandhi A, Chen G. 2021. Comparing physicochemical properties and sorption behaviors of pyrolysis-derived and microwave-mediated biochar. *Sustainability* 13(4):2359
[180] Song X, Zhang Y, Cao N, Sun D, Zhang Z, et al. 2021. Sustainable chromium (VI) removal from contaminated groundwater using nano-magnetite-modified biochar *via* rapid microwave synthesis. *Molecules* 26(1):103
[181] Qi G, Pan Z, Zhang X, Chang S, Wang H, et al. 2023. Microwave biochar produced with activated carbon catalyst: characterization and adsorption of heavy metals. *Environmental Research* 216(4):114732
[182] Antunes E, Jacob MV, Brodie G, Schneider PA. 2017. Silver removal from aqueous solution by biochar produced from biosolids via microwave pyrolysis. *Journal of Environmental Management* 203:264–272
[183] Sui H, Chen Y, Chen H, Zhao Y, Tian C, et al. 2025. Characterization and mechanistic insights into coke formation on biochar-based catalysts under microwave-assisted biomass pyrolysis. *Industrial Crops and Products* 226:120645
[184] Wang Y, Liu Z, Deng H, Cao P, Tan T, et al. 2024. Study on the properties and components of solid-liquid products by co-pyrolysis of sludge and cotton stalk. *Journal of Analytical and Applied Pyrolysis* 182:106712
[185] An Q, Liu Y, Cao X, Yang P, Cheng L, et al. 2024. Microwave catalytic pyrolysis of solid digestate for high quality bio-oil and biochar. *Journal of Analytical and Applied Pyrolysis* 182:106683
[186] Leite JCS, Suota MJ, Ramos LP, Lenzi MK, Luz LFL Jr. 2024. Development of a microwave-assisted bench reactor for biomass pyrolysis using hybrid heating. *ACS Omega* 9(23):24987–24997

[187] Correia I, Ilkaeva M, Castellino M, Bocchini S, Novais RM, et al. 2024. Impact of pyrolysis heating methods on biochars with enhanced CO_2/N_2 separation and their incorporation in 3D-printed composites. *Journal of Environmental Chemical Engineering* 12(5):113875

[188] Minaei S, Benis KZ, McPhedran KN, Soltan J. 2024. Adsorption of sulfamethoxazole and lincomycin from single and binary aqueous systems using acid-modified biochar from activated sludge biomass. *Journal of Environmental Management* 358:120742

[189] Nazari M, Aguilar MM, Ghislain T, Lavoie JM. 2024. Microwave-assisted pyrolysis of biomass waste for production of high-quality biochar: corn stover and hemp stem case studies. *Biomass and Bioenergy* 187:107302

[190] Tsai WT, Kuo LA, Tsai CH, Huang HL, Yang RY, et al. 2023. Production of porous biochar from cow dung using microwave process. *Materials* 16(24):7667

[191] Nam WL, Phang XY, Su MH, Liew RK, Ma NL, et al. 2018. Production of bio-fertilizer from microwave vacuum pyrolysis of palm kernel shell for cultivation of Oyster mushroom (*Pleurotus ostreatus*). *Science of The Total Environment* 624:9–16

[192] Kuo LA, Tsai WT, Yang RY, Tsai JH. 2023. Production of high-porosity biochar from rice husk by the microwave pyrolysis process. *Processes* 11(11):3119

[193] Mabaso T, Lo SL, Chiueh PT. 2024. Effect of pyrolytic temperature on the adsorption of Pb (II) from synthetic wastewater onto bamboo chopstick biochar: a conventional vs. microwave-assisted pyrolysis approach. *Sustainable Environment Research* 34(1):31

[194] Qi G, Pan Z, Zhang X, Wang H, Chang S, et al. 2024. Novel pretreatment with hydrogen peroxide enhanced microwave biochar for heavy metals adsorption: characterization and adsorption performance. *Chemosphere* 346:140580

[195] Nguyen DK, Dinh VP. 2025. Highly efficient removal of Cr (VI) by biochar derived from vietnamese young durian fruit: comparison of traditional and microwave-assisted pyrolysis. *Langmuir* 41(1):518–531

[196] Benis KZ, Minaei S, Soltan J, McPhedran KN. 2022. Adsorption of lincomycin on microwave activated biochar: batch and dynamic adsorption. *Chemical Engineering Research and Design* 187:140–150

[197] Luo J, Chen Y, Huang H, Ma R, Ma N, et al. 2023. Microwave-coordinated KOH directionally modulated N/O co-doped porous biochar from Enteromorpha and its structure-effect relationships in efficient CO_2 capture. *Chemical Engineering Journal* 473:145279

[198] dos Reis GS, Bergna D, Tuomikoski S, Grimm A, Lima EC, et al. 2022. Preparation and characterization of pulp and paper mill sludge-activated biochars using alkaline activation: a box–behnken design approach. *ACS Omega* 7(36):32620–32630

[199] Zamiri MA, Niu CH. 2022. Development and characterization of novel activated carbons based on reed canary grass. *Industrial Crops and Products* 187(A):115316

[200] Sousa ÉML, Otero M, Rocha LS, Gil MV, Ferreira P, et al. 2022. Multivariable optimization of activated carbon production from microwave pyrolysis of brewery wastes - application in the removal of antibiotics from water. *Journal of Hazardous Materials* 431:128556

[201] Liu C, Wang H, Karim AM, Sun J, Wang Y. 2014. Catalytic fast pyrolysis of lignocellulosic biomass. *Chemical Society Reviews* 43(22):7594–7623

[202] Sharma A, Pareek V, Zhang D. 2015. Biomass pyrolysis—a review of modelling, process parameters and catalytic studies. *Renewable and Sustainable Energy Reviews* 50:1081–1096

[203] Akazawa M, Kojima Y, Kato Y. 2016. Effect of pyrolysis temperature on the pyrolytic degradation mechanism of β-aryl ether linkages. *Journal of Analytical and Applied Pyrolysis* 118:164–174

[204] Liu WJ, Jiang H, Yu HQ. 2015. Thermochemical conversion of lignin to functional materials: a review and future directions. *Green Chemistry* 17(11):4888–4907

[205] Zhang Y, Fan S, Liu T, Fu W, Li B. 2022. A review of biochar prepared by microwave-assisted pyrolysis of organic wastes. *Sustainable Energy Technologies and Assessments* 50:101873

[206] Motasemi F, Afzal MT. 2013. A review on the microwave-assisted pyrolysis technique. *Renewable and Sustainable Energy Reviews* 28:317–330

[207] Asomaning J, Haupt S, Chae M, Bressler DC. 2018. Recent developments in microwave-assisted thermal conversion of biomass for fuels and chemicals. *Renewable and Sustainable Energy Reviews* 92:642–657

[208] Bundhoo ZMA. 2018. Microwave-assisted conversion of biomass and waste materials to biofuels. *Renewable and Sustainable Energy Reviews* 82:1149–1177

[209] Yin P, Lan D, Lu C, Jia Z, Feng A, et al. 2025. Research progress of structural regulation and composition optimization to strengthen absorbing mechanism in emerging composites for efficient electromagnetic protection. *Journal of Materials Science & Technology* 204:204–223

[210] He M, Hu J, Yan H, Zhong X, Zhang Y, et al. 2025. Shape anisotropic chain-Like CoNi/polydimethylsiloxane composite films with excellent low-frequency microwave absorption and high thermal conductivity. *Advanced Functional Materials* 35(18):2316691

[211] Kumar P, Pathak S, Singh A, Verma R, Khanduri H, et al. 2024. Augmented magnetic nanoparticle assimilation in rGO sheets for tailored static and dynamic magnetic properties in surface functionalized $Co_{0.8}Zn_{0.2}Fe_2O_4$ nanoferrite–rGO hybrid structures. *Journal of Materials Chemistry C* 12(44):18036–18047

[212] Yang H, Jiang X, Sun J, Zhang B, Su X, et al. 2024. Ferrite doped sucrose-derived porous carbon composites inspired by Pharaoh's Serpent for broadband electromagnetic wave absorption. *Journal of Alloys and Compounds* 989:174402

[213] Zhang B, Qu Z, Ruiz-Agudo C, Yang L, Chi B, et al. 2025. Lightweight magnetic carbon nanotube/cellulose nanofibre aerogels with microstructure engineering for enhanced microwave absorption. *Carbon* 234:120020

[214] Meng X, Xu W, Ren X, Zhu M. 2024. Progress and challenges of ferrite matrix microwave absorption materials. *Materials* 17(10):2315

[215] Ma M, Tao W, Liao X, Chen S, Shi Y, et al. 2023. Cellulose nanofiber/MXene/FeCo composites with gradient structure for highly absorbed electromagnetic interference shielding. *Chemical Engineering Journal* 452(4):139471

[216] Xie Y, Guo Y, Cheng T, Zhao L, Wang T, et al. 2023. Efficient electromagnetic wave absorption performances dominated by exchanged resonance of lightweight PC/Fe_3O_4@PDA hybrid nanocomposite. *Chemical Engineering Journal* 457:141205

[217] Gu W, Sheng J, Huang Q, Wang G, Chen J, et al. 2021. Environmentally friendly and multifunctional shaddock peel-based carbon aerogel for thermal-insulation and microwave absorption. *Nano-Micro Letters* 13(1):102

[218] Zhou X, Liu S, Hu Y, He J, Zhang W, et al. 2024. Green synthesis of porous bamboo-based activated carbon with high VOCs adsorption performance *via* steam activation method. *Journal of Porous Materials* 31(2):737–746

[219] Zhu Y, Li Z, Tao Y, Zhou J, Zhang H. 2022. Hierarchical porous carbon materials produced from heavy bio-oil for high-performance supercapacitor electrodes. *Journal of Energy Storage* 47:103624

[220] Xu H, He Z, Li Y, Wang Y, Zhang Z, et al. 2023. Porous magnetic carbon spheres with adjustable magnetic-composition and synergistic effect for lightweight microwave absorption. *Carbon* 213:118290

[221] Du Y, Liu Y, Wang A, Kong J. 2023. Research progress and future perspectives on electromagnetic wave absorption of fibrous materials. *iScience* 26(10):107873

[222] Zhang X, Jia Z, Zhang F, Xia Z, Zou J, et al. 2022. MOF-derived $NiFe_2S_4$/porous carbon composites as electromagnetic wave absorber. *Journal of Colloid and Interface Science* 610:610–620

[223] Liang J, Wei Z, Zhang X, Chen F, Cao X, et al. 2023. Lightweight cementite/Fe anchored in nitrogen-doped carbon with tunable dielectric/magnetic loss and low filler loading achieving high-efficiency microwave absorption. *Carbon* 210:118080

[224] Zhang S, Lan D, Zheng J, Kong J, Gu J, et al. 2024. Perspectives of nitrogen-doped carbons for electromagnetic wave absorption. *Carbon* 221:118925

[225] Hou T, Jia Z, Dong Y, Liu X, Wu G. 2022. Layered 3D structure derived from MXene/magnetic carbon nanotubes for ultra-broadband electromagnetic wave absorption. *Chemical Engineering Journal* 431(1):133919

[226] Li J, Lan D, Cheng Y, Jia Z, Liu P, et al. 2024. Constructing mixed-dimensional lightweight magnetic cobalt-based composites heterostructures: an effective strategy to achieve boosted microwave absorption and self-anticorrosion. *Journal of Materials Science & Technology* 196:60–70
[227] Zhang S, Lan D, Zheng J, Feng A, Pei Y, et al. 2024. Rational construction of heterointerfaces in biomass sugarcane-derived carbon for superior electromagnetic wave absorption. *International Journal of Minerals, Metallurgy and Materials* 31(12):2749–2759
[228] Wang J, Zhang S, Liu Z, Ning T, Yan J, et al. 2023. Graphene-like structure of bio-carbon with CoFe Prussian blue derivative composites for enhanced microwave absorption. *Journal of Colloid and Interface Science* 652:2029–2041
[229] Zhu M, Lei Y, Wu H, Kong L, Xu H, et al. 2022. Porous hybrid scaffold strategy for the realization of lightweight, highly efficient microwave absorbing materials. *Journal of Materials Science & Technology* 129:215–222
[230] Zhao X, Yan J, Huang Y, Liu X, Ding L, et al. 2021. Magnetic porous CoNi@C derived from bamboo fiber combined with metal-organic-framework for enhanced electromagnetic wave absorption. *Journal of Colloid and Interface Science* 595:78–87
[231] Wang D, Zhang M, Guo Y, Bai T, Liu H, et al. 2022. Facile preparation of a cellulose derived carbon/BN composite aerogel for superior electromagnetic wave absorption. *Journal of Materials Chemistry C* 10(13):5311–5320
[232] Zhao X, Zhu D, Wu J, Zhang R, Lu X, et al. 2022. Environmentally friendly a multifunctional cellulose-based carbon foam for superior electromagnetic wave absorption performance. *Composites Communications* 35:101320
[233] Yang S, Sun X, Wang S, Ning Y, Yuan Y, et al. 2022. Electromagnetic wave absorbing properties of coconut shell-derived nanocomposite. *Carbon* 196:354–364
[234] Mou P, Zhao J, Wang G, Shi S, Wan G, et al. 2022. BCN nanosheets derived from coconut shells with outstanding microwave absorption and thermal conductive properties. *Chemical Engineering Journal* 437(2):135285
[235] Wen X, Li C, Liu H, Fan G, Tang Y, et al. 2024. Green carbonization of waste coffee grounds into porous C/Fe hybrids for broadband and high-efficiency microwave absorption. *Journal of Materials Science & Technology* 170:1–10
[236] Lu Z, Wang Y, Di X, Wang N, Cheng R, et al. 2022. Heterostructure design of carbon fiber@graphene@layered double hydroxides synergistic microstructure for lightweight and flexible microwave absorption. *Carbon* 197:466–475
[237] Dong S, Hu P, Li X, Hong C, Zhang X, et al. 2020. $NiCo_2S_4$ nanosheets on 3D wood-derived carbon for microwave absorption. *Chemical Engineering Journal* 398:125588
[238] Lu X, Zhu D, Li X, Li M, Chen Q, et al. 2021. Protein-derived hybrid carbon nanospheres with tunable microwave absorbing performance in the X-band. *ACS Applied Electronic Materials* 3:2685–2693
[239] Liu C, Dong C, Wang S, Yang D, Lei D, et al. 2024. Electromagnetic wave absorbing biomass kelp derived porous carbon anchored by Fe_3O_4 nanocomposites. *Diamond and Related Materials* 146:111211
[240] Lu C, Geng H, Ma J, Zhao J, Wang R, et al. 2023. Hierarchical porous carbon/Co nanocomposites derived from biomass for high-performance microwave absorption. *ACS Applied Nano Materials* 6(18):16778–16789
[241] Liu J, Liu C, Tong Y, Liu C, Sun H, et al. 2023. *In-situ* generated Ni/Ni_3Si to enhance electromagnetic wave absorption properties of Ni/PDCs/biomass ceramic composites. *Colloids and Surfaces A: Physicochemical and Engineering Aspects* 663:131035
[242] Zhang R, Qiao J, Zhang X, Yang Y, Zheng S, et al. 2022. Biomass-derived porous carbon for microwave absorption. *Materials Chemistry and Physics* 289:126437
[243] Wang Y, Di X, Chen J, She L, Pan H, et al. 2022. Multi-dimensional C@NiCo-LDHs@Ni aerogel: structural and componential engineering towards efficient microwave absorption, anti-corrosion and thermal-insulation. *Carbon* 191:625–635
[244] Li Z, Lin H, Wu S, Su X, Wang T, et al. 2022. Rice husk derived porous carbon embedded with Co_3Fe_7 nanoparticles towards microwave absorption. *Composites Science and Technology* 229:109673
[245] Yu W, Wang Z, Lin J, Xiao Y, Zhu L, et al. 2024. Rose-derived porous carbon and in-situ fabrication of cobalt/nickel nanoparticles composites as high-performance electromagnetic wave absorber. *Engineered Science* 30:1113
[246] Ren L, Wang Y, Jia Z, He Q, Wu G. 2022. Controlling the heterogeneous interfaces of Fe_3O_4/N-doped porous carbon *via* facile swelling for enhancing the electromagnetic wave absorption. *Composites Communications* 29:101052
[247] He Y, Wang Y, Ren L, He Q, Wu D, et al. 2022. Construction of heterointerfaces and honeycomb-like structure for ultrabroad microwave absorption. *Journal of Colloid and Interface Science* 627:102–112
[248] Elhassan A, Li J, Abdalla I, Xu Z, Yu J, et al. 2025. Ant-nest-inspired biomimetic composite for self-cleaning, heat-insulating, and highly efficient electromagnetic wave absorption. *Advanced Functional Materials* 35(18):2407458
[249] Shi Q, Zhao Y, Li M, Li B, Hu Z. 2023. 3D lamellar skeletal network of porous carbon derived from hull of water chestnut with excellent microwave absorption properties. *Journal of Colloid and Interface Science* 641:449–458
[250] Li Z, Lin H, Xie Y, Zhao L, Guo Y, et al. 2022. Monodispersed Co@C nanoparticles anchored on reclaimed carbon black toward high-performance electromagnetic wave absorption. *Journal of Materials Science & Technology* 124:182–192
[251] Gong X, Liu Q, Zhao W, Lu Z, Zhang T. 2022. Almond C/Fe_xO_y composite material based on biomass porous carbon structure with high-efficiency microwave absorbing properties. *Journal of Materials Science-Materials in Electronics* 33(16):13166–13179
[252] Cheng T, Guo Y, Xie Y, Zhao L, Wang T, et al. 2023. Customizing the structure and chemical composition of ultralight carbon foams for superior microwave absorption performance. *Carbon* 206:181–191
[253] Wang Z, Xu G. 2022. 3D porous Ni@BPC composites for enhanced electromagnetic wave absorption. *Journal of Alloys and Compounds* 926:166923
[254] Yue J, Yu J, Jiang S, Chen Y. 2022. Biomass carbon materials with porous array structures derived from soybean dregs for effective electromagnetic wave absorption. *Diamond and Related Materials* 126:109054
[255] Wu Z, Tian K, Huang T, Hu W, Xie F, et al. 2018. Hierarchically porous carbons derived from biomasses with excellent microwave absorption performance. *ACS Applied Materials & Interfaces* 10(13):11108–1115
[256] Xi J, Zhou E, Liu Y, Gao W, Ying J, et al. 2017. Wood-based straightway channel structure for high performance microwave absorption. *Carbon* 124:492–498
[257] Wu Z, Meng Z, Yao C, Deng Y, Zhang G, et al. 2022. Rice husk derived hierarchical porous carbon with lightweight and efficient microwave absorption. *Materials Chemistry and Physics* 275:125246
[258] Wu Z, Guo X, Meng Z, Yao C, Deng Y, et al. 2022. Nickel/porous carbon derived from rice husk with high microwave absorption performance. *Journal of Alloys and Compounds* 925:166732
[259] Yao C, Wu Z, Liu J, Guo X, Zhang W, et al. 2023. Construction of lychee-like MoS_2 microspheres on rice husk-derived porous carbon for enhanced dielectric loss and efficient electromagnetic wave absorption. *Journal of Materials Science-Materials in Electronics* 34(15):1213
[260] Peng Q, Gao C, Song C, Liu Z, Fatehi P, et al. 2024. Wood-derived porous carbon foams filled with $Ti_3C_2T_x$MXene/CoFe-MOF for electromagnetic shielding with flame retardant, heat insulation and excellent cycle stability. *Journal of Industrial and Engineering Chemistry* 133:333–344
[261] Jiang Y, Xie X, Chen Y, Liu Y, Yang R, et al. 2018. Hierarchically structured cellulose aerogels with interconnected mxene networks and their enhanced microwave absorption properties. *Journal of Materials Chemistry C* 6(32):8679–8687

[262] Huang Y, Xie A, Seidi F, Zhu W, Li H, et al. 2021. Core-shell heterostructured nanofibers consisting of Fe_7S_8 nanoparticles embedded into S-doped carbon nanoshells for superior electromagnetic wave absorption. *Chemical Engineering Journal* 423:130307

[263] Zhou X, Jia Z, Feng A, Wang X, Liu J, et al. 2019. Synthesis of fish skin-derived 3D carbon foams with broadened bandwidth and excellent electromagnetic wave absorption performance. *Carbon* 152:827–836

[264] Xia C, Zhang S, Ren H, Shi S, Zhang H, et al. 2016. Scalable fabrication of natural-fiber reinforced composites with electromagnetic interference shielding properties by incorporating powdered activated carbon. *Materials* 9(1):10

[265] Zhang Y, Qu M, Zhang K, Liu W, Wang J, et al. 2025. Effect mechanisms of microwave on CO_2 adsorption with cellulosic and non-cellulosic biochar. *Separation and Purification Technology* 373:133610

[266] Lv Q, Peng Z, Meng Y, Pei H, Chen Y, et al. 2022. Three-dimensional printing to fabricate graphene-modified polyolefin elastomer flexible composites with tailorable porous structures for electromagnetic interference shielding and thermal management application. *Industrial & Engineering Chemistry Research* 61(45):16733–16746

[267] Fan M, Chen R, Lu Y, Liu R, Ma Y, et al. 2022. Flexible microfibrillated cellulose/carbon nanotube multilayered composite films with electromagnetic interference shielding and thermal conductivity. *Composites Communications* 35:101293

[268] Xie C, Wang Y, Wang W, Yu D. 2022. Flexible, conductive and multifunctional cotton fabric with surface wrinkled MXene/CNTs microstructure for electromagnetic interference shielding. *Colloids and Surfaces A: Physicochemical and Engineering Aspects* 651:129713

[269] Ai Y, Xing R, Huang R, Kong J, Su R. 2024. Biomass-derived fire-retardant porous carbon towards efficient electromagnetic wave absorption and shielding. *Carbon* 227:119268

[270] Xie X, Zhang B, Wang Q, Zhao X, Wu D, et al. 2021. Efficient microwave absorber and supercapacitors derived from puffed-rice-based biomass carbon: effects of activating temperature. *Journal of Colloid and Interface Science* 594:290–303

[271] Xia C, Shi SQ. 2016. Self-activation for activated carbon from biomass: theory and parameters. *Green Chemistry* 18(7):2063–2071

[272] Tian N, Lu BA, Yang XD, Huang R, Jiang YX, et al. 2018. Rational design and synthesis of low-temperature fuel cell electrocatalysts. *Electrochemical Energy Reviews* 1(1):54–83

[273] Ali Abdelkareem M, Elsaid K, Wilberforce T, Kamil M, Sayed ET, et al. 2021. Environmental aspects of fuel cells: a review. *Science of The Total Environment* 752:141803

[274] Aizudin M, Goei R, Ong AJ, Tan YZ, Lua SK, et al. 2022. Sustainable development of graphitic carbon nanosheets from plastic wastes with efficient photothermal energy conversion for enhanced solar evaporation. *Journal of Materials Chemistry A* 10(37):19612–19617

[275] Zhu L, Shen D, Luo KH. 2020. A critical review on VOCs adsorption by different porous materials: species, mechanisms and modification methods. *Journal of Hazardous Materials* 389:122102

[276] Rosli NHA, Lau KS, Winie T, Chin SX, Chia CH. 2021. Microwave-assisted reduction of graphene oxide for an electrochemical supercapacitor: structural and capacitance behavior. *Materials Chemistry and Physics* 262:124274

[277] Gopalakrishnan A, Badhulika S. 2020. Effect of self-doped heteroatoms on the performance of biomass-derived carbon for supercapacitor applications. *Journal of Power Sources* 480:228830

[278] Joshi B, Samuel E, Kim YI, Yarin AL, Swihart MT, et al. 2022. Review of recent progress in electrospinning-derived freestanding and binder-free electrodes for supercapacitors. *Coordination Chemistry Reviews* 460:214466

[279] Khedulkar AP, Dang VD, Thamilselvan A, Doong RA, Pandit B. 2024. Sustainable high-energy supercapacitors: metal oxide-agricultural waste biochar composites paving the way for a greener future. *Journal of Energy Storage* 77:109723

[280] Guardia L, Suárez L, Querejeta N, Pevida C, Centeno TA. 2018. Winery wastes as precursors of sustainable porous carbons for environmental applications. *Journal of Cleaner Production* 193:614–624

[281] Sri Shalini S, Palanivelu K, Ramachandran A, Raghavan V. 2020. Biochar from biomass waste as a renewable carbon material for climate change mitigation in reducing greenhouse gas emissions—a review. *Biomass Conversion and Biorefinery* 11(5):2247–2267

[282] Karnan M, Subramani K, Sudhan N, Ilayaraja N, Sathish M. 2016. *Aloe vera* derived activated high-surface-area carbon for flexible and high-energy supercapacitors. *ACS Applied Materials & Interfaces* 8(51):35191–35202

[283] Deng J, Peng Z, Xiao Z, Song S, Dai H, et al. 2020. Porous doped carbons from anthracite for high-performance supercapacitors. *Applied Sciences* 10(3):1081

[284] Okonkwo CA, Lv T, Hong W, Li G, Huang J, et al. 2020. The synthesis of micromesoporous carbon derived from nitrogen-rich *spirulina* extract impregnated castor shell based on biomass self-doping for highly efficient supercapacitor electrodes. *Journal of Alloys and Compounds* 825:154009

[285] Song P, He X, Shen X, Sun Y, Li Z, et al. 2019. Dissolution-assistant all-in-one synthesis of N and S dual-doped porous carbon for high-performance supercapacitors. *Advanced Powder Technology* 30(10):2211–2217

[286] Peng L, Liang Y, Huang J, Xing L, Hu H, et al. 2019. Mixed-biomass wastes derived hierarchically porous carbons for high-performance electrochemical energy storage. *ACS Sustainable Chemistry & Engineering* 7(12):10393–10402

[287] Li C, Feng Y, Zhong F, Deng J, Yu T, et al. 2022. Optimization of microwave-assisted hydrothermal carbonization and potassium bicarbonate activation on the structure and electrochemical characteristics of crop straw-derived biochar. *Journal of Energy Storage* 55(D):105838

[288] Cheng BH, Tian K, Zeng RJ, Jiang H. 2017. Preparation of high performance supercapacitor materials by fast pyrolysis of corn gluten meal waste. *Sustainable Energy & Fuels* 1(4):891–899

[289] Li J, Jiang Q, Wei L, Zhong L, Wang X. 2020. Simple and scalable synthesis of hierarchical porous carbon derived from cornstalk without pith for high capacitance and energy density. *Journal of Materials Chemistry A* 8(3):1469–1479

[290] Jin H, Wang X, Shen Y, Gu Z. 2014. A high-performance carbon derived from corn stover via microwave and slow pyrolysis for supercapacitors. *Journal of Analytical and Applied Pyrolysis* 110:18–23

[291] Chen H, Wang G, Chen L, Dai B, Yu F. 2018. Three-dimensional honeycomb-like porous carbon with both interconnected hierarchical porosity and nitrogen self-doping from cotton seed husk for supercapacitor electrode. *Nanomaterials* 8(6):412

[292] Tian X, Ma H, Li Z, Yan S, Ma L, et al. 2017. Flute type micropores activated carbon from cotton stalk for high performance supercapacitors. *Journal of Power Sources* 359:88–96

[293] Fang K, Chen M, Chen J, Tian Q, Wong CP. 2019. Cotton stalk-derived carbon fiber@Ni-Al layered double hydroxide nanosheets with improved performances for supercapacitors. *Applied Surface Science* 475:372–379

[294] Zhang X, Yu Z, Ma X, Yi Y, Yue W, et al. 2024. Preparation of nitrogen-rich porous carbon by microwave-assisted two-step co-pyrolysis of kapok wood and chlorella vulgaris. *Journal of Analytical and Applied Pyrolysis* 179:106523

[295] Peng L, Cai Y, Luo Y, Yuan G, Huang J, et al. 2018. Bioinspired highly crumpled porous carbons with multidirectional porosity for high rate performance electrochemical supercapacitors. *ACS Sustainable Chemistry & Engineering* 6(10):12716–12726

[296] Lei W, Yang B, Sun Y, Xiao L, Tang D, et al. 2021. Self-sacrificial template synthesis of heteroatom doped porous biochar for enhanced electrochemical energy storage. *Journal of Power Sources* 488:229455

[297] Luo J, Zhang H, Zhang Z, Yu J, Yang Z. 2019. In-built template synthesis of hierarchical porous carbon microcubes from biomass toward electrochemical energy storage. *Carbon* 155:1–8

[298] Jin H, Hu J, Wu S, Wang X, Zhang H, et al. 2018. Three-dimensional interconnected porous graphitic carbon derived from rice straw for high performance supercapacitors. *Journal of Power Sources* 384:270–277

[299] Charoensook K, Huang CL, Tai HC, Lanjapalli VVK, Chiang LM, et al. 2021. Preparation of porous nitrogen-doped activated carbon

derived from rice straw for high-performance supercapacitor application. *Journal of the Taiwan Institute of Chemical Engineers* 120:246–256

[300] Yang S, Wang S, Liu X, Li L. 2019. Biomass derived interconnected hierarchical micro-meso-macro-porous carbon with ultrahigh capacitance for supercapacitors. *Carbon* 147:540–549

[301] Li M, Xiao H, Zhang T, Li Q, Zhao Y. 2019. Activated carbon fiber derived from sisal with large specific surface area for high-performance supercapacitors. *ACS Sustainable Chemistry & Engineering* 7(5):4716–4723

[302] Feng H, Hu H, Dong H, Xiao Y, Cai Y, et al. 2016. Hierarchical structured carbon derived from bagasse wastes: a simple and efficient synthesis route and its improved electrochemical properties for high-performance supercapacitors. *Journal of Power Sources* 302:164–173

[303] Zhang S, Su Y, Zhu S, Zhang H, Zhang Q. 2018. Effects of pretreatment and $FeCl_3$ preload of rice husk on synthesis of magnetic carbon composites by pyrolysis for supercapacitor application. *Journal of Analytical and Applied Pyrolysis* 135:22–31

[304] Chen T, Luo L, Luo L, Deng J, Wu X, et al. 2021. High energy density supercapacitors with hierarchical nitrogen-doped porous carbon as active material obtained from bio-waste. *Renewable Energy* 175:760–769

[305] Song X, Ma X, Li Y, Ding L, Jiang R. 2019. Tea waste derived microporous active carbon with enhanced double-layer supercapacitor behaviors. *Applied Surface Science* 487:189–197

[306] Zhao C, Huang Y, Zhao C, Shao X, Zhu Z. 2018. Rose-derived 3D carbon nanosheets for high cyclability and extended voltage supercapacitors. *Electrochimica Acta* 291:287–296

[307] Wang X, Kong D, Zhang Y, Wang B, Li X, et al. 2016. All-biomaterial supercapacitor derived from bacterial cellulose. *Nanoscale* 8:9146–9150

[308] Li S, Huang D, Zhang B, Xu X, Wang M, et al. 2014. Flexible supercapacitors based on bacterial cellulose paper electrodes. *Advanced Energy Materials* 4(10):1301655

[309] Tang YH, Liu SH, Tsang DCW. 2020. Microwave-assisted production of CO_2-activated biochar from sugarcane bagasse for electrochemical desalination. *Journal of Hazardous Materials* 383:121192

[310] Lu Q, Zhou S, Li B, Wei H, Zhang D, et al. 2020. Mesopore-rich carbon flakes derived from lotus leaves and it's ultrahigh performance for supercapacitors. *Electrochimica Acta* 333:135481

[311] Simon S, Harikumar P, Sreeja PB. 2025. Green power: the role of plant-based biochar in advanced energy storage. *ChemPhysChem* 26(1):e202400569

[312] Zhang Y, Gao H, Song X, Kong X, Xu H. 2019. Preparation of hierarchical porous carbon from wheat bran for free-standing electrode of high areal capacitance supercapacitor. *ChemElectroChem* 6(21):5486–5491

[313] Thines KR, Abdullah EC, Ruthiraan M, Mubarak NM, Tripathi M. 2016. A new route of magnetic biochar based polyaniline composites for supercapacitor electrode materials. *Journal of Analytical and Applied Pyrolysis* 121:240–257

[314] Jiang W, Li L, Pan J, Senthil RA, Jin X, et al. 2019. Hollow-tubular porous carbon derived from cotton with high productivity for enhanced performance supercapacitor. *Journal of Power Sources* 438:226936

[315] Zhang Y, Chen H, Wang S, Shao W, Qin W, et al. 2020. Facile fabrication and structure control of SiO_2/carbon *via in situ* doping from liquefied bio-based sawdust for supercapacitor applications. *Industrial Crops and Products* 151:112490

[316] Shang T, Xu Y, Li P, Han J, Wu Z, et al. 2020. A bio-derived sheet-like porous carbon with thin-layer pore walls for ultrahigh-power supercapacitors. *Nano Energy* 70:104531

[317] Guo R, Guo N, Luo W, Xu M, Zhou D, et al. 2021. A dual-activation strategy to tailor the hierarchical porous structure of biomass-derived carbon for ultrahigh rate supercapacitor. *International Journal of Energy Research* 45(6):9284–9294

[318] Wang J, Wu L, Shen L, Zhou Q, Chen Y, et al. 2023. CoO embedded porous biomass-derived carbon as dual-functional host material for lithium-sulfur batteries. *Journal of Colloid and Interface Science* 640:415–422

[319] Nguyen TKA, Huynh TV, Doong RA. 2023. Enhanced capacitive deionization of Cr(VI) using functionalized metal carbide 2D framework and badam tree leaf-derived carbon as the asymmetric electrode materials. *Chemical Engineering Journal* 475:146439

[320] Liu SH, Tang YH. 2020. Hierarchically porous biocarbons prepared by microwave-aided carbonization and activation for capacitive deionization. *Journal of Electroanalytical Chemistry* 878:114587

[321] Inal IIG, Holmes SM, Yagmur E, Ermumcu N, Banford A, et al. 2018. The supercapacitor performance of hierarchical porous activated carbon electrodes synthesised from demineralised (waste) cumin plant by microwave pretreatment. *Journal of Industrial and Engineering Chemistry* 61:124–132

[322] Liu Y, Pan L, Chen T, Xu X, Lu T, et al. 2015. Porous carbon spheres via microwave-assisted synthesis for capacitive deionization. *Electrochimica Acta* 151:489–496

[323] Adorna J, Borines M, Dang VD, Doong RA. 2020. Coconut shell derived activated biochar–manganese dioxide nanocomposites for high performance capacitive deionization. *Desalination* 492:114602

[324] Liu C, Chen W, Li M, Hong S, Li W, et al. 2019. Rapid microwave activation of waste palm into hierarchical porous carbons for supercapacitors using biochars from different carbonization temperatures as catalysts. *RSC Advances* 9(34):19441–19449

[325] Chen D, Li L, Xi Y, Li J, Lu M, et al. 2018. Self-assembly of biomass microfibers into 3D layer-stacking hierarchical porous carbon for high performance supercapacitors. *Electrochimica Acta* 286:264–270

[326] Li D, Lin J, Lu Y, Huang Y, He X, et al. 2020. MnO_2 nanosheets grown on N-doped agaric-derived three-dimensional porous carbon for asymmetric supercapacitors. *Journal of Alloys and Compounds* 815:152344